ALMA MATER STUDIORUM – UNIVERSITY OF BOLOGNA

SCHOOL OF ENGINEERING AND ARCHITECTURE

CHEMICAL AND PROCESS ENGINEERING

Sustainable Technologies and Biotechnologies for Energy and Materials

MASTER THESIS

in

Fluid Mechanics and Transport Phenomena M

ULTRA-THIN GRAPHENE-BASED MEMBRANES FOR HYDROGEN PURIFICATION

Student

Roberta Di Carlo

Supervisor

Prof. Matteo Minelli

Co-supervisor

Dr. Giacomo Foli

Session III

A.Y. 2021-2022

Table of Contents

Abstract

Hydrogen is emerging as a versatile raw material and energy vector. However, current hydrogen production methods rely on fossil fuels, leading to greenhouse gas emissions and contributing to global warming. Carbon capture technologies are being explored as a potential solution to this issue. One approach for carbon capture and storage (CCS) is to use membranes, which are perm-selective barriers that, in this specific case, can allow for the separation of hydrogen from carbon dioxide. Polymeric membranes, in particular, are becoming increasingly important thanks to their great versatility and processability. However, there is a limitation in separation performance known as the Robeson upper bound, which means that as permeability increases, selectivity decreases. Mixed matrix membranes (MMM) have been introduced to integrate polymeric materials with organic or inorganic fillers that have excellent separation properties. Low dimensional materials, such as graphene and its derivatives, have emerged as promising fillers due to their high permeability and selectivity. Two types of graphene-based membranes are possible: nanoporous graphene and multilayered graphene-based membranes. This thesis work is focused on graphene oxide (GO) multilayered membranes. Polyimides, specifically Matrimid, are used as polymeric support onto which GO multilayered coating is deposited by means of dipping Layer by Layer (LbL) technique. By carrying out permeation tests, effect of temperature, GO concentration, thermal reduction, number of bilayers and deposition of the coating on one side only have been investigated. Furthermore, since several factors have an influence on the LbL assembly, a standardization procedure has been started in order to improve reproducibility and scalability of the process. Overall, GO nanocomposite membranes result to be highly effective in gas separations and offer many insight and potential to be exploited in the production of competitive systems.

1. Introduction

The global energy need is increasing as the population is growing worldwide. The immediate consequence is the paramount transition towards low-carbon sources of energy. However, today's economy and life still rely on fossil-based energy leading to the emissions of greenhouse gases. Greenhouse gases (GHG), i.e., CO_2, CH_4, H_2O, N_2O, and CFC, may be defined as substances able to absorb the infrared solar radiation coming from Earth and re-emit it in all directions. In this way, they are responsible for a global increase in temperature causing the so-called Greenhouse effect.

Since CO2 is probably the most relevant GHG, emissions are measured in carbon dioxide equivalent. This is a reference quantity to compare the effect of different greenhouse gases on the basis of their Global Warming Potential (GWP). Indeed, GWP is an environmental indicator that accounts for the contribution to global warming for a pulse of 1 kg of the gas and relative to 1 kg of carbon dioxide.

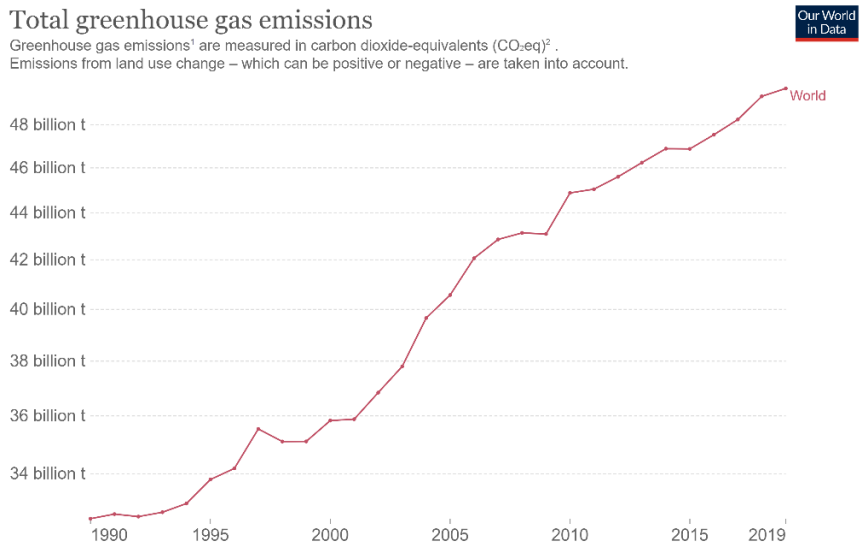

Figure 1, Total greenhouse gas emissions [1]

As one can see from the chart, the total greenhouse gas emissions are exponentially increasing and such trend has not reached a peak yet, so it is expected that it will continue to rise.

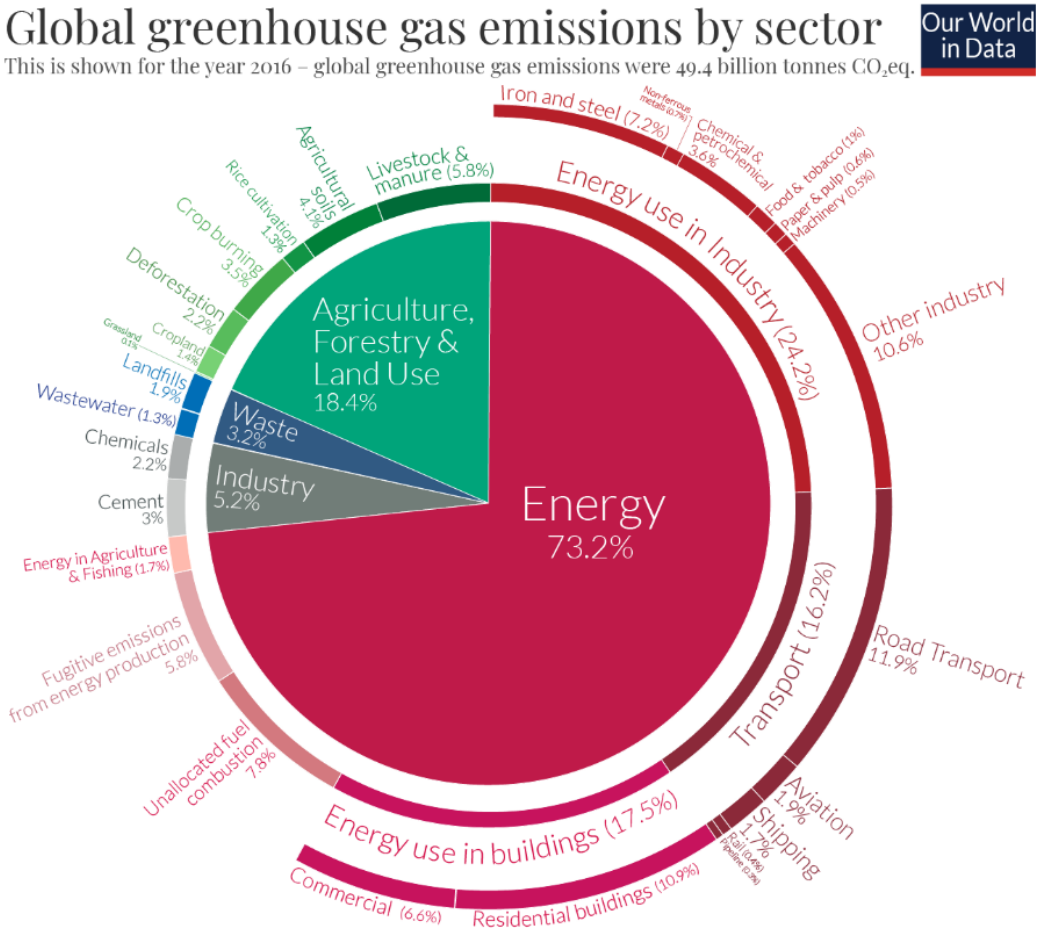

Figure 2, Global greenhouse gas emissions by sector [1]

GHG emissions are produced by several different sectors. Therefore, one of the main challenges is to find new and sustainable raw materials to feed all industrial and technological needs. More precisely, sustainability refers to the connection of scientific and industrial progress to environmental, social, and economic needs in order not to compromise the development of future generations.

In this context, in recent years, the development of a new energy strategy based on hydrogen has been widely inspected in view of its remarkable versatility. Hydrogen can be produced from various sources, namely water, biomass, natural gas, or coal, and using various processes. The majority of current production methods include the formation of CO and CO_2 as byproducts. This means that hydrogen needs to be purified from these substances. The purification from CO_2 is

essential and it allows to find an application also for carbon dioxide which can be explored in turn as a raw material. This investigation ended in the development of the Carbon Capture Utilization and Storage (CCUS) method.

Hydrogen purification is based on several conventional technologies: pressure swing adsorption, temperature swing adsorption, and cryogenic distillation. In recent years membrane separation has obtained more importance because it is a versatile and environmentally friendly process that allows having extremely high-purity products.

The main aim of this thesis work is to find an efficient process to carry out the separation of gases and, specifically, hydrogen from carbon dioxide, using graphene oxide nanostructured membranes. Theoretical background will be provided together with experimental results which have been obtained in laboratories at Unibo, Dicam department.

1.1 Hydrogen

Hydrogen is the first, and lightest element in the periodic table. At standard conditions, it is a colorless, tasteless, and odorless gas represented by the formula H_2. Hydrogen is the most abundant element in the universe, representing 75% of its composition, even if it is not present in the atmosphere because it is lighter than air. This means that, on Earth, hydrogen is not available in the free state, but combined with other atoms such as oxygen in water, carbon in methane, and other hydrocarbons.

Currently, hydrogen is considered a precious and versatile raw material. The hydrogen market covers two main sectors: refineries and the chemical industry.

H_2 properties can be exploited in

- The industrial field for chemical processes and refinery usage
    - Ammonia is the dominant product using hydrogen as raw material and it is obtained through the Haber-Bosch process; nitrogen and hydrogen are treated at high pressures and temperatures (15-25 MPa, 300-500°C) with an iron catalyst. The reaction is the following:

$$N_2 + 3H_2 \rightarrow 2NH_3$$

- Methanol is also synthesized starting from hydrogen, more specifically from syngas, in two exothermic reactions:

  $$2H_2 + CO \rightarrow CH_3OH$$

  $$3H_2 + CO_2 \rightarrow CH_3OH + H_2O$$

- Fischer-Tropsch process for hydrocarbons production
- Oil and fat hydrogenation to produce cosmetics and food
- Hydrocracking and hydro refining in the petroleum industry

- Energy field as an energy vector
- Decarbonization in hard-to-abate sectors (i.e., those sectors for which the transition to net zero CO_2 emissions is difficult from both technical and economic POV). [2]

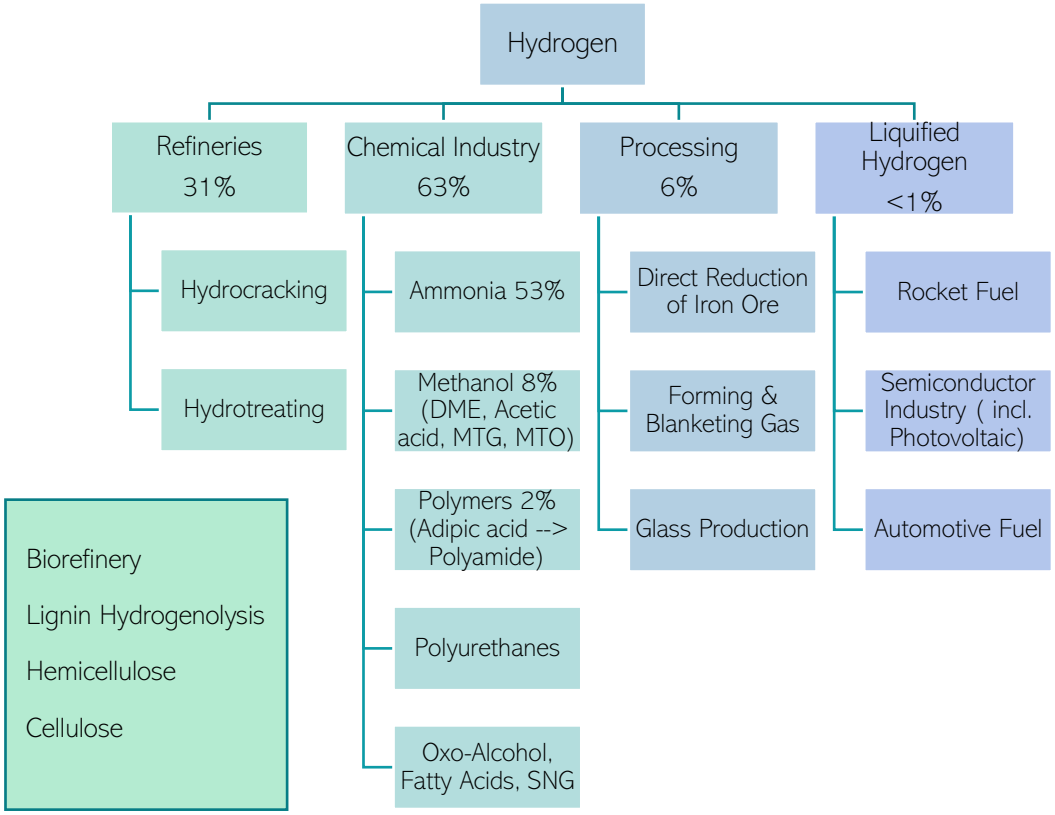

Figure 3, Possible utilization of hydrogen [2]

The potential decarbonization ability of hydrogen is the main driving force to push on the transition toward the so-called Hydrogen Economy. Such term has been coined in 1970 by Prof John Bockris and, as can be foreseen from the name itself, it is the development of a hydrogen-based economy

to reach sustainability goals. But hydrogen can be a green substance only if its production processes are nonpolluting and the emitted CO_2 is captured and reused somehow. So, the goal is to have carbon-free or less carbon-intensive energy systems with respect to the current ones based on fossil fuels.

1.1.1 Production

Depending on the production route of hydrogen, it is possible to distinguish three types of hydrogen. [3]

Grey hydrogen is produced starting from fossil fuels such as natural gas or coal and the emitted CO_2 and other GHGs are not sequestered but dispersed in the atmosphere. Hence, it is a harmful production route for the planet. Moreover, this term is also used when hydrogen is produced with electrolysis, but the electricity comes from fossil fuels. The most common production path used to get grey hydrogen is natural gas reforming. Here steam at 700°C-1000°C is used to produce hydrogen from methane, in an endothermic reaction that takes place at 3-25 bar.

$CH_4 + H_2O$ (+ heat) → $CO + 3H_2$

The following step is called the "water-gas shift reaction" and it is needed to increase the hydrogen yield and to convert carbon monoxide into CO_2. [4]

$CO + H_2O \rightarrow CO_2 + H_2$

Blue hydrogen (or purple hydrogen) is obtained starting from natural gas, biomethane, or even biomass through the same process as before (reforming), but CO_2 is then captured and stored. Of course, this process is costlier than the previous one because it consists of an additional stage for the CCS.

Last, green hydrogen is originated from water, thanks to electrolysis. This process uses electric energy, and it is much more expensive than the other two, and the main advantage is that it does not produce CO_2 or any other GHG.

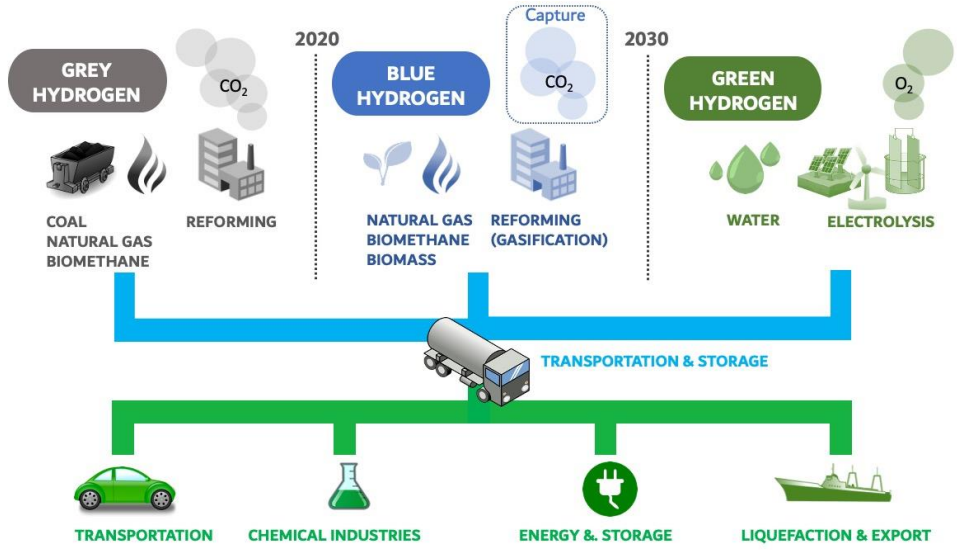

Figure 4, Hydrogen production routes [5]

Focusing on natural gas, three processes are possible: steam reforming, partial oxidation, and autothermal reforming.

Steam reforming

Steam reforming is the process that produces the highest ratio of H_2/CO_2. A gaseous stream is desulphurized and then it is contacted with a nickel-based catalyst and steam in heated tubes. The gaseous stream contains hydrocarbons that can be converted into synthesis gas. Typical conditions are characterized by high temperatures (750°C-900°C) and pressures (3-25 bar).

$$CH_4 + H_2O \rightarrow CO + 3H_2$$

This reaction is coupled with the so-called water gas shift where oxygen coming from the water molecule is used to oxidize carbon monoxide in carbon dioxide.

$$CO + H_2O \rightarrow H_2 + CO_2$$

In this way, it is possible to reach that high H_2/CO_2 ratio.

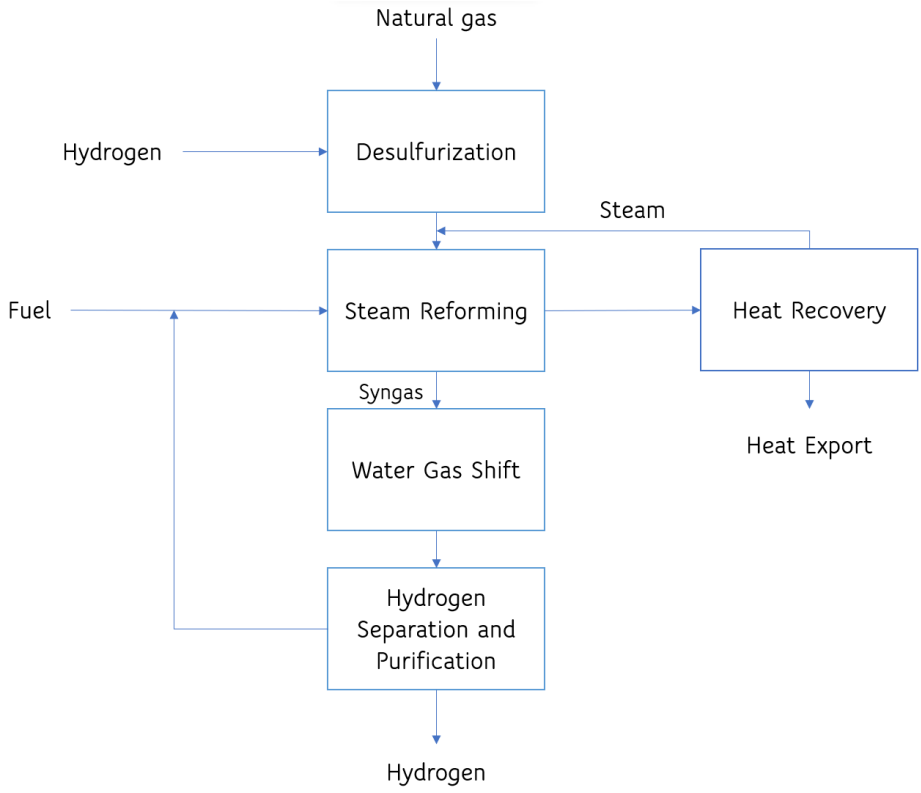

Figure 5, Hydrogen production through steam reforming [2]

Steam reforming is an endothermic process, for this reason, it is needed to recover heat in an efficient way to achieve economic sustainability.

Partial oxidation

Partial oxidation is a sort of variation of steam reforming. Here the gaseous stream reacts with under stoichiometric oxygen resulting in partial combustion.

$$CH_4 + \frac{1}{2}O_2 \rightarrow CO + 2H_2$$

Oxygen can be obtained from purified air and carbon monoxide is again converted to CO_2 by following the water gas shift reaction. The main advantage of the partial oxidation process is that it removes the need for an external heat supply: being the combustion exothermic, the reaction releases enough energy to conduct the process.

Autothermal reforming [6,7]

Autothermal reforming tries to combine the endothermic conventional steam reforming and exothermic partial oxidation: heat released from the partial oxidation is used to produce syngas through the steam reforming route.

$$2CH_4 + H_2O + \frac{1}{2}O_2 \rightarrow CO + 5H_2$$

This combination allows the reaction to take place in one single reactor with a nickel-based catalyst, high temperatures (900-1150 °C), and pressures (1-80 bar).

Gasification

Gasification is a process that can be carried out with every carbon-containing material. The process can be generalized through the following reaction:

$$C_xH_y + xH_2O \rightarrow xCO + \left(x + \frac{y}{2}\right)H_2$$

The ratio H_2/CO depends on the specific feedstock, but in a general view, it can be adjusted with the water gas shift process.

Among all the possibilities, coal is the most frequently used, but also biomass may be one of the employed feedstocks. This is interesting because the gasification process is responsible for greenhouse gases emission: therefore, using wastes or biomass, in general, could be a balancing choice. [7]

Electrolysis [8]

Electrolysis is a process that uses electric energy and converts it into chemical energy stored in a fuel.

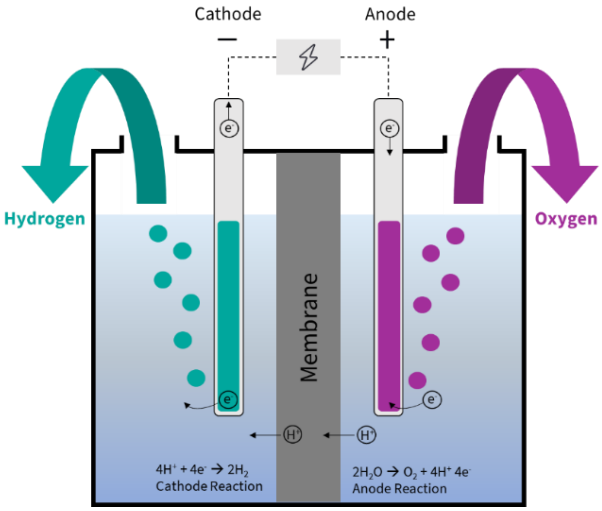

Figure 6, Example of an electrolytic cell for hydrogen production [87]

The main component of an electrolysis unit is the electrolytic cell. The electrolytic cell is composed of two electrodes (i.e., anode and cathode) immersed in an electrolyte and it is supplied with external power to make the direct current flow between the anode and the cathode. In the specific case of hydrogen production, it is water electrolysis that is used to split water into its constituents: oxygen and hydrogen. When a certain critical voltage is reached, hydrogen starts to be produced. [9,10]

$$H_2O_{(l)} \rightarrow H_{2(g)} + \frac{1}{2}O_{2(g)}$$

The reductive half-reaction takes place at the cathode, therefore producing hydrogen; whilst the oxidation occurs at the anode where oxygen is produced. A diaphragm is also needed to avoid the recombination of oxygen and hydrogen.

Three main electrolysis routes are available for the production of hydrogen: alkaline electrolysis, Proton Exchange Membrane (PEM) water electrolysis, and steam electrolysis.

Alkaline electrolysis is a mature technology: alkaline environments are usually preferred because they consent to better control corrosive phenomena, therefore cheaper materials can be used. It requires a liquid alkaline electrolyte such as sodium or potassium hydroxide solutions.

PEM water electrolysis uses polymeric membranes as solid electrolytes. The electrodes are usually noble metals like platinum or iridium. Through this version of electrolysis, it is possible to get hydrogen with higher purity with respect to alkaline electrolysis and higher electrical density can be exploited. This option is usually chosen for safety reasons.

Steam electrolysis tries to increase the efficiency of the process by focusing on the energetic requirement. The key point is to use water steam at high temperatures (800-900°C): in this way, part of the energy is supplied in form of heat that is cheaper than electric energy; moreover, heat also boosts the reaction kinetics. [9]

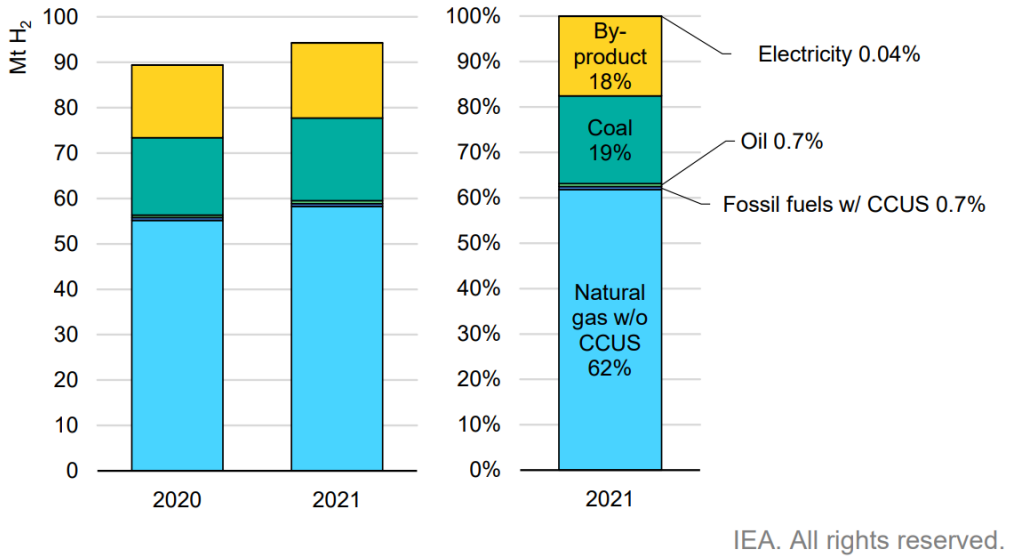

Figure 7, Hydrogen production mix, 2020 and 2021 [11]

At present, most of the hydrogen is still produced from natural gas without CO_2 capture, meaning that it is highly impacting on global warming. The percentage of blue and green hydrogen is still below 1%, although several projects are now devoted to increase the amount of low emissions

hydrogen production, and many of them are coupled with CCUS (Carbon Capture Utilization and storage).

1.2 Carbon Capture Utilization and Storage

CCUS is a set of technologies to capture, utilize and/or store CO_2 that is available from large point sources, such as industrial facilities or power generation plants. [12,13] Such technology may represent a step forward in the reduction of carbon emitted in the atmosphere and the development of its circularity. [13]

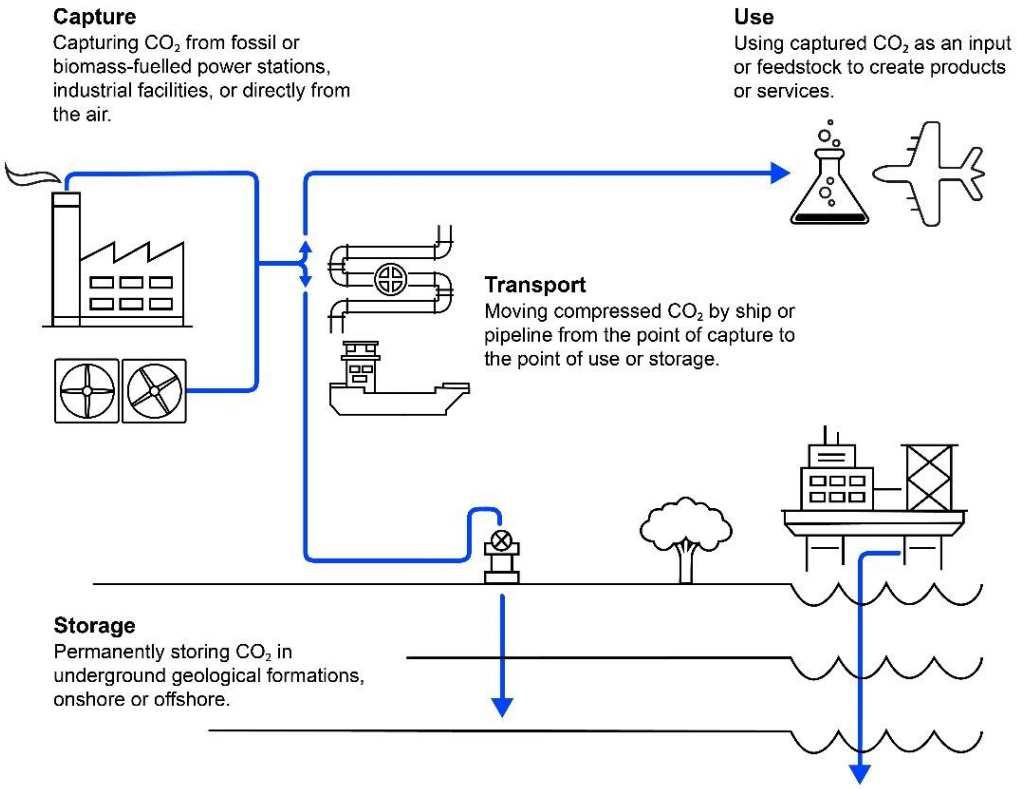

Figure 8, Carbon capture, utilization, transport and storage [12]

There are three main approaches to capture CO_2: [14]

- Pre-combustion is the capture of CO_2 from a gas mixture before combustion takes place. The fuel is reacted with oxygen to produce syngas (CO and hydrogen); carbon monoxide is then converted to CO_2 through the use of a water gas shift converter. In the end, CO_2 is

separated from the gas mixture. The concentration of CO_2 in the mixture can be in the range of 15-60%.

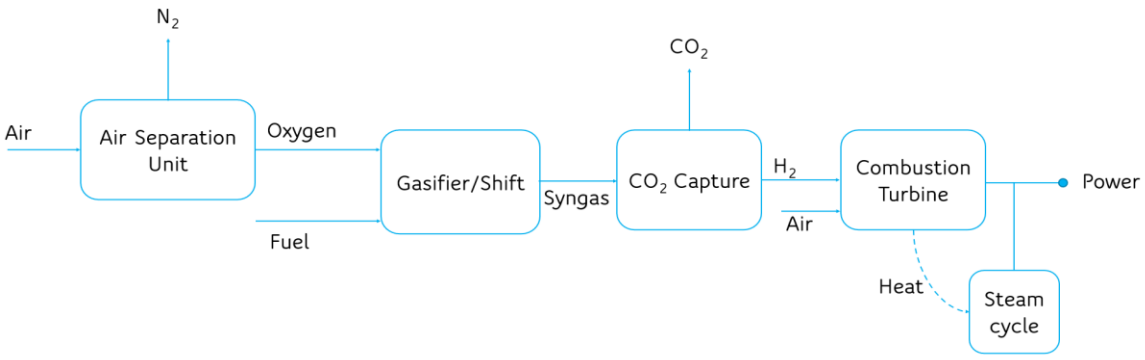

Figure 9, Pre-combustion CCS [39]

- Post-combustion: separation takes place only after the combustion of fossil fuels. During the combustion, flue gas is produced: instead of discharging it in the atmosphere, it is processed to separate most of the present CO_2. It is a versatile technique; indeed, it results to be applicable to most industrial plants. A drawback is that flue gases are commonly diluted and removal of CO_2 is not as easy as in the pre-combustion capture. This is the main reason why chemical absorption is the most common technique employed in post-combustion plants.

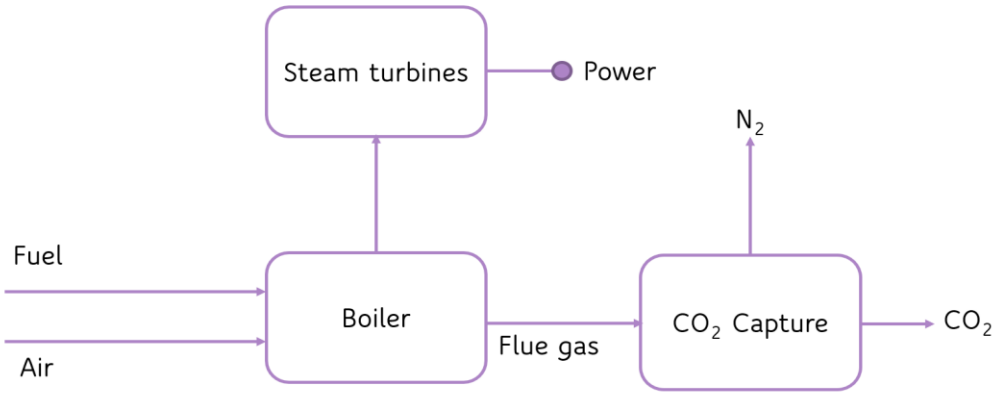

Figure 10, Post-combustion CCS [15]

- Oxycombustion: pure oxygen is used to have controlled combustion where flue gas will be mainly composed of CO_2 and water vapor. Water vapor can be easily condensed and the resulting CO_2 concentrated stream can be further processed and purified before the storage of CO_2. Pure oxygen is typically obtained from air through cryogenic distillation or other air separation techniques.

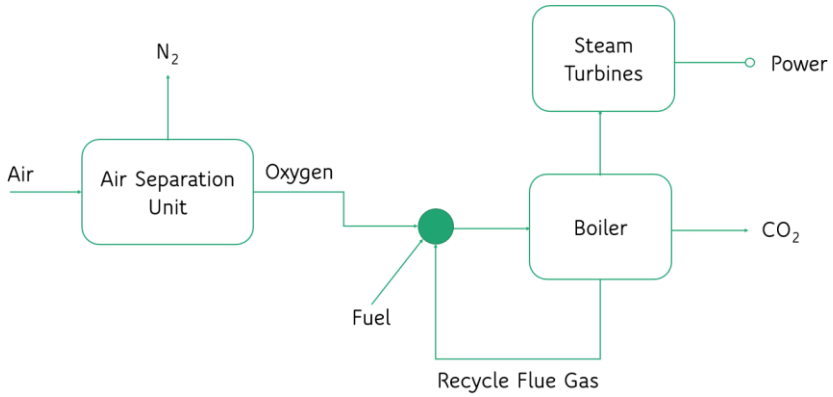

Figure 11, Oxy-combustion CCS [15]

CO_2 capture has been considered a promising technique since 2010. In these years there has been significant progress, but we are still far from what would be needed to reach net zero emissions. [12]

Interestingly, hydrogen production can be conveniently coupled with pre-combustion CCUS.

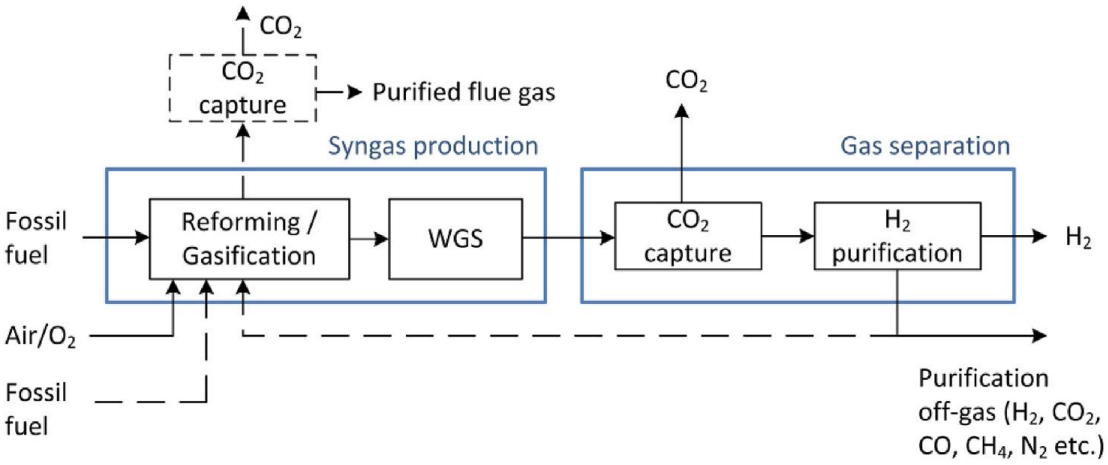

Figure 12, Pre-combustion system to separate hydrogen from carbon dioxide [16]

This system can support the scale-up of low-carbon hydrogen production. Indeed, it has been estimated that global hydrogen use will increase sevenfold by 2070. This low-carbon hydrogen will be produced mostly by using water electrolysis, but still, 40% will be obtained from fossil-based plants coupled with CCS.

At present different technologies may be used as summarized in the following table.

Separation task	*Pre-combustion capture*
Capture technologies	CO_2/H_2
Absorption	Physical solvent
	Chemical solvents
Membranes	Polymeric
Adsorption	Zeolites
	Activated carbon
	Alumina
Cryogenic	Liquefaction

Table 1, Summary of CO_2/H_2 separation techniques [14]

These techniques will be explained in the following paragraph.

1.3 Hydrogen purification

Once hydrogen has been produced it is called “crude hydrogen” and in most cases, it is not ready to be directly used. The required purity of hydrogen in the majority of applications is higher than 98%. The crucial step to get to hydrogen utilization is hydrogen purification.

Component [%]	**H_2**	**CO**	**CO_2**	**CH_4**	**N_2**	**Ar**	**Total Sulfur**	**H_2O**	**O_2**	**Others**
Coal gasification	25-35	35-45	15-25	0.1-0.3	0.5-1	-	0.2-1	15-20	-	-
Natural gas reforming	70-75	10-15	10-15	1-3	0.1-0.5	-	-	-	-	-
Methanol reforming	75-80	0.5-2	20-25	-	-	-	-	-	-	-
Coke oven gas	45-60	5-10	2-5	25-30	2-5	-	0.01-0.5	-	0.2-0.5	2-5
Methanol purge gas	70-80	4-8	5-10	2-8	5-15	0.1-2	-	-	-	-
Synthetic ammonia tail gas	60-75	-	-	-	15-20	-	-	1-3	10-15	-
Biomass gasification	25-35	30-40	10-15	10-20	1	-	0.2-1	-	0.3-1	-

Table 2, Composition of diverse types of crude hydrogen [4]

Hydrogen purification methods can be categorized into physical and chemical methods. Physical methods are adsorption, absorption, cryogenic distillation, and innovative membrane separation; whilst chemical methods comprise metal hydride separation and absorption.

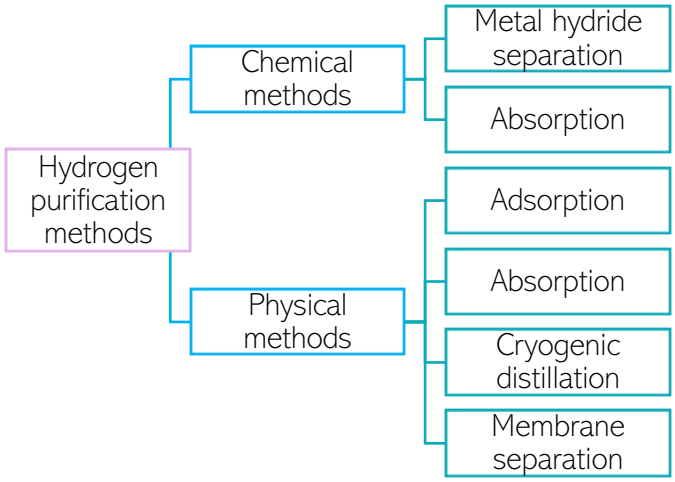

Figure 13, Hydrogen purification methods [17]

1.3.1 Chemical methods

Metal hydride separation

Metal hydride separation is a process based on the reversible equilibrium absorption of hydrogen in metal alloys. By increasing the pressure and at low-temperature crude hydrogen is absorbed by the system: molecular hydrogen is decomposed through a reaction that is catalyzed by metal alloys, therefore metal hydrides are produced, and impurities are trapped inside the metal alloy. The temperature is then increased so that the system will release hydrogen to lower the pressure and get back to the equilibrium conditions.

1.3.2 Physical methods

Adsorption

Adsorption processes are based on selective adsorption on solid surfaces of specific molecules. These processes include Pressure Swing Adsorption (PSA), and Temperature Swing Adsorption (TSA). The basic principle is the same for both: a gas mixture in contact with a solid will end up in molecules that are more or less attracted to the solid surface and, depending on this aspect, less adsorbed molecules can be separated from the others. The process is exothermic and spontaneous. Traditional adsorbents are porous materials to increase the available surface area per unit volume, such as zeolites, activated carbons, silica, and alumina gels.

Pressure Swing Adsorption

PSA is a method based on the evidence that, at high pressures, gases tend to be selectively adsorbed to solid surfaces. The gaseous mixture is contacted with adsorbents in a packed column to produce high-purity hydrogen. Being hydrogen a light gas, it is less adsorbable than other gaseous components present in the mixture such as CO_2 and CO; these impurities are more strongly adsorbed and through PSA, one can recover the hydrogen stream flowing out of the column. Then, the adsorbed molecules are desorbed in an endothermic process by lowering the gas-phase partial pressure.

A typical process scheme consists of two vessels working in parallel. The gaseous mixture is fed at the bottom of the first vessel, impurities are adsorbed, and the gas can pass through the vessel

and be collected on the top. During the purification step, the other vessel is working to regenerate the adsorbents: by reducing the pressures, impurities are desorbed so that the vessel is ready for another purification step.

A four-step PSA cycle has been developed to increase the efficiency of the process by recovering the high-pressure gas from the regeneration adsorber and part of the purified hydrogen that is trapped inside the voids of the adsorber. Five steps are needed to carry out this type of hydrogen purification:

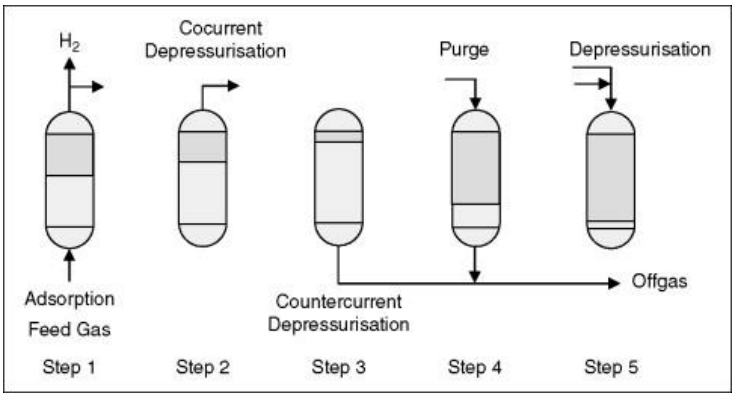

Figure 14, Pressure Swing Adsorption scheme [18]

1. Adsorption of impurities in the first vessel.
2. Co-current depressurization to recover high-purity hydrogen trapped in voids of the adsorber.
3. Counter-current depressurization, i.e., blow off to release the remaining gas impurities trapped in voids of the adsorber.
4. The purge of the regenerated adsorber with high-pressure hydrogen that is taken from another adsorber in the depressurization step.
5. Re-pressurization of the adsorber through hydrogen coming from the co-current depressurization.

PSA is used since the 1970s to produce high-purity hydrogen. Since one of the principal limitations of the PSA apparatus invented by Batta, was the low final yield due to the insufficient number of beds, the most frequently used version of PSA is patented by Union Carbide Corporation of the U.S.A and it consists of eleven cyclic steps and at least 7 beds (usually 10).

Temperature Swing Adsorption

Temperature swing adsorption is an alternative to PSA and relies on the tendency of gases to be more easily adsorbed at lower temperatures. The gas mixture is fed to the adsorber at a low temperature to make the adsorption of impurities possible. Desorption will take place by heating up the vessel with a hot and clean gaseous stream. Then the bed is cooled down and the operation can restart. TSA is advantageous because it allows a faster and more accurate regeneration of molecular sieves that are used as adsorbers. On the other hand, the main drawback is related to the possibility of overheating for the adsorber because of temperature cycles. [19,20]

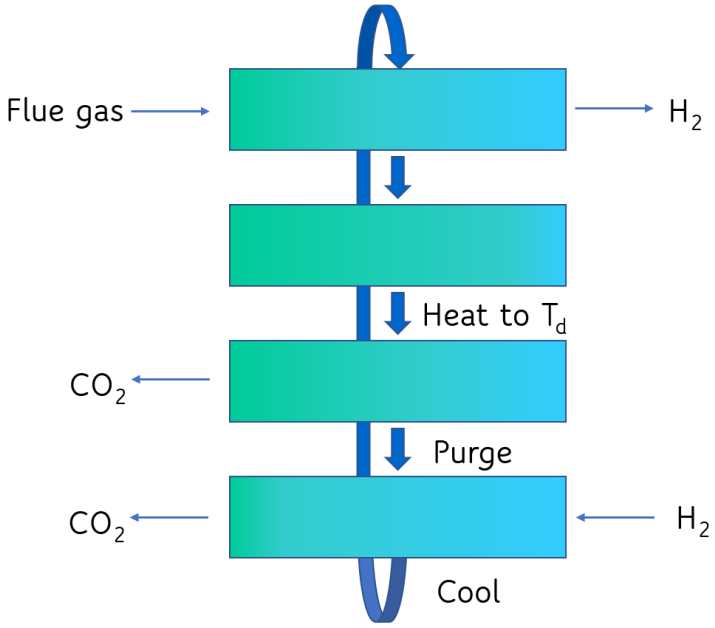

Figure 15, Temperature Swing Adsorption scheme [21]

Cryogenic process

Distillation is a unit operation whose aim is to separate different components taking advantage of their different relative volatilities, without the use of a third component or solvent. Specifically, cryogenic distillation is a distillation process performed at high pressure and low temperature and this technology can be exploited to separate and purify hydrogen from gaseous mixtures.

As a result, it is possible to separate hydrogen from other components that condense first. Specifically, hydrogen has high volatility: hydrocarbons, carbon monoxide, and other gases

condense first. The purity of hydrogen that one can reach throughout this process is not sufficient in several cases and this needs to be considered together with the high energy requirements for compressors and cooling equipment. [22]

Absorption

As one can see from table 2, CO_2 is one of the main impurities in the hydrogen-containing gaseous stream, so, notably, carbon dioxide capture and separation have become relevant issues.

Aside from the techniques that have already been introduced in the previous paragraphs, another process that can be used for CO_2 capture is absorption.

Absorption is a phenomenon in which molecules can cross the surface of the considered material so that they can enter the bulk of the material volume. Specifically, gas absorption is a unit operation where soluble gaseous components are dissolved in a liquid.

It is possible to distinguish chemical absorption where there is a chemical reaction between the absorbed molecules and our material; and physical absorption which is, instead, an unreactive process, based thus on the physical dissolution of the gas in the liquid solvent phase. [23]

Dealing with the separation of hydrogen from CO_2, chemical absorption ends up in an exothermic reversible reaction where a solvent reacts with a gas stream containing CO_2, preferably at low temperatures. This process is particularly suitable for gases with CO_2 at low partial pressure and the two most used solvents are amines and carbonate solutions. At the end of the process, the chemical reaction is reverted through the stripping step at high temperatures, to restore solvents. [24,25] The main advantages of this technology are the low cost, high efficiency, and the fact that it is a mature method if compared with others (such as membranes, for example).

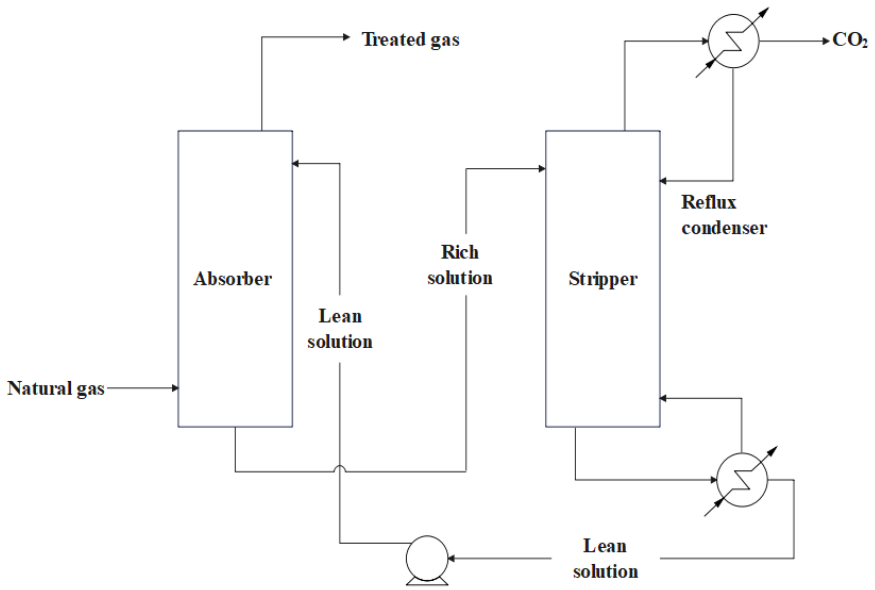

Figure 16, Absorption process scheme [88]

Key parameters for an absorption process are: [14]

- Solvent flowrates determine the dimensions of the plant
- The CO_2 content in the gaseous stream and CO_2 removal
- Energy requirement that will be the sum of the thermal energy to regenerate solvents and electrical energy needed to carry out the operation
- Solvent choice

The choice of solvent is based on three main requirements: reactivity, low regeneration energy, and high CO_2 loading capacity. The most frequently used solvents are amines or carbonates.

Amines are compounds deriving from ammonia where one or more hydrogen atoms have been replaced by organic substituents. Depending on the number of substituted hydrogen atoms, it is possible to have primary, secondary, and tertiary amines, and all of them apply to CO_2 capture.

Monoethanolamine (MEA) is a primary amine and the most used one to separate CO_2.

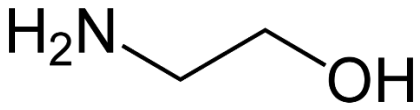

Figure 17, MEA chemical structure [89]

The utilization of amines to capture CO_2 shows several limitations in the high energy requirement for regeneration, corrosion action towards equipment, and easy degradation. For this reason, a different process has been developed using carbonate-based solutions. Here the absorption process is carried out at high pressure and temperature, whilst the stripping section is characterized by lower pressures.

Carbonate-based absorption is beneficial thanks to lower desorption and solvent regeneration energy requirements, but reaction rates are lower if compared to amine-based absorption.

Physical absorption is a technology based on vapor-liquid equilibria. For a wide range of gases, the equilibrium relationship is based on Henry's law which states that, at a given temperature, the amount of dissolved gas in a unit volume of a solvent is proportional to the gas's partial pressure.

$$p_{CO_2} = Hx_{CO_2} \qquad (1)$$

Generally, the solubility increases with pressure and decreases with temperature, so the best condition to perform a physical separation is working with high-pressure and low-temperature CO_2 streams.

The solvent choice is a key aspect of this technology:

- Liquids with high solubilities for the solute should be preferred in order to reduce the amount of solvent that is needed
- It should not be expensive, corrosive, viscous and hazardous (for instance, flammability should be avoided)
- It should also be easily recoverable.

Methanol, propylene carbonate, and dimethyl ethers are only some of the available possibilities to capture CO_2. The desorption heat requirements are much lower than chemical absorption, but chemical solvents can achieve high loading at low partial pressure.

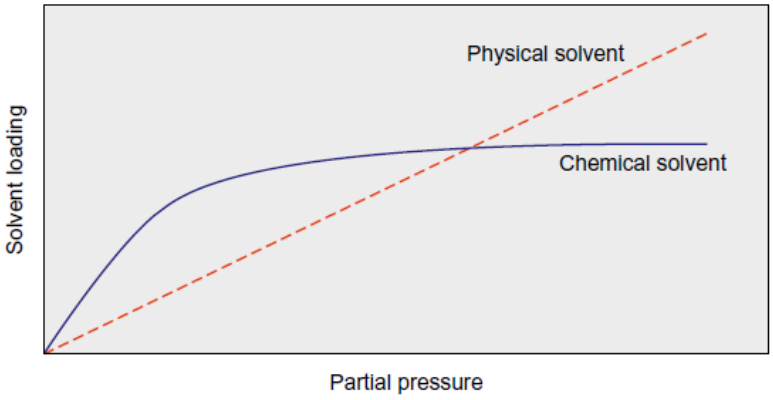

Figure 18, Solvent loading of chemical and physical solvents [26]

1.3.3 Membrane separation

In recent years, membrane separation has become an innovative and highly debated technology to perform hydrogen separation and purification.

Membranes may be defined as thin selective films capable of transporting one component more readily than other because of chemical or physical interactions. [27]

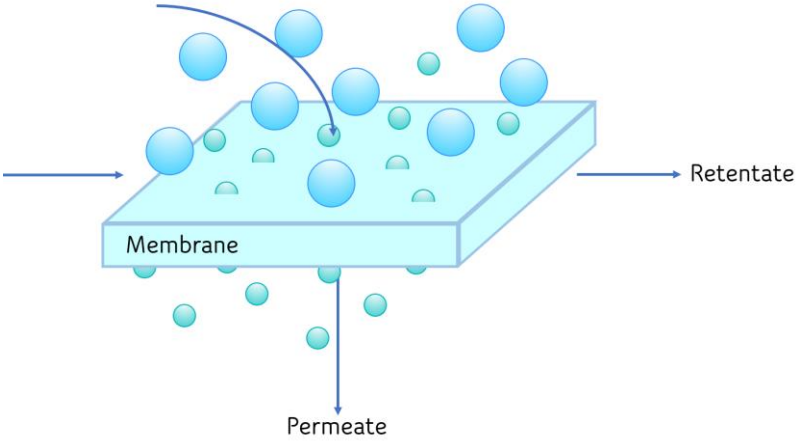

Figure 19, Gas separation membrane scheme

A gaseous stream is fed to the membrane and the driving force for the separation is the chemical potential gradient. [28] Thanks to the intrinsic selectivity of the membrane, the different components of the gaseous streams are separated: from one side species able to cross the membrane

will be collected in the permeate stream; on the opposite side, rejected molecules will be collected in the retentate stream.

Specifically, the crude hydrogen mixture is fed to the system: for instance, in the case of Hydrogen-selective membranes, hydrogen will be able to cross the membrane, being collected on the permeate side, whilst CO_2 will be rejected.

Membrane separation shows different advantages:

- No phase change or usage of chemical additives
- Easiness of the operation and scale up
- High efficiency
- Low energy requirements
- Compactness

Further details will be provided in the following chapter.

2. Membranes for gas separation

Thomas Graham was the first to propose the use of membrane technology in gas separation in 1829. He was then followed by Barrer to give the foundation of the modern gas permeation theory.

Membrane gas separation is a pressure-driven process through which different components of a gaseous mixture are separated by exploiting the intrinsic barrier properties of the membrane. Such technology has been introduced at the industrial level in 1980 to reduce the complexity of conventional separation techniques plants and increase the energetic efficiency of the process. Furthermore, it should be remarked that gas separation membranes do not require any phase change, meaning that the energy need of this technology is significantly lower than the other process mentioned in paragraph 1.3.

Several membrane typologies exist based on material, morphology, structure, and preparation method.

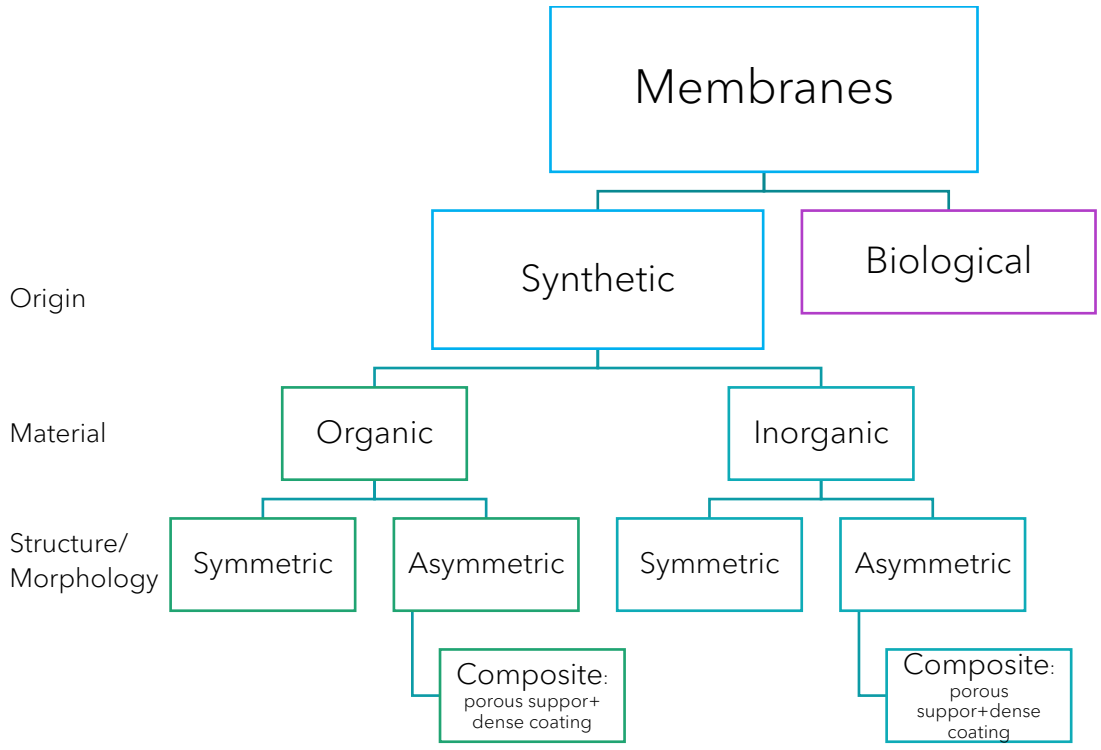

Figure 20, Classification of membranes

Membrane properties are dependent on several factors. Among the others, membrane material plays a significant role in determining the main characteristics and performances of the membrane; indeed, one can distinguish:

- Inorganic membranes are characterized by great thermal and chemical stability, and high mechanical properties. At the same time, their major problem is rigidity and fragility.
  Inorganic membranes can also be classified as:
  - Ceramic membranes
  - Metallic membranes
  - Carbon-based membranes
- Polymeric membranes show the major advantages in their versatility in terms of ease of processability, cost efficiency, and corrosion resistance. Being polymers, they will be limited to specific pressure and temperature ranges and lower chemical stability, as drawbacks.
- Hybrid membranes or mixed matrix membranes (MMM) are aimed to combine the advantages of polymeric membranes with the performances of inorganic ones.

2.1 Modules

Aiming to extend the use of membrane on an industrial scale, large membrane areas are required. Thus, membranes need to be packed in units called modules. Membrane modules are the basic building blocks in a membrane separation system.

The feed gaseous mixture is characterized by a certain composition and flowrate that will change inside the module as a function of distance. In the end, the feed stream is separated into permeate and retentate streams. Module designs are grouped in two basic types of membranes: flat and tubular. Flat membranes include plate-and-frame and spiral-wound modules; whilst tubular ones comprise tubular, capillary and hollow fiber modules. [27]

Among these modules, spiral-wound and hollow fibers are the most common.

2.1.1 Spiral wound

In the spiral wound modules, two flat sheets are sealed together and separated by a spacer to maintain a gap and to promote turbulence. In the end these sheets are rolled into a spiral format where the permeate is collected from a central channel. The permeate flow is a cross flow: the feed flows through the channel spacer, just certain molecules will be able to cross the membrane being collected at the center, whilst the other ones will be collected at the end of the tube as retentate.

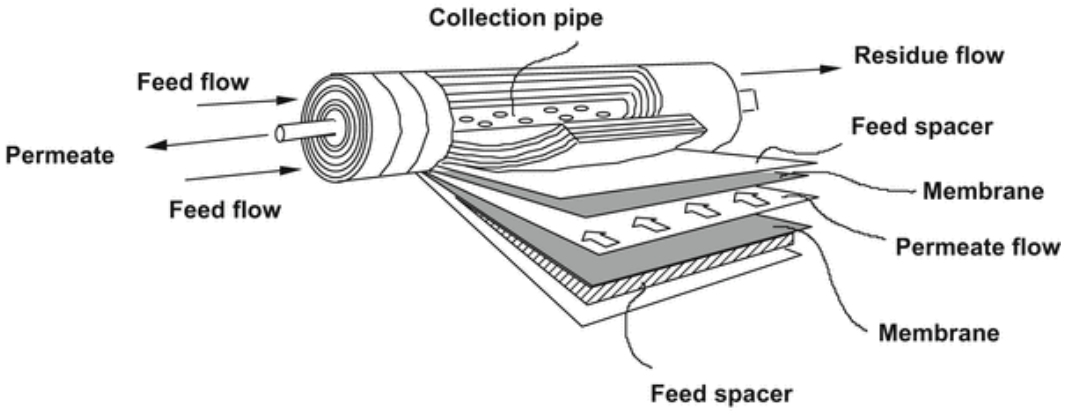

Figure 21, Spiral wound module [27]

Spiral wound configuration may be beneficial when penetrant fluxes are higher because pressure drop and mass transfer can be tuned by selecting a proper spacer. Moreover, the packing density is about 300-1000 m^2/m^3, so it is quite high even if it is strongly dependent on the channel height.

2.1.2 Hollow fibers

Hollow fibers modules consist of a large number of these capillaries with a very small inner diameter; these fibers are self-supporting and are arranged in parallel in bundles with a synthetic resin at the ends.

In hollow fibers modules, two arrangements are possible:

- Inside out: the feed solution enters the system shell-side and permeate is collected outside of the capillaries, still shell-side.

- Outside in: the feed solution enters the system shell-side, but permeate is collected tube-side. Smaller molecules will be able to cross the hollow fibers and they go inside these little tubes, whilst other molecules will exit shell-side.

Hollow fibers module allows the highest packing density possible, 30000 m^2/m^3.

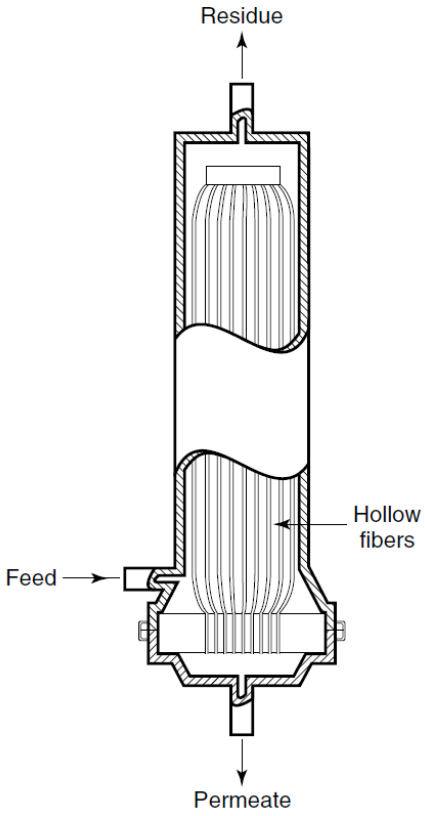

Figure 22, Hollow fibers module scheme [29]

In gas separation, generally the outside-in configuration is used because it avoids high pressure losses inside the fiber. The typical lumen diameters are 50-200 μm. One of the main limitations is about the obtainment of too high pressure drops that can affect the membrane performance, but as a benefit, hollow fibers are the best choice for packing density, their cost per square meter of membrane is usually lower than other configurations and hollow fibers are self-supporting guaranteeing ease of manufacturing and replacement operation.

	Tubular	*Plate-and-frame*	*Spiral-wound*	*Capillary*	*Hollow fiber*
Packing density	Low	---------->			Very high
Investment	High	---------->			Low
Fouling tendency	Low	---------->			Very high
Cleaning	Good	---------->			Poor
Membrane replacement	Yes/No	Yes	No	No	No

Table 3, Comparison of membrane configurations [30]

The idea of exploiting all the advantages of polymeric materials in gas separation dates to the late 1800s. However, it is only from 1950 onward that polymeric membranes began to be under the concrete attention of scientific and industrial research. [27,29]

2.2 Polymeric membranes

Polymers are macromolecules composed of small repeating units called monomers. The polymeric structure may be semicrystalline or amorphous: crystallinity is a long-range order in the three-dimensional polymeric structure and the amount of crystallinity influences the properties of the final material. In most cases, gas separation polymeric membranes make use of amorphous glassy polymers because semicrystalline materials present extremely low permeability for all the gaseous penetrants. Amorphous materials are characterized by the glass transition temperature, which is a parameter used to describe the transition due to thermal effect [31].

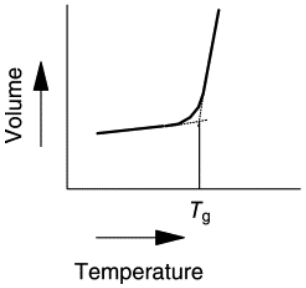

Figure 23, Volume change as a function of temperature for amorphous polymers [32]

The glass transition temperature, T_g, is related to the mobility of the polymeric chain. Below T_g, the polymer has a quite rigid structure, and it is in the glassy state, showing a solid-like behavior; above T_g, the so-called rubbery state shows a liquid-like behavior with quite good mobility of the polymeric chains. Glassy polymers are frozen in a non-equilibrium structure, and they present a rigid polymeric chain; instead, rubbers are equilibrium phases that can be approached thermodynamically as liquids; indeed they show good mobility and high values of diffusion coefficients for all the gaseous species. [33]

The distinction between the rubbery and glassy phases of polymers is crucial because their different properties will reflect on membrane performances.

From a general point of view, the flux across a membrane can be approached thermodynamically: [27,28,29]

$$J_i = -L_i \left(\frac{d\mu_i}{dx_i}\right) \qquad (2)$$

Where L_i is a proportionality factor between the flux J_i and the chemical potential driving force μ_i. In the case of gas separation processes, μ_i includes only concentration and pressure as driving forces.

$$d\mu_i = RTdln(\gamma_i c_i) + v_i dp \qquad (3)$$

γ_i is the activity coefficient, c_i the molar concentration, v_i the molar volume and dp the pressure gradient.

Such relation applies to the solid membrane which is an incompressible phase and to the permeant gases, being instead compressible.

$$\mu_i^i = \mu_i° + RTln(\gamma_i c_i) + v_i(p - p_i°) \qquad (4)$$

$$\mu_i^c = \mu_i° + RTln(\gamma_i c_i) + RTln\left(\frac{p}{p_i°}\right) \qquad (5)$$

μ_i^i is the chemical potential of the incompressible phase, μ_i^c the one of the compressible gas; $\mu_i°$ refers to the chemical potential of the pure component i, at the reference pressure $p_i°$; in the

equation of compressible phases the molar volume $v_i = \frac{RT}{p}$. However, the chemical potential should be the same at the equilibrium conditions: for this reason, the reference pressure is taken as the saturation vapor pressure of component i.

$$\mu_i^i = \mu_i° + RTln(\gamma_i c_i) + v_i(p - p_{i,sat}°) \qquad (6)$$

$$\mu_i^c = \mu_i° + RTln(\gamma_i c_i) + RTln\left(\frac{p}{p_{i,sat}°}\right) \qquad (7)$$

From this point onward, the gas transport mechanism depends on whether the membrane is porous or not. Indeed, one can distinguish:

- Porous membranes, whose dimension of pores is the key point. If the pores of the membrane are too large, no separation will occur. If the porosity is in the order of a micron, then the Knudsen diffusion mechanism takes place. Then, if the dimension of the pores is in the order of an Angstrom, the molecular sieving effect will be seen, and it will be needed to consider diffusion in the gaseous phase of pores together with diffusion of the adsorbed penetrants on the surface of pores. [29] The basic idea is that molecules larger than the pores' dimension will be rejected from the membrane; small molecules whose diameter is lower than the pores will pass through.

  The transport mechanism is the so-called pore-flow model. It is based on the presence of a pressure gradient within the membrane, whereas concentration is uniform.
- Dense membranes: membranes without porosity where the theoretical model that is taken as a reference is the solution-diffusion theory. There is no pressure gradient across the membrane, it is a concentration gradient to drive the process.

  The process can be analyzed by considering two phenomena:
  - Solution, where temperature, pressure, and composition of the fluids on the two sides of the membrane will determine the concentration of diffusing species in equilibrium with the fluid.
  - Diffusion, where dissolved molecules will permeate in the bulk of the membrane. Inside the polymeric network, there are microcavities between polymer chains

representing the so-called free volume. Depending on their dimensions, molecules are able to diffuse throughout these microcavities.

Gas separation is performed by using dense membranes. This is the reason why in the following chapter there will be a more detailed explanation of the transport mechanism in dense polymers.

Transport in dense polymeric phases is governed by the so-called solution diffusion mechanism. In 1968 Crank and Park proposed a 5-step structure for this process. [34]

1. Diffusion through the upstream boundary layer.
2. Sorption of the penetrant gas by the membrane
3. Gas diffusion in the bulk of the membrane
4. Downstream desorption
5. Diffusion out of the downstream boundary layer

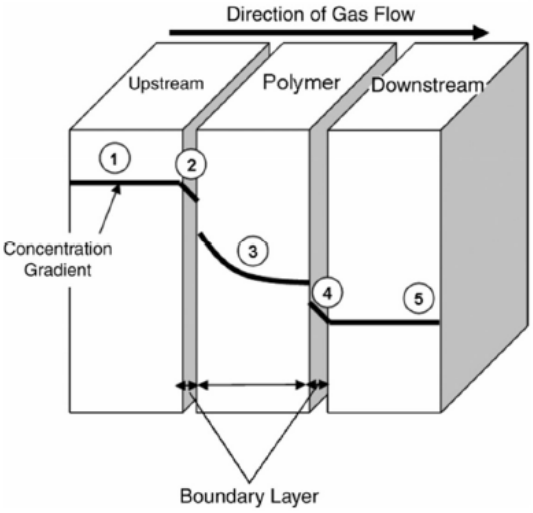

Figure 24, Concentration profile and schematization of solution-diffusion mechanism across a dense polymeric film [34]

In the solution diffusion model, it is assumed that, within the membrane, the pressure is constant, therefore the transport mechanism can be described by using Fick's law.

$$\frac{\partial c}{\partial t} = D \cdot \nabla^2 c \qquad (8)$$

Where D is the diffusion coefficient, assumed constant in a wide concentration range.

$$\frac{\partial c}{\partial t} = D \cdot \frac{\partial^2 c}{\partial x^2} \qquad (9)$$

To solve the problem, it is necessary to couple this equation with the proper boundary and initial conditions.

On the two sides of the membrane, concentration can be considered as the equilibrium concentration. At the initial time, the concentration of component i in the membrane is constant and typically equal to 0.

$$c(x = 0, t) = c_u \qquad (10)$$

$$c(x = l, t) = c_d \qquad (11)$$

$$c(x, t = 0) = 0 \qquad (12)$$

At the initial times, a transient can be observed: at time zero, the equilibrium concentration is present just at the upstream interface, in all the other regions concentration is null. Then, diffusion starts, and the concentration profile increases up to reach the steady state condition.

At the steady state:

$$D \cdot \frac{\partial^2 c}{\partial x^2} = 0 \rightarrow \frac{d^2 c}{dx^2} = 0 \qquad (13)$$

$$x = 0 \quad c(x) = c_u \qquad (14)$$

$$x = l \quad c(x) = c_d \qquad (15)$$

Solving the problem, the following concentration profile is obtained:

$$\frac{c(x) - c_u}{c_d - c_u} = \frac{x}{l} \qquad (16)$$

It means that there is a linear concentration profile within the membrane.

By using the first Fick's law, the flux is constant within the membrane:

$$J_i = D_i \cdot \frac{\partial c}{\partial x} = D_i \frac{c_{i,u} - c_{i,d}}{l} \qquad (17)$$

Concentration may be rewritten thanks to the equilibrium condition:

$$c_i = S_i \cdot p_i \qquad (18)$$

This relation defines S_i as the solubility coefficient of component i in the membrane; p_i is instead the partial pressure of gas outside the membrane.

The flux becomes:

$$J_i = D_i \frac{S_{i,u} p_{i,u} - S_{i,d} p_{i,d}}{l} \qquad (19)$$

Two particular cases are commonly considered:

- The solubility coefficient is a constant:

  $$J_i = D_i S_i \frac{p_{i,u} - p_{i,d}}{l} \qquad (20)$$

- The downstream partial pressure is much smaller than the upstream one:

  $p_{i,d} \ll p_{i,u}, p_{i,d} \to 0$

  $$J_i = D_i S_i \frac{p_{i,u}}{l} \qquad (21)$$

In both cases, there is a proportionality coefficient $D_i S_i$. This can be used to define a new quantity called permeability:

$$\mathbb{P}_i = D_i S_i \qquad (22)$$

Therefore, permeability is strictly related to diffusivity and solubility coefficients. The diffusivity coefficient is a measure of penetrant mobility inside the membrane; the solubility coefficient is a thermodynamic parameter that accounts for the dissolution of the penetrant in the polymeric membrane.

As already mentioned, the solution-diffusion mechanism provides that transport phenomenon is split into diffusivity-driven and solubility-driven transport. Permeation properties are strongly affected by the polymeric structure. Researchers tried to find a quantitative correlation between these two aspects, introducing the well-known fractional free volume.

$$FFV = \frac{v - v_0}{v} \qquad (23)$$

Where v is the specific volume of the polymer and v0 is the volume occupied by the molecules. In the polymeric structure, there are small spaces between the molecules standing for this free volume.

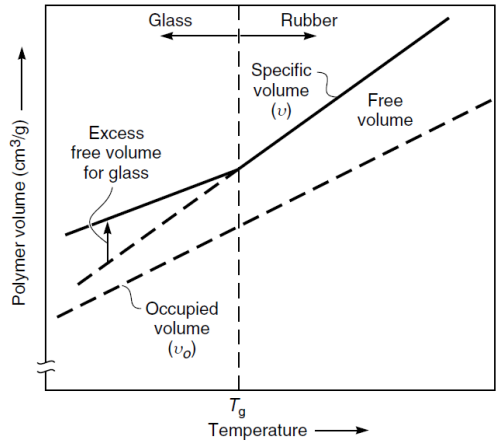

Figure 25, Free volume as a function of temperature [29]

Free volume is dependent on temperature. Starting from $T>T_g$, the polymer is in the rubbery (or molten) state, and it possesses a certain free volume deriving from the amorphous structure. By decreasing the temperature, also the free volume will diminish, following a roughly linear relationship. The expectation is that, if one further lowers the temperature going below the T_g, the free volume will continue to decrease following the same trend as before. Actually, this is not the case: in the glassy state chain mobility is hindered and the free volume is frozen in the structure. This non-equilibrium condition is indeed characterized by an excess free volume. [29]

An estimation of the free volume provides information about the available space for gaseous penetrant diffusion within the membrane. The larger the gaseous molecules, the higher the sensitivity to the free volume, and this is the basis for a dimensions-based selective process.

2.3 Performance parameters: permeability & selectivity

The effectiveness of gas separation technology is based on two main parameters: permeability and selectivity.

Permeability is the intrinsic capacity of the membrane to accept a certain flux across itself. From a numerical point of view, it can be described as the flux normalized in terms of pressure.

$$\mathbb{P}_i = \frac{J_i}{p_{i,u} - p_{i,d}} \cdot l \qquad (24)$$

Having a membrane with high permeability means that the required area to accomplish a certain objective will be low. Ultimately, since productivity is proportional to the area exposed to the feed stream, permeability may be seen as a quantification of the productivity of a given gas separation process. Permeability may be also seen as an intrinsic parameter, it is normalized, therefore it points out the invariancy with respect to geometrical features (i.e., thickness and membrane area) and driving force. [27]

The accomplishment of high efficiency in a membrane-based process is not only related to the amount of achievable flux through the film; the main aim of the process is to have a selective process where the different components are separated. The membrane selectivity is defined as follows:

$$\alpha_{i,j} = \frac{y_i^d / y_j^d}{y_i^u / y_j^u} \qquad (25)$$

where y is the molar fraction of species i and j, d stands for the downstream side, and u is the upstream side of the membrane. Under the assumption that downstream pressure is close to zero, the selectivity can be rewritten:

$$\alpha_{i,j} = \frac{y_i^d / y_j^d}{y_i^u / y_j^u} = \frac{1}{y_i^u / y_j^u} \frac{\mathbb{P}_i}{\mathbb{P}_j} \frac{p_i^u - p_i^d}{p_j^u - p_j^d} \cong \frac{\mathbb{P}_i}{\mathbb{P}_j} \qquad (26)$$

Ultimately, it is possible to define the ideal selectivity of the membrane as the ratio between the permeabilities of the different pure components. The higher the selectivity, the better the separation process; therefore, selectivity may be identified as a parameter representing the efficiency and effectiveness of the separation process.

Actually, the ideal selectivity is only an estimation of the real selectivity because the presence of a mixture characterized by the copresence of different gases can lead to effects given by the mutual interactions between the species. [33]

Two factors contribute to the overall selectivity of the membrane: diffusivity selectivity and solubility selectivity.

$$\alpha_i = \frac{\mathbb{P}_i}{\mathbb{P}_j} = \frac{D_i}{D_j}\frac{S_i}{S_j} = \alpha_D \alpha_S \qquad (27)$$

The first factor, diffusivity selectivity, is the ability of the membrane to discriminate penetrants thanks to a difference in diffusivity factors, so it is related to the shape and size of the gaseous feed stream. Solubility selectivity is, instead, based on solubility and it is influenced by the condensability and the affinity between the penetrant and the polymer. Condensability refers to the ability of a gas to be converted into a liquid through cooling or compression and it is usually quantified as critical temperature or boiling point. More precisely, solubility increases with the condensability of the gas.

In the specific case of hydrogen separation from carbon dioxide, it is possible to have hydrogen-selective membranes or CO_2-selective membranes.

Hydrogen-selective membranes are designed to maximize the flux of hydrogen on the permeate side. This can be achieved by basing the separation process on diffusivity: hydrogen has a low critical temperature predicting low solubility, and one of the smallest kinetic diameters (2.89 Å). CO_2 is instead a larger molecule, with a kinetic diameter of 3.3 Å: it is the kinetic diameter difference to drive the separation process. On the other hand, CO_2-selective membranes rely on thermodynamic factors, and the separation mechanism is based on the higher solubility of carbon dioxide with respect to hydrogen.

Gas properties	*H_2*	*CO_2*
Molecular weight [g/mol]	2.02	44.01
Kinetic diameter [Å]	2.89	3.30
Critical temperature T_c [K]	33.2	304.1
Density at 0°C and 1 atm (g/L)	0.0899	1.977

Table 4, Properties of H_2 and CO_2 [35]

In polymeric materials, permeability is strongly affected by the glass transition temperature that, as already mentioned, is related to the chain mobility; indeed, it is quite easy for gases to permeate

through rubbery amorphous regions that are characterized by more available energy for macromolecular motion, rather than in glassy ones. This explains why permeability is typically higher in rubbery polymers. [27]

Generally, rubbery polymers show high solubility selectivity, whilst glassy polymers are more sensitive to diffusivity selectivity. Indeed, in the glassy state polymers are intrinsically more selective towards the size and shape of penetrants: having such low chain mobility, the molecular size difference of the gases will influence the relative mobility in a relevant way. [36] This is the reason why it is preferable to choose glassy polymers to produce a hydrogen-selective membrane and a rubbery matrix for a CO_2-selective process. [37]

ADVANTAGES	DISADVANTAGES
H_2-SELECTIVE MEMBRANES	
Higher thermal stability	Need of permeate recompression
Tolerance towards higher compression stresses	Deterioration in the presence of plasticizing agents
Higher H_2 purity level	
CO_2-SELECTIVE MEMBRANES	
No need for permeate recompression	Low thermal stability
No side effects due to the presence of plasticizing agents	Low compression resistance
	Low condensability impurities may remain in the retentate stream

Table 5, Comparison between H_2-selective and CO_2-selective membranes [35]

2.4 Robeson upper bound

Polymeric membranes have been under the attention of researchers thanks to their versatility, easiness of processability, relatively minimal cost, and good mechanical strength. As explained in the previous chapter, the best membrane should be characterized by high permeability and high selectivity, simultaneously. Unfortunately, Robeson in 1991 demonstrated that the main drawback of polymeric membranes for gas separation was the inability to reach simultaneously high permeability and selectivity. In this regard, Robeson collected all the polymeric membranes data available in the literature to build a log-log plot showing the tradeoff line that was then called "Robeson upper bound."

$$P_i = k\alpha_{i,j}^n \qquad (28)$$

Where P is the permeability, α the selectivity, and k and n are two experimental parameters.

Specifically, for H_2/CO_2 mixtures, the first upper bound was presented in 1994 and then revisited in 2008. [38]

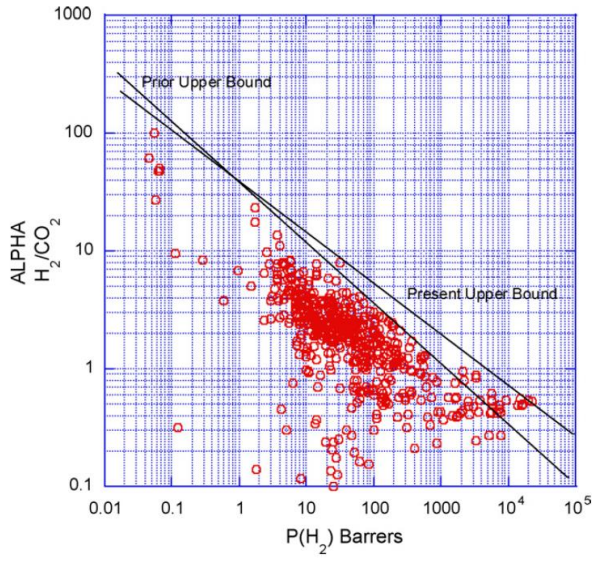

Figure 26, Robeson Upper Bound [38]

H_2/CO_2	k [Barrers]	α
1994	1200	-1.9363
2008	2570	-2.302

Table 6, Parameters of Robeson Upper Bound

The shift from the first upper bound is mainly due to the perfluorinated polymer data that were not available in the literature in 1994.

Glassy H_2 selective systems show a large advantage in higher thermal resistance so that they can be used at higher operating temperatures.

The effect of temperature on perm-selectivity can be explained accounting for the dependence of diffusivity and solubility on temperature itself. Rowe et al. report a view of diffusion as an Arrhenius-like temperature-activated process [39].

$$lnD_a = lnD_{0,A} - \frac{E_{D,A}}{RT} \qquad (29)$$

Where D_0 is a pre-exponential factor, $E_{d,A}$ is the activation energy, R is the universal gas constant, and T is the absolute temperature. This relation is valid for broad temperature ranges. Activation energy is defined as the energy needed to move the polymeric chain such that molecules can pass through the material. Unsurprisingly, activation energy depends on the size of molecules: the larger the molecules, the higher will be the activation energy; but there is also a strong correlation between activation energy and pre-exponential factor.

$$lnD_{0,A} = a\frac{E_{D,A}}{RT} - b \qquad (30)$$

This is quite relevant because it indicates that there is a strong dependence of diffusivity on temperature. On the other hand, it is needed to consider the effect of temperature on solubility. Solubility is related to the penetrant condensability, and it depends on temperature following a Van't Hoff-like equation:

$$\frac{d(lnS_A)}{d\left(\frac{1}{T}\right)} = -\frac{\Delta H_{S,A}}{R} \qquad (31)$$

Where S_A is the solubility coefficient, $\Delta H_{S,A}$ is the heat of sorption: solubility decreases as the temperature increases. In the end, both permeability and selectivity may be seen as dependent on temperature as a result of the two contributions of diffusivity and selectivity dependence on temperature.

Permeability in polymers is an activated energy process. Far below or well above T_g, gas permeability may be written referring to an Arrhenius like behavior: [33,27]

$$P = D_0 S_0 \exp\left(-\frac{\Delta H_{S,A} + E_{D,A}}{RT}\right) = P_0 \exp\left(-\frac{E_p}{RT}\right) \qquad (32)$$

Where E_p is the activation energy of permeability, R the gas universal constant, T the temperature expressed in Kelvin and P_0 is a pre-exponential factor. [40,27]

For small gases it is the diffusion process to determine the permeability, instead for larger molecules the two effects of solubility ad diffusivity are opposing and their behavior is more complex.

This phenomenon is interesting because Rowe et al. demonstrated that, for H_2/CO_2, the Robeson upper bound is shifted to higher selectivity with increasing operating temperature. [39] Indeed, CO_2 solubility strongly decreases with increasing temperature, so increasing the temperature means decreasing the solubility selectivity of the process because it is the solubility selectivity to dominate the temperature effect on the upper bound. [41]

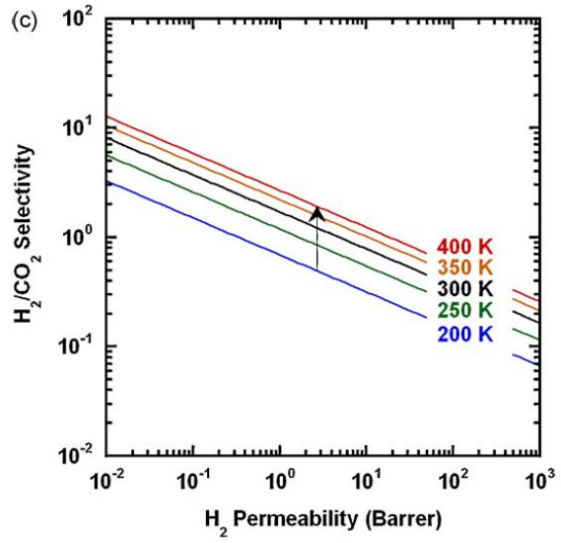

Figure 27, Effect of temperature on Robeson Upper Bound [39]

Nevertheless, the Robeson upper bound remains a major problem and achieving high performance gas separation membranes with both high permeability and selectivity is a great challenge. A potential solution to overcome this trade-off involves the development of mixed matrix membranes.

Polymeric membranes are of particular interest thanks to their economical and practical advantages, such as easiness of processability. The addition of fillers can increase the perm

selectivity of membranes by creating additional selective transport pathways for the gas molecules. This kind of membranes integrate polymeric material with organic and/or inorganic filler to achieve benefits from both components. [42]

Among MMMs, one can distinguish:

- Symmetric nanocomposite membranes, where there is a uniform dense composite film that is selective. They are the most frequently produced MMMs for the ease of fabrication.
- Asymmetric nanocomposite membranes, characterized by the presence of a dense thin selective layer (<1μm) deposited onto a non-selective support layer. Typically, it is the selective skin to contain nanofillers. Their morphology allows a strong reduction in the overall membrane resistance since the selective layer is very thin.

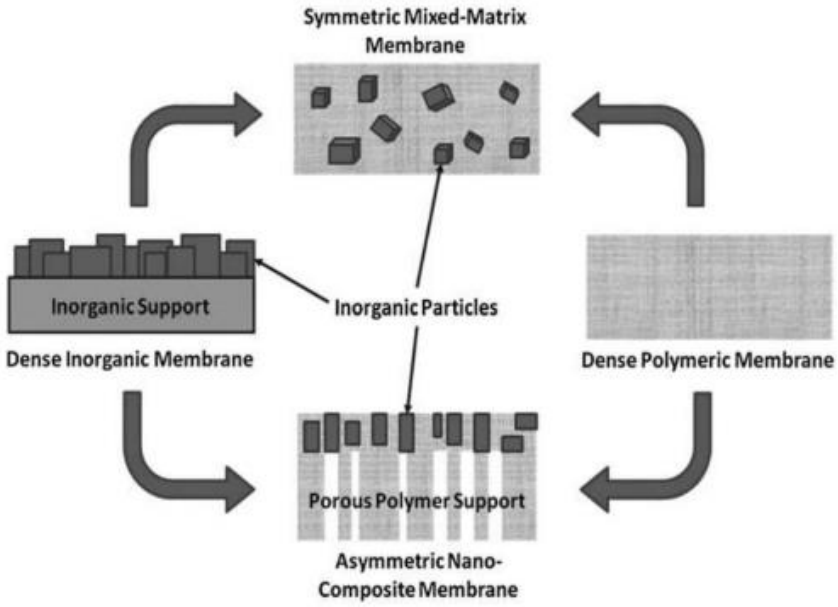

Figure 28, Possible inorganic filler dispersion [43]

Nanofillers can be classified according to their dimensions: 1D nanomaterials such as nanotubes, nanorods and nanowires; 2D nanomaterials like graphene, nanolayers and nanofilms with plate-like shape and 3D nanomaterials including spherical and cubical nanoparticles. [43,44]

The utilization of ordered nanomaterials has the potential to enhance membranes performance. These fillers manage to increase the resistance to fouling and degradation, thereby improving the

overall stability of the membrane. Due to their high surface area-to-volume ratio, they can expand the membrane available surface area, which essential for increasing productivity. Additionally, these oriented materials can be engineered to have specific physical and chemical properties, which can make the membrane much more selective. As a result, nanometric fillers play a crucial role in exceeding the Robeson upper bound.

To meet the productivity and high selectivity requirements of an industrial-scale membrane module, developing multilayered membrane is a feasible solution. Furthermore, multilayered membranes are applicable to both glassy and rubbery polymers and various deposition techniques can be used to introduce the selective multilayer, making the fabrication method versatile. [44]

2.5 Low dimensional materials

Low-dimensional materials (LDM) can be defined as materials with atomic dimensions. LDM have been under the attention of researchers in all the membrane separation processes, but these materials are particularly attractive for sub-nanometer separations such as water desalination and gas separations which are the most expensive processes. In gas separation, LDM promise to increase permeability thanks to their incredibly low thickness without having a negative effect on selectivity, but on the contrary, improving it.

LDM may be used to produce nanostructured materials, which are defined as those materials containing structural elements in the order of nanometers.

As of now, among all the materials that have been used in MMM, graphene-based materials are defined as rising stars as membrane materials thanks to their very small thickness, high mechanical strength, and high stability.

3. Graphene-based materials

3.1 Graphene

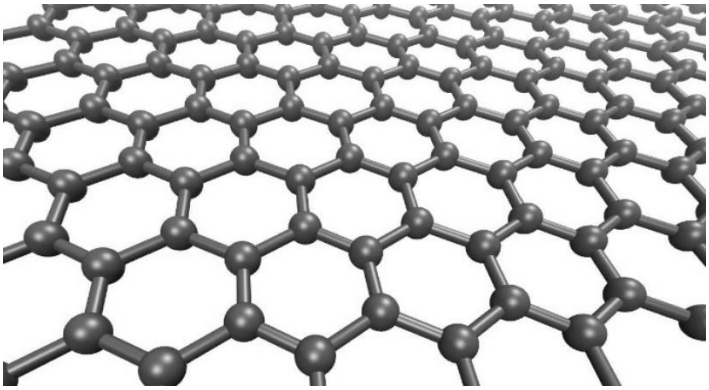

Figure 29, Graphene structure [45]

Graphene is a 2D material, officially discovered in 2004 by Geim et Novoselov who also won the Nobel Prize in 2010 for this. Graphene is a monolayer of sp2 hybridized carbon atoms arranged in a honeycomb structure. Until 2004 graphene was known, but no one had been able to isolate this material and demonstrate that it was possible to have a monoatomic layer stable material. The two Nobel prize winners managed to obtain graphene in a very simple way: using adhesive tape on bulk graphite they peeled off graphene layers and transfer them onto silicon dioxide on a silicon wafer. [46]

Graphene is almost transparent, but it has a very dense structure indeed it is almost impermeable also to the smallest substances such as helium. Even though it is the thinnest material known, it is still one of the strongest. Graphene has many interesting properties such as high specific surface area, strength, elasticity, and thermal conductivity for which it has captured the attention of the scientific community.

3.2 Graphene oxide

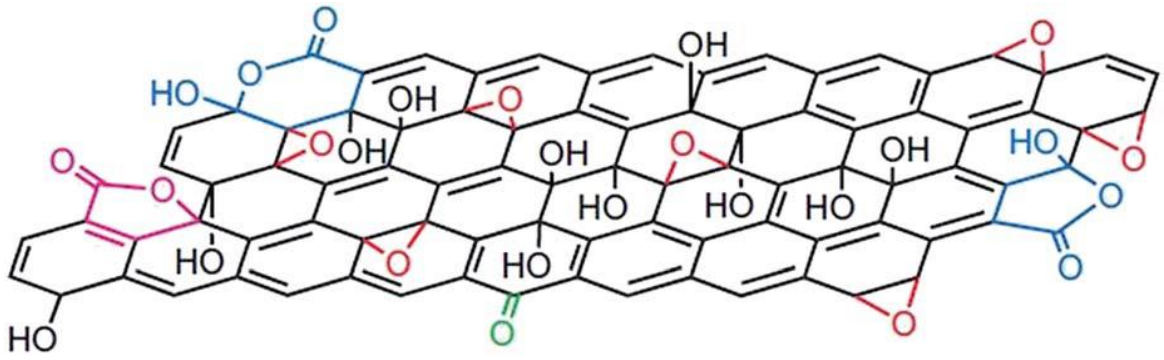

Figure 30, Graphene oxide structure [47]

The first official appearance of graphene oxide in scientific research dates back to 1859 when a British chemist, Brodie, oxidized graphite reacting it with potassium chlorate and fuming nitric acid. The product of the reaction was a substance containing carbon, hydrogen, and oxygen. This reaction produces a suspension of graphene oxide, indeed Brodie found out that GO could be dispersed in water, but not in acid environments so that its first name has been graphic acid. [48]

Brodie's discovery was then deepened in the following years and several other methods to oxidize graphite have been developed to overcome some limitations, such as long reaction time and release of toxic gases [47]. Staudenmaier in 1898 improved Brodie's method by adding the potassium chlorate at different times of the reaction and concentrated sulfuric acid to increase mixture acidity, thus reducing the reaction time. The product was a highly oxidized GO, but this process was hazardous because of the generation of explosive byproducts such as ClO_2. [48]

Hofmann in 1937 proposed an innovative method using concentrated nitric acid and potassium chlorate to oxidize graphite. The oxidation level was lower than that reached by Brodie, indeed it was found that there was an inverse proportionality between the concentration of nitric acid and the level of oxidation [49].

20 years later Hummers and Offeman developed another oxidation route by using potassium permanganate ($KMnO_4$), concentrated sulfuric acid (H_2SO_4), and sodium nitrate at low concentrations. This process avoids the production of ClO_2, but it is not an environment-friendly

method because nitrogen oxides are generated and evolve during the reaction. As a positive aspect, GO oxidation levels and reaction yields are very similar to the Brodie method. [49]

The C:H:O composition of the oxidative reaction results to be variable. It depends on the specific chemical process that is used and also on the variability of the raw material. In this respect, the most common source of graphite is flake graphite: its overall structural complexity is inherent in the natural source, indeed flake graphite is a mineral that needs to be purified from contaminants.

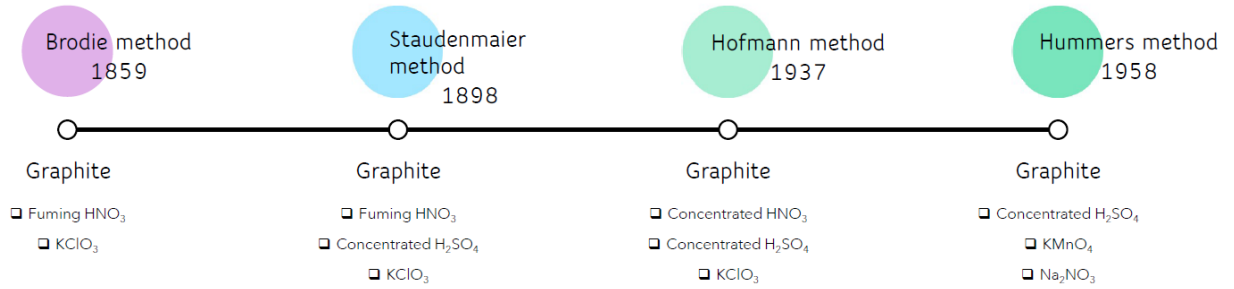

Figure 31, Graphene oxide production methods [47]

The final level of oxidation is a relevant parameter because it changes the properties of the material.

Ultimately, graphene oxide may be defined as one single layer of graphite oxide. Its structure is characterized by the presence of oxygenated functional groups enhancing graphene oxide processability. Furthermore, these groups are much easier to be functionalized and modified making graphene oxide to be a versatile material. Even macroscopically, it is possible to notice a change in color, from black to brownish yellow, as the degree of oxidation increases.

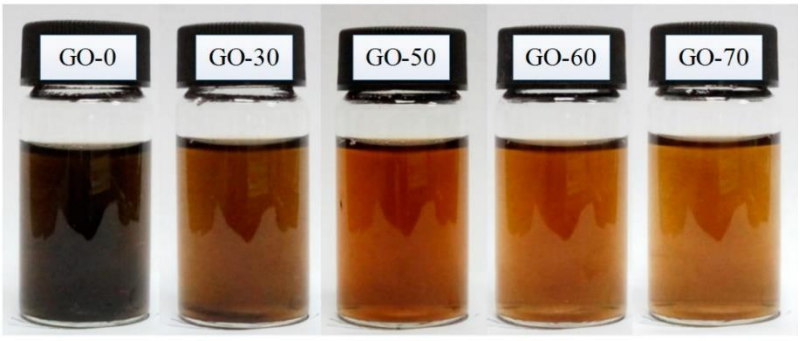

Figure 32, Change in color in graphene oxide due to the increasing degree of oxidation [50]

Clearly, differences are also evident by carrying out chemical analyses of the compound such as X-Rays Diffraction Analysis (XRD), Raman spectroscopy, and so on. An interesting point is that by increasing the oxidation level it is possible to have higher exfoliation reaching monolayers of graphene oxide after ultrasonication. [51] Moreover, also zeta potential is affected by the degree of oxidation: there is a linear increase of zeta potential measurements with the oxidation level. This can be explained by considering that a larger amount of electronegative functional groups is present on the GO nanosheets, due to the dissociation in the aqueous medium of acidic groups:

$$COOH \rightarrow COO^- + H^+$$

Furthermore, according to ASTM standards, higher zeta potential means higher stability for suspension and this is quite relevant when dealing with an aqueous suspension of GO. [52]

Still, also the distribution of functional groups and, thus, the precise structure of graphene oxide is strongly dependent on the extent of oxidation, and it is not possible to have a general univocal representation. [47] The most frequently used structure has been introduced in 1998 by Lerf and Klinowski. Graphene oxide is divided in two regions:

1. Region with aliphatic oxidized rings
2. Region with non-oxidized benzene rings

The amount of these two regions depends on the oxidation level of GO. [49]

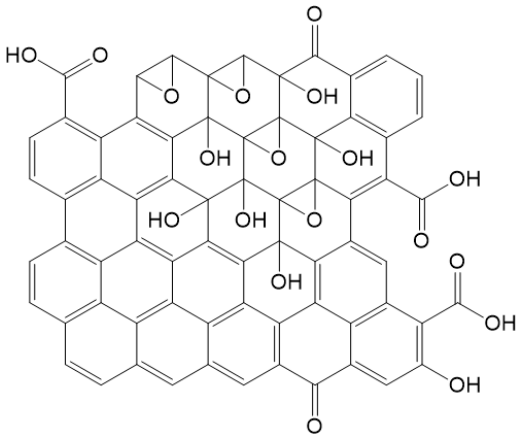

Figure 33, Lerf&Klinowski GO structure [49]

Even if GO composition and structure are still under debate, it can be seen as the oxidized form of graphene where oxygen is introduced through chemical oxidation. The different oxygen-containing functional groups that are present, such as epoxide, hydroxyl, carbonyl, and carboxyl groups make graphene oxide hydrophilic, versatile, and able to well interact with polymeric matrices. [53]

3.3 Graphene production methods

Graphene production is a challenging process whose aim is to obtain high-quality graphene at a large scale. The synthesis of graphene can be performed through top-down or bottom-up approaches.

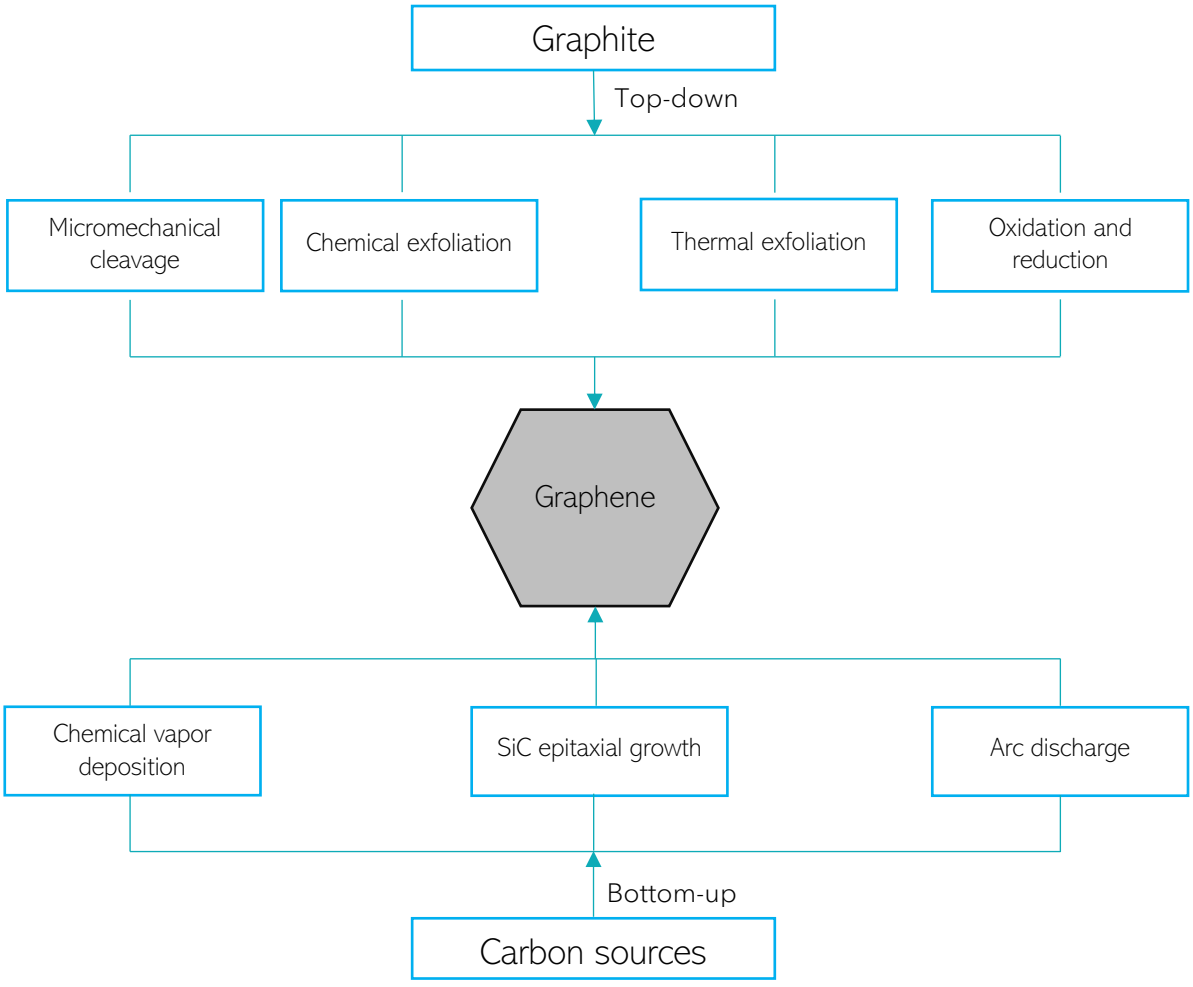

Figure 34, Graphene production methods

3.3.1 Top-down

In the top-down approach, a detachment of the graphene layer from graphitic structures takes place. Top-down methods are a variation of exfoliation, and they include micro-mechanical cleavage, chemical exfoliation, thermal exfoliation, and oxidation and reduction.

Micro-mechanical cleavage has been introduced by Novoselov et al.: it is a peeling process where graphite is peeled off using scotch tape; then, exfoliated layers are placed on a SiO_2/Si substrate. This technique is easy to be scaled at the industrial level and it guarantees high-quality graphene sheets. But, it is not efficient because the size and thickness of sheets are not tunable, so other methods have been developed.

Chemical exfoliation is possible by dispersing graphite in solvents with a surface energy similar to the one of graphite. Graphite is exfoliated into nanosheets thanks to the exposure to ultrasonication. The solvent is needed to avoid aggregation of particles. One of the most used solvents is N-methyl pyrrolidone (NMP) and, as shown by Coleman et al., one can produce single-layer graphene with this solvent. The main limitations of the technique are the low yield and concentration of graphene because, even in the presence of solvents, reaggregation of graphene sheets will take place sooner or later. The same exfoliation procedure can be performed without ultrasonication but in presence of a smart surfactant. The latter is able to delaminate graphene layers from graphite thanks to non-covalent interactions.

Chemical exfoliation is even possible after the oxidation of graphite. Graphite reacts with strong oxidants in the presence of a mixture of acids (usually nitric and sulfuric acid as in the Hummers method). Graphite oxide is obtained and it consists of oxidized graphene sheets stacked together. Since graphite oxide is soluble in water, a suspension is prepared and then it is exposed to ultrasonication: layers will acquire a negative charge and reaggregation will be avoided thanks to electrical repulsion. To achieve the goal of producing graphene, GO needs to be reduced and this is possible through microwave irradiation or using strong chemical reductants.

The chemical treatment with an oxidizing solution can also be carried out together with thermal exfoliation by means of very rapid heating. GO is easily formed thanks to the thermal expansion of graphite in presence of oxidizing solution.

3.3.2 Bottom-up

The bottom-up approach consists in depositing a graphene layer onto a substrate using hydrocarbons as sources of carbon: the main techniques are chemical vapor deposition (CVD), epitaxial growth on SiC, and arc discharge.

Chemical vapor deposition is one of the most common methods to produce graphene. The mechanism takes place on metal surfaces: for instance, carbon atoms come from a precursor, usually methane. Methane diffuses through the boundary layer; it is adsorbed on the substrate surface which can be a copper foil that catalyze the conversion in graphene. A chemical reaction occurs, the byproducts are desorbed, and they diffuse out of the boundary layer, whilst graphene will stay adsorbed on the surface. In the end, graphene sheets are transferred to a dielectric surface or other substrates. This technique allows to have square meters of graphene, and it is highly scalable, but the process is expensive because of energy consumption and the cost of the metal substrate.

Silicon Carbide, SiC, consist of silicon atoms is bonded each to four carbon atoms; each carbon atom is, in turn, attached to four silicon atoms. By heating up SiC crystals, silicon sublimates, and a graphene or graphite layer is formed. Graphene is then transferred by using a chemical reaction producing oxygen peroxide. The latter intercalates between SiC and graphene causing delamination. SiC wafers are costly and, since very high temperatures (1000-1500°C) are required, also the energetic aspect represents a drawback. On the other hand, the number of layers of graphene can be controlled by tuning process parameters and the quality of graphene can be very high.

The arc discharge is another production method for graphene. Graphite electrodes are used, and they are placed a few millimeters apart. Direct current is generated and, under an inert gas atmosphere (such as high-pressure hydrogen or helium), discharge occurs, plasma is generated and some carbon evaporates. Then, soot is produced and it deposits on the chamber walls in the form of graphene. Arc discharge allows the production of high-quality graphene and it does not require any metal catalyst, but impurities may be present leading to a poor yield of the process. [54]

4. Graphene-based membranes

As for what concern graphene-based membranes, two main categories are available:

- Single layer nanoporous graphene
- Multilayered graphene-based membranes

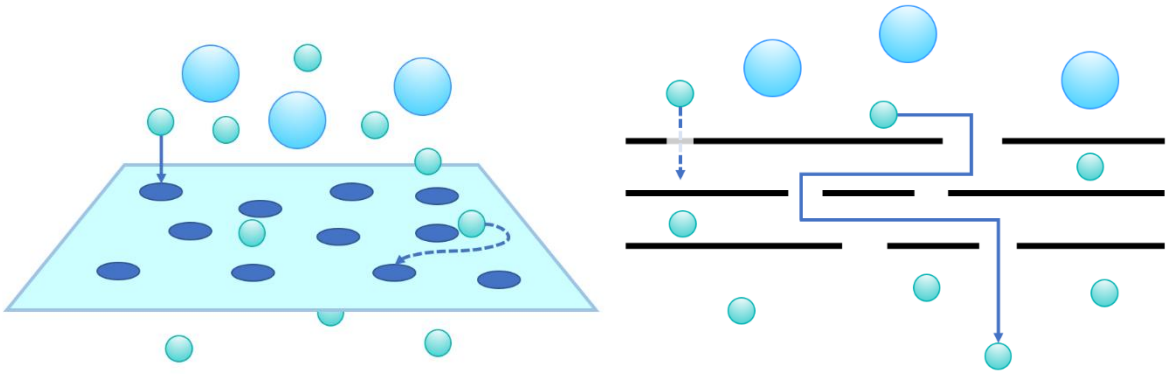

Figure 35, Nanoporous graphene membrane on the left; multilayered graphene-based membrane on the right

A single graphene sheet is, indeed, impermeable to all gases: that is the reason why pores need to be generated onto a sheet of graphene in order to have the passage of some specific molecules. On the other hand, graphene is not so reactive and processable: to be assembled in a multilayer it should be functionalized to have interaction between the different sheets.

4.1 Porous graphene film

The basic idea behind the production of porous graphene film is the possibility of drilling holes in the graphene layers. The process ends up in the creation of pores that, from one side increase the permeability of the film and, on the other hand, suitable selectivity can be achieved by tuning the dimension of pores and making use of the sieving mechanism.

The first study that reports on nanoporous graphene films dates back to 2008 thanks to Liu et al. from Columbia University: they managed to make pores on the graphene surface by using oxidative etching. Graphene was encapsulated into a mullite tube; the tube is then inserted in a furnace where it is invested by a gaseous mixture of oxygen and argon at high temperature and atmospheric

pressure: depending on the flow rate of the gas, one can tune pores dimensions in a range from 0 to tens of nanometers. [55]

Another technology that allows the creation of pores is focused electron beam irradiation making use of a Scanning Electron Microscope or Transmission Electron Microscope. The focused electron beam bombarded the graphene film and stable pores are generated. Drndic et al used a TEM at room temperature as the electron-beam source: generated nanopores are stable, but they usually show a concentric ring-like structure that is probably due to the introduction of defects because of the electron irradiation. [56] Zhang et al. used instead a SEM with a low-energy electron beam together with nitrogen ions. Nitrogen gas molecules are ionized by the electron beam; graphene reacts with nitrogen ions and the product of this reaction is removed from the surface of graphene causing the formation of a small pore. The reaction proceeds with the edge of the pore as a preferential site to react with nitrogen ions and the dimension of the pores increases. In this way, one can obtain very well-defined pores, but it would be a difficult challenge to scale up such technology at the industrial level. [55,56]

Other researchers used ion beam irradiation and they managed to obtain a nanoporous graphene sheet with proper dimensions, small pores, and quite good density of pores. Bell and coworkers reported that it was possible to create very precise pores with helium ions using a microscope for lithography. [55,57]

An additional strategy is plasma etching and it can be performed by using oxygen or hydrogen. Yang et al. used hydrogen plasma to hydrogenate the graphene carbon atoms: methane is generated and it is expelled giving rise to nanopores. This technique allows good tunability of hole dimensions and it is applicable to large areas. [58]

Koenig et al. used ultraviolet-induced oxidative etching to create very small pores in a large area. Ultraviolet irradiation manages to ionize gas molecules, oxygen-rich radicals are generated and, therefore pores are produced onto the graphene surface. Wide pore distribution and small pore density are the main drawbacks. [58]

Perforation can also be carried out by means of a chemical method. Potassium permanganate, hydrogen peroxide, nitric acid, and phosphoric acid can create pores in GO sheets. This technique

is beneficial from an economic perspective because it has relatively low cost and it is scalable, but there is limited control over pore sizes and distribution. [59]

Technique	Pore dimensions [nm]	Advantages	Disadvantages
Focused electron beam irradiation	2-40	Well defined dimensions of pores	Small areas
Ultraviolet induced oxidative etching	<10	Possibility to treat large areas	Low density of pores
Ion bombardment and chemical oxidative etching	0.40	Tunable dimensions of pores and large areas	Low porosity
Oxygen plasma etching	0.5-1	Tunable dimensions of pores	Low porosity
Focused ion beam	7.6-1000	Well defined dimensions of pores	Small areas

Table 7, Summary of pore generation techniques

Although numerous different techniques have been proposed and studied, the main limitation of nanoporous graphene membranes still remains in the dimensions of pores, in case the target is the separation of gas molecules: in order to have an effective separation of hydrogen from carbon

dioxide, indeed, pores should be in the order of an Angstrom, instead, as it is possible to notice from the table above, only nanometric pores are obtained.

4.2 Multilayered membranes

Thin-layered membranes are the alternative to single-layer nanoporous graphene. In this case, it is not graphene to be directly involved in the preparation of membranes, but its derivative graphene oxide. Thanks to its lower inertness, which is due to the presence of oxygen containing functional groups, graphene oxide can interact with other species by creating chemical bonds. Therefore, it can be arranged in multiple layers structures: GO sheets are positioned on top of each other.

4.2.1 Coating methods

The preparation of multilayer graphene-based membranes is possible by using several different deposition methods. Multilayer GO membranes may be classified in:

- Self-standing GO membranes, without a polymeric support
- Composite GO membranes: a polymeric membrane is used to support the GO multilayer.

Self-standing GO membranes can be obtained by the flow-directed assembly of GO sheets, in particular vacuum filtration, pressure-assisted filtration, but also solvent evaporation. These methods result in tightly packed interlocking sheets along the hexagons surface. [60]

Concerning the vacuum filtration method, a homogeneous suspension of GO is placed on filter paper, and, by a filtration system, the dispersion is vacuum-filtrated. As a result, a superimposed membrane on the filter is obtained. This composite membrane is transferred in a specific solvent that allows the separation of the graphene oxide film from the filter and a graphene oxide free-standing film is produced.

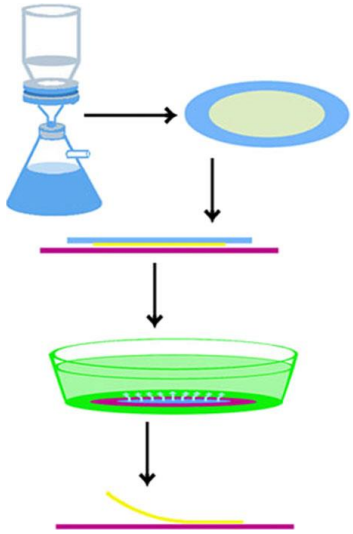

Figure 36, Vacuum filtration scheme [61]

The nanostructure of GO laminates is highly dependent on the driving force of the filtration.

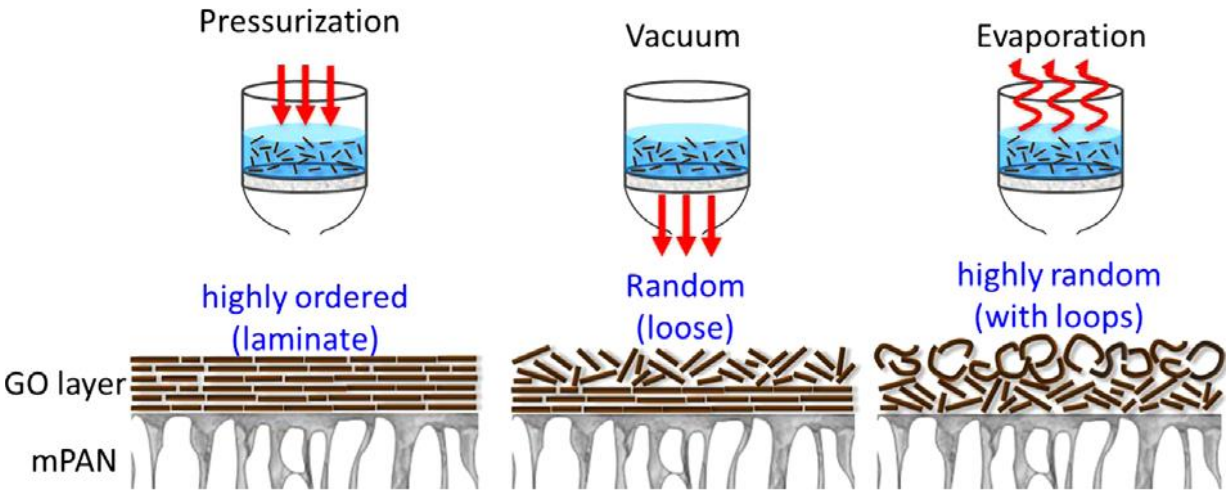

Figure 37, Comparison in the multilayered structure for Pressurization method, vacuum assisted method and evaporation method [60]

The surface roughness of the pressure-assisted filtration (PAF) results to be the smoothest, that of the membrane from evaporation-assisted filtration (EAF) is instead the roughest, and the vacuum-assisted filtration (VAF) one is in the middle. This is probably due to the fact that, in the PAF, the constant pressure ensures precise deposition in a highly ordered structure. In VAF the filter cake thickness increases and the filtration rate decreases with time so that the layers far from the filter

become more loosely packed. The application of a certain pressure as a driving force is needed to guarantee the formation of a compact multilayered structure. In the evaporation method, there is not a strong driving force for the filtration and a lot of environmental conditions influence the formation of the laminate, the latter indeed will be highly disordered. [62]

Composite membranes

Graphene-based composite membranes are characterized by the presence of a multilayer of GO placed on a polymeric support. The permselective performances of the membrane are guaranteed by the GO multilayer that is considered as a coating with respect to the polymer. In addition, graphene oxide makes a better adhesion to the polymeric matrix possible, thanks to the possibility of creating many diverse types of chemical bonding.

The coating should be:

- Highly permeable
- Highly selective toward the interested specie
- Thermally and chemically stable
- Cost-effective

The coating technique is fundamental in order to achieve good adhesion between the two parts and to obtain ultra-thin layers.

Thin film deposition techniques		
Interfacial deposition processes	Vapor deposition	Advanced deposition processes

• Colloidal solutions
  • Dip coating
  • Spin coating
  • Sol-gel
• Langmuir-Blodgett
	• Physical
	• Chemical
		• Atomic layer
		• Electrochemical
		• Electron-beam

Table 8, Deposition techniques

Casting is the oldest method to prepare polymer membranes and films. [63]

Solution casting is one of the simplest methods. Graphene-based material is dissolved in a solvent and the solution is then cast on the polymeric support. The drying is usually performed in an oven. This procedure is performed until the proper number of layers is achieved. Two limitations arise: it is difficult to obtain very thin layers (thickness lower than 1 μm); it can be a quite long procedure depending on the boiling point of the utilized solvent.

Spin coating is a three-phase process:

1. Preparation of the solution
2. High-speed rotation
3. Solvent evaporation

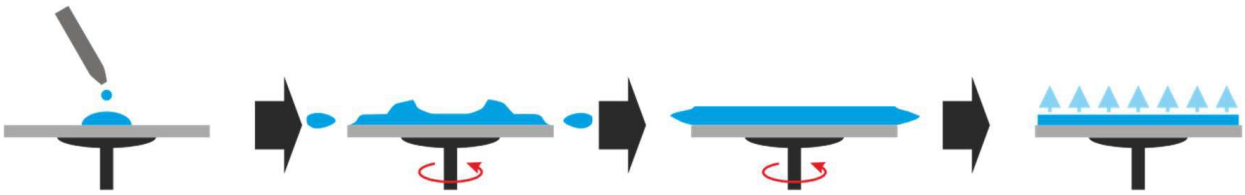

Figure 38, Spin coating scheme [64]

A drop of GO suspension is placed at the center of the polymeric substrate. Then a torque is applied to have a certain rotational velocity, thus spreading the drop on the whole polymer. The multilayer thickness can be tuned through the GO concentration, the spin velocity, and the number of spin-coating cycles. Indeed, by increasing the GO concentration thicker layers are generated and, in some extreme cases, GO sheets may aggregate; but insufficient GO concentration leads to non-uniform deposition on the polymer. Even the spin velocity is a crucial factor: there is an inverse proportionality with the thickness of the multilayer so that, to lower the thickness it is possible to increase the rotational velocity. The multilayer structure is strongly affected by edge-to-edge repulsive forces generated by the negatively charged carboxylic groups in solution and face-to-face attractive interactions that are produced by the evaporation of the solvent.

Similar to spin coating, there is spin casting.

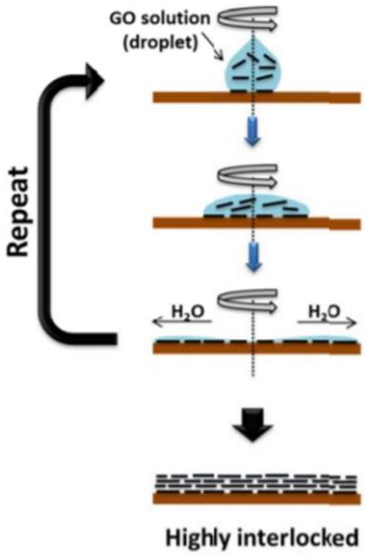

Figure 39, Spin casting scheme [65]

Here the deposition of the drop takes place when centrifugation is already present. In this way, attractive capillary forces generated by the rotation will be stronger than the repulsive ones causing the formation of a denser deposition and thicker layers. [66]

An additional technique is spray coating. It is applicable at the industrial-scale production since it can be cost effective and time efficient. [63] Spray coating is a multi-step hydrodynamic process. the spraying setup is composed of a feed system, injection system, atomization system, and collection system.

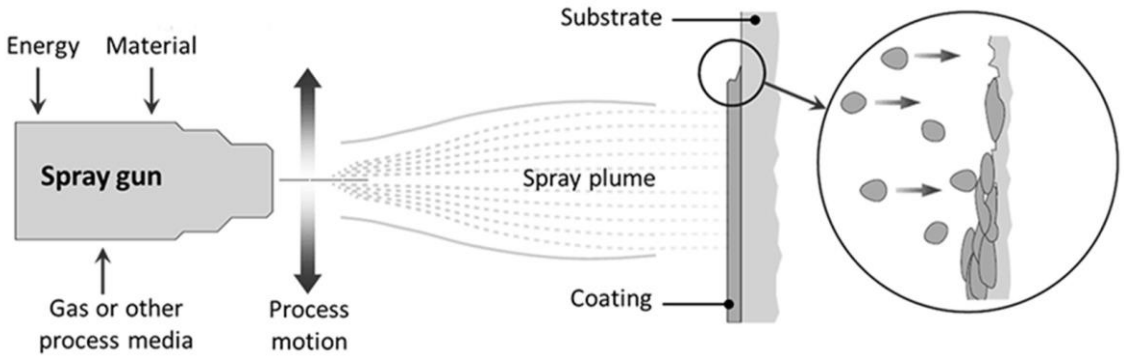

Figure 40, Spray coating scheme [67]

The solution is stored in a liquid storage tank that is one of the main components of the feed system together with a flowmeter and a liquid feed pump. Then, the injection system is basically an air compressor that pumps the solution to the atomization system. The latter atomizes the solution, and the atomized droplets are collected by the collection system. Once ultrafine droplets have been produced, they impinge on the surface of the substrate. Evaporation takes place and the membrane is produced. Relevant parameters in this technique are: viscosity of the solution because it is related to the size distribution of the atomized particles and to their spreading; evaporation rate that is critical to achieve uniformity of the membrane and surface wettability that is still related to the degree of spreading of droplets.

Spray coating is available in many different typologies, but step-by-step spraying is usually employed for the preparation of multilayer membranes.

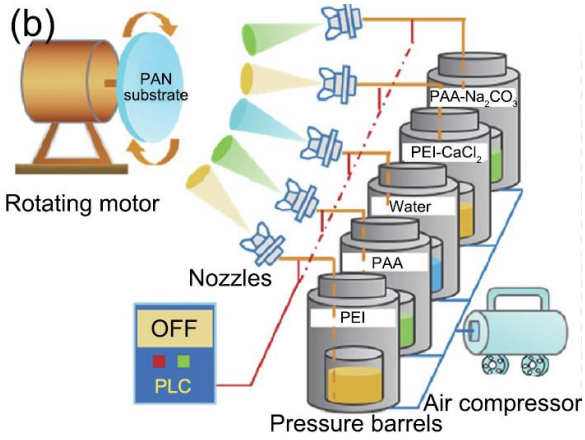

Figure 41, Example of a cyclic spray coating apparatus [66]

It is a computer-aided technique in order to have an automated cyclic procedure and at least two liquid solution reservoirs and two spray nozzles are employed to atomize the different interacting species of the multilayer. [68]

Dip coating is another important method to produce thin coatings or supported membranes and one of the most commonly used techniques. The polymeric membrane is dipped inside a GO suspension with a constant speed, and then it is pulled out.

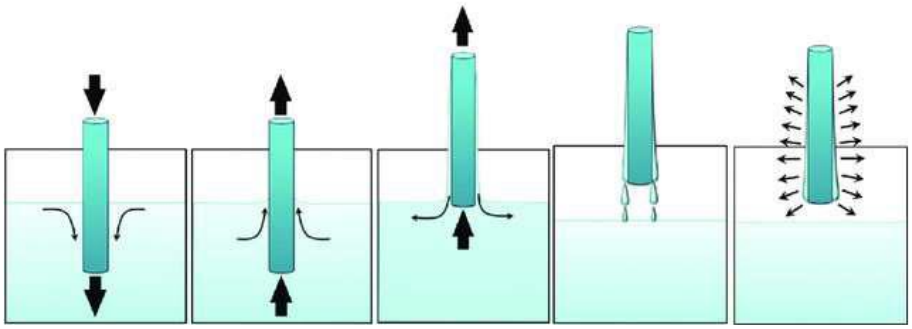

Figure 42, Dip coating scheme [69]

More precisely, three steps are needed:

1. Dipping of the substrate in the GO solution
2. The membrane is left in the bulk of the solution in order to allow a good coating deposition
3. Withdrawal of the substrate from the GO solution and drying

Because of its success, various mathematical models have been proposed to estimate the thickness of the layers based on the solution properties and process conditions. Landau and Levich developed one of these models:

$$l = 0.944 \cdot Ca^{\frac{1}{6}} \cdot \left(\frac{\eta U}{\rho g}\right)^{\frac{1}{2}} \qquad (33)$$

Where $Ca = \frac{\eta U}{\sigma}$ is the capillary number, η the viscosity of the liquid, U is the withdrawal speed and σ is the surface tension of the liquid, ρ the density of the liquid and g is the gravitational acceleration constant.

All of these factors need to be tuned precisely to control the layer thickness and, to do so, crucial parameters are the solution concentration, the soaking time, the withdrawal speed, and the evaporation conditions. [70]

The main critical points of such process are related to defects caused by aggregation of particles, air bubbles in the solution, and contamination of irregularities present on the substrate surface. But, as a benefit, dip coating is an easy technique, and it can be used for large areas of membranes.

The fabrication of multilayered membranes is possible by the so-called Layer by Layer (LbL) dip coating. LbL assembly birth dates back to the mid-1930s and it has been intensively studied. Until then, multilayered materials were produced by using the Langmuir-Blodgett technique: after the formation of monolayers on a water surface, they are transferred onto a solid support. Decher et al in 1997 used the LbL technique to obtain polyelectrolyte multilayer: their aim was to overcome all the limitations of the Langmuir-Blodgett technique such as the inability to produce self-standing films based on covalent bonds, limited yield, and dependence of film quality and stability on substrate size and topology [71]. LbL is a cyclization of the dip coating technique and it may be defined as a cyclic process in which alternately charged materials are adsorbed onto a substrate: a one-dimensional structure along the layer normal is developed. Currently, it is an automated process that allows very small layer thickness: Decher et al. and Dubas et al. claim to produce layers characterized by 1-2 nm thicknesses. [72]

LbL assembly takes place in 4 steps:

1. Immersion of the substrate in the polycationic solution for a certain amount of time is needed to allow polyelectrolyte adsorption
2. Rinsing in deionized water to remove the polyelectrolyte excess
3. Immersion of the substrate in the polyanionic solution for a certain amount of time is needed to allow the polyelectrolyte adsorption.
4. Rinsing in deionized water to remove the polyelectrolyte excess

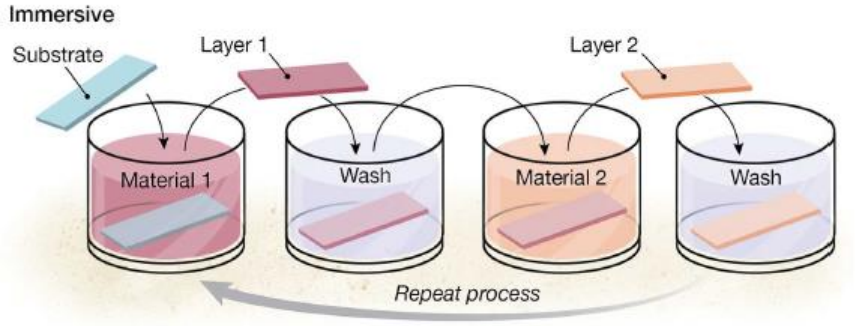

Figure 43, Dipping LbL scheme [71]

The concentrations of the polyelectrolytic solutions are much greater than those required to have the adsorption plateau that is usually reached in some minutes, but the excess allows for conservative work. The washing steps are needed to avoid contamination of the following solution and also to stabilize the weakly adsorbed polymer layers. and to remove the excess of polyelectrolyte that remains on the polymer surface due to evaporation.

One of the most promising aspects of LbL is that many different materials can be used in this multilayer approach and the final film structure will depend on the deposition sequence. [71] Furthermore, nanoscale-level control of the thickness and composition is possible and this technique can be used without specific instrumentation.

LbL assembly allows to obtain homogeneous and uniform structures at the nanoscale, preserving the main features of its constituents, and that is what makes it interesting for graphene-based materials. The first one to report on graphene-based LbL assembly was Kotov et al. in 1996: he used non-exfoliated graphite oxide platelets and polyelectrolytes. From that moment onward, several scientific studies have been performed to understand completely this technique.

Since LbL is based on electrostatic interactions, it is not possible to use graphene as it is, because it does not possess any charge. On the other hand, GO sheets can be easily packed in multilayers by LbL. Two approaches are possible: as prepared GO is negatively charged in aqueous solution thanks to the presence of carboxylic groups; graphene oxide can also be functionalized by introducing amine groups on the surface of GO sheets for instance, obtaining positively charged GO.

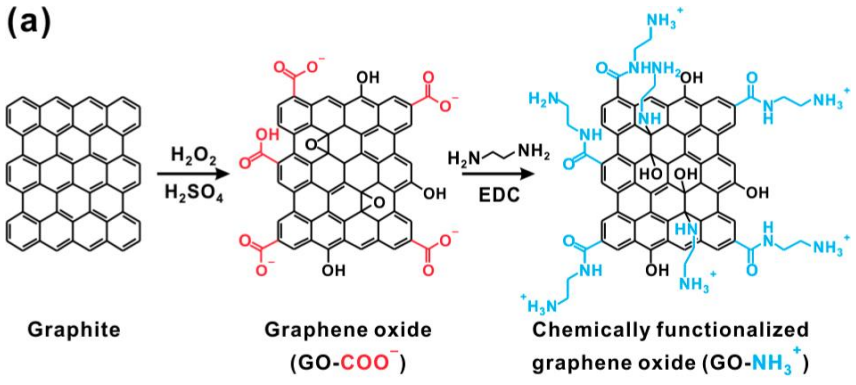

Figure 44, Graphite, graphene oxide and functionalized graphene oxide structures [73]

4.2.2 State of the art

One of the most relevant features of graphene oxide is that it can be easily dispersed in water thanks to the electrostatic repulsion between the ionized functional groups. Preparing membranes using water GO suspensions is a promising technique and that is one of the reasons why GO multilayer membranes have been widely studied. When GO sheets are arranged in a multilayered structure, some space between the layers is formed and it has been estimated to be in the range of 0.6-1.2 nm as a function of the degree of oxidation and amount of intercalated water. The separation mechanism is based on molecular sieving; therefore, the gas permeability increases with decreasing kinetic diameter of gases as reported by Park and Suda.

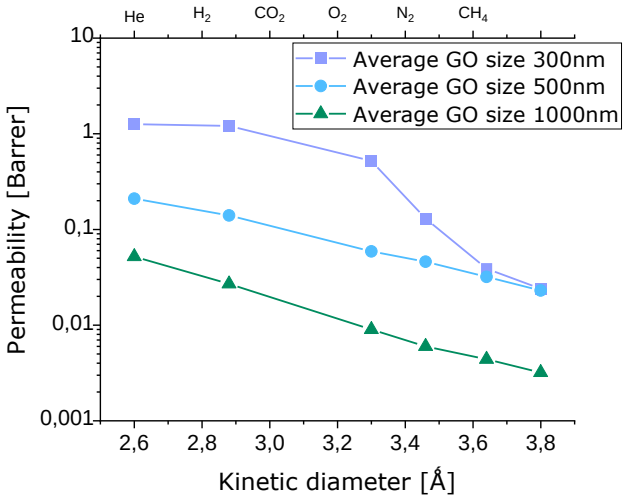

Figure 45, Gas permeability as a function of kinetic diameter and average GO size [74,75]

In addition, it has been proved that the permeability is inversely proportional to the multilayer thickness. At this concern, Li et al prepared ultrathin GO onto an anodized aluminum oxide support, and their resulting permeability was much higher than conventional thick membranes; also Pierleoni et al. produced GO membranes on Matrimid and PET, and they proved that by increasing the number of layers, as well as the thickness of the multilayer, permeability decreases.

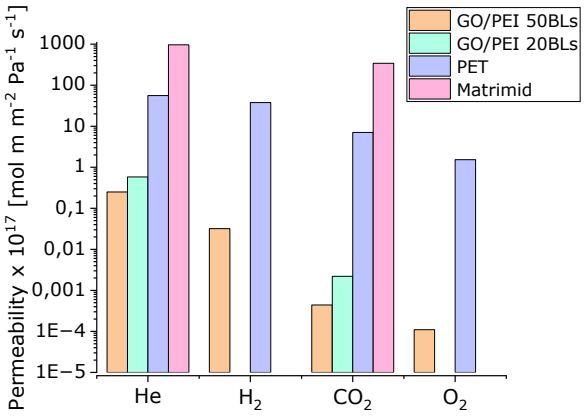

Figure 46, Permeability as a function of number of layers [76]

Even Liu et al. in 2017 reported the same trend for LbL-assembled GO membranes. In their work, the LbL procedure results to be dependent not only on electrostatic interactions but also on hydrogen bonding. It is the pH of the solutions to change the interaction that is mainly involved in the LbL technique: at pH=4 electrostatic interactions are strong, so the LbL will be based on them; on the other hand, when pH=10 electrostatic interactions are minimized and a hydrogen bonding LbL can be carried out. Even if in the hydrogen bonding LbL assembled membranes, the thickness of the multilayer is higher, in both two methods, by increasing the number of layers permeability is decreased.

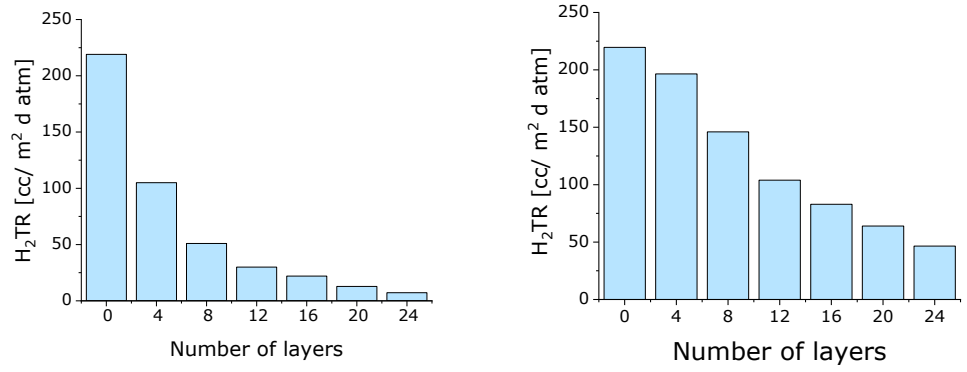

Figure 47, Hydrogen transfer rate as a function of number of layers for membranes produced by hydrogen bonding LbL (on the left) and electrostatic interactions LbL (on the right) [77]

The same evidence is reported by Kim and coworkers who, in 2013, fabricated GO-coated PTMSP membranes following two different methods. In method 1, they contacted the polymeric membranes with the air-liquid interface of a GO solution and, in the end, they perform a spin coating procedure; in method two they prepared GO membranes by spin-casting. As a result, membranes obtained by method 1 have heterogeneous graphene oxide deposition: the stacked GO sheets arrange themselves in an "island-like" manner; instead membranes obtained by spin casting show higher GO density and homogeneity. This is probably due to the balancing between electrostatic interactions, particularly edge-to-edge repulsive forces, and face-to-face attractive ones: in method one, the repulsion prevails on the attraction between the different layers. Of course, this will be reflected in perm-selectivity, spin-coated membranes show higher permeability towards hydrogen but also carbon dioxide; instead, spin-casted membranes result in lower permeability, but a highly selective system.

To have a positive contribution to permeance, it is also possible to tune the concentration of the GO solution. In 2018 Zeynali and coworkers, produced three different alumina supported GO membranes: in sample 1 they have the maximum concentration of GO (1 mg/mL), in sample 2 the solution was diluted 2 times, and in sample 3 three times. By analyzing their results, it can be easily seen that, by decreasing the concentration of the GO suspension, permeability will increase without having a too strong effect on selectivity. [78]

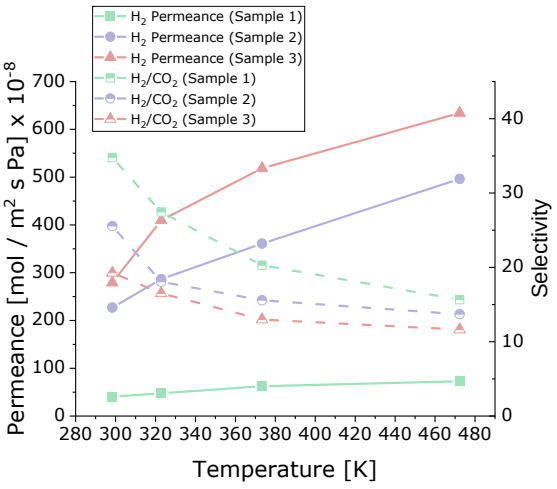

Figure 48, Effect of temperature on permeance and selectivity for all three GO membrane samples at pressure gradient 1 bar. [78]

Another key parameter is the average GO size that can be conveniently tuned by using sonicating the GO suspensions for different times. Intensive ultrasound allows to reach remarkably high temperatures, pressure, and rapid cooling rates in very short times. Han Lyn et al. [79] measured the size of GO after different sonication times, they noticed that by increasing the sonication time there was an effective reduction in the size of GO sheets through exfoliation. Such reduction affects both the lateral size of GO flakes and the resulting thickness of GO-based nanocomposite films. Gas permeability increases with decreasing size of GO sheets and this is due to the diffusional pathways shortening. [55] Another effect of size reduction is the presence of a slightly lower amount of oxygen functional groups on the basal plane of GO. The presence of these oxygen functional groups is relevant because it can tune the interlayer spacing between the different flakes and this is also due to the fact that oxygen groups will attract water molecules in the multilayer structure resulting in an increased interlayer spacing. [80]

Interestingly, in LbL assembly the interlayer spacing can also be controlled by changing the pH values of GO and polyelectrolytic solutions. Different pH conditions will affect the protonation level of oxygen functional groups inducing stronger or weaker face-to-face attraction between the different layers. An explanation can be retrieved from the concept of persistence length. The persistence length is a measure of the structural rigidity of a polymer. [81] Indeed, the persistence length of a polyelectrolyte depends on the ionic strength that, in its turn, depends on the protonation level, therefore on pH values. By decreasing the pH, the protonation level will be higher, causing also stronger edge-to-edge repulsion with a flattening of each layer and higher persistence length, therefore a decrease in the interlayer spacing. [80]

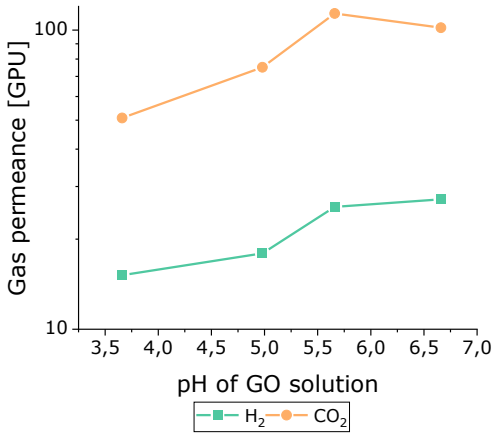

Figure 49, Gas permeance as a function of pH of the GO solution [80]

Since graphene oxide can be easily functionalized, the interlayer distance is highly tunable. From one side, this is a positive aspect because it is possible to increase the permeability of the overall system, but there is a constraint related to the fact that, if this space is increased excessively, then the membrane will lose the sieving capacity, therefore selectivity will reach very low values.

In the table below, numerical values of the best case of each system reported in previous charts are reported.

Membrane	*H_2 Permeability [Barrer]*	*CO_2 Permeability [Barrer]*	*H_2/CO_2 Selectivity*	*Notes*	*Ref.*
PTMSP/GO	1.26	0.52	2.42	GO average size: 300 nm	60
PEI/GO	0.00955	1.3E-05	72.72	Coating only	68
PEI/GO, PET as polymeric substrate	0.33	0.0072	46.67		68
Few-layers graphene oxide membranes	0.15	0.68	0.23	pH=5.66	73
GO, alumina tube as a support	3501	100.71	34.8		70
PET/rGO	0.0002	-	-	LbL governed by hydrogen bonding	69
PET/rGO	0.00004	-	-	LbL governed by electrostatic forces	69

Table 9, Perm-Selectivity of GO-based membranes available in literature.

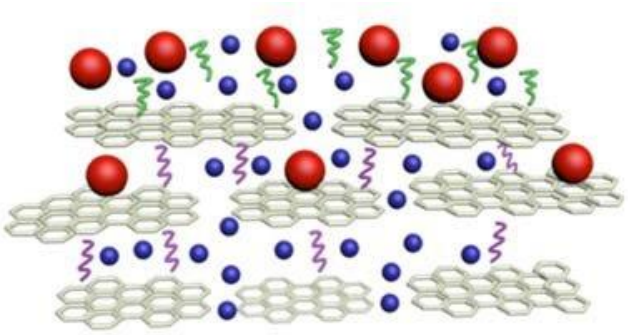

Figure 50, GO multilayered membrane representation.

In graphene oxide multilayers the transport of molecules is allowed following two pathways:

- Interlayer nanochannels
- Structural defects introduced upon functionalization of graphene

Tunable interlayer distance is one of the key parameters to allow a selective transport: in pristine graphene, the interlayer distance was about 0.334 nm causing an almost total impermeability to any molecule. Graphene oxide interlayer distance is instead around 0.6-1.2 nm guaranteeing the possibility of certain gas molecules passing through.

On the other side, on graphene sheets, defects might be present resulting in shortcuts for molecules crossing the membranes. These defects can also improve the membrane's overall selectivity because they can exhibit molecular sieving properties. [57]

In the following tables a summary of existing GO membranes is reported.

5. Thesis aim

As the world moves towards cleaner and more sustainable energy sources, hydrogen is emerging as an alternative to fossil fuels. In the introduction chapter it is reported that, a paramount step in hydrogen production is its purification. Here membranes come in showing several advantages with respect to conventional purification technologies. The development of proper membrane system to purify hydrogen is an important step towards making hydrogen a sustainable and viable energy vector and raw material.

The main goal of this thesis work is to find a perm-selective membrane system to carry out diffusivity-driven gas separation and, specifically, hydrogen purification. As previously mentioned in paragraph 1.3, the main separation that is required is between hydrogen and carbon dioxide. Therefore, the permeation tests will be focused on these two gases. Nanocomposite membranes have been produced: a polymeric substrate is used as a support and, graphene oxide, is deposited on it as a coating in a multilayered structure.

Starting from Matrimid, a polyimide that will be presented in the following chapter, preliminary attempts to extend the study to other types of polymeric substrate have been done in order to investigate the versatility of the process. In this perspective, it has been tried to produce asymmetric supported thin films with the aim of creating a system in which the polymeric substrate does not influence in a relevant way the performances of the coating.

6. Experimental

6.1 Materials

6.1.1 Matrimid

Matrimid 5218 is a commercial thermoplastic polyimide. It is obtained by polycondensation of 3,3’,4,4’-benzophenone tetracarboxylic dianhydride (BTDA) and a mixture of cycloaliphatic monomers. [82] Matrimid can be used to obtain membrane, indeed it is possible to get films with excellent adhesion, chemical resistance, and good thermal stability. Furthermore, upon

polymerization and casting, an amorphous glassy structure is obtained creating a polymeric network where the available free volume makes the film a selective towards H_2. However, this selectivity is not enough to reach high purity hydrogen and that leads to the need of developing more selective systems.

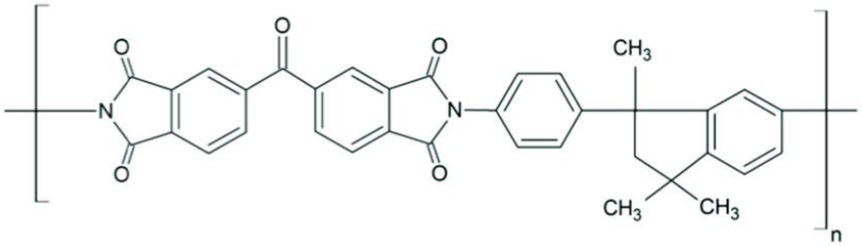

Figure 51, Matrimid chemical structure [83]

Matrimid 5218 has been provided in powder by Huntsman; self-standing film and supported thin film have been obtained through solvent casting.

SELF-STANDING POLYMERIC FILM

A 1.5 wt.% solution of Matrimid in high-purity dichloromethane (DCM) has been prepared. 20 mL of the solution has been poured into a Petri dish, covered with the lid, and left for 48 hours in a hood to allow a controlled slow evaporation of the solvent.

The second step for the film production is a thermal treatment: Matrimid film is positioned in a vacuum oven at 200°C for 18h in order to complete the total evaporation of the solvent and to remove polymerization volatile residues that may affect the barrier properties of the membrane. In the end, the film is cooled down slowly still in a vacuum atmosphere.

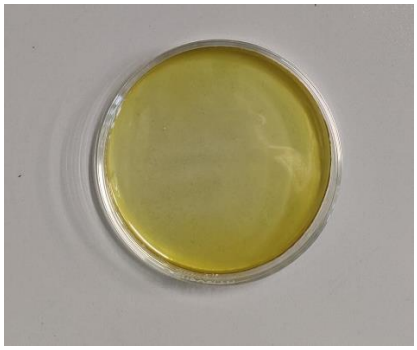

Figure 52, Matrimid film

Since Matrimid films are hydrophobic, surface hydrolyzation is performed by immersing the membrane in sodium hydroxide (NaOH) aqueous solution with 1M concentration, for 18 hours. Such step is needed because there should be a negative charge on the surface of the membrane in order to allow the polycation deposition during the multilayer preparation.

THIN FILM ON A POROUS SUPPORT

A 0.75 wt.% solution of Matrimid in chloroform is prepared. 5 mL of the solution are poured onto a paper support; through solvent casting a 20 μm film Matrimid film can be obtained.

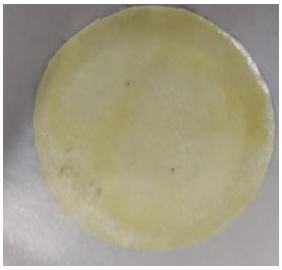

Figure 53, Matrimid thin film on a porous support

Thermal treatment is not carried out to avoid degradation of the paper support; to avoid the presence of polymerization residues, these films are prepared by using thermal-treated Matrimid that is re-dissolved in DCE. Also in this case, an important step is hydrolyzation: some drops of aqueous NaOH solution 1M are placed onto the thin film, and after 5 minutes the sodium hydroxide is removed by blotting with a napkin; afterward repeated washing with some drops of water is performed by using a 3ml pipette.

Some permeation tests have been conducted on these thin films, but the main problem was about reproducibility: through this method it was not possible to produce films with uniform thickness, therefore the final performances could not be determined in a proper way.

6.1.2 Other polymeric supports

PPO

Polyphenylene oxide is a high-temperature thermoplastic polymer, it is aromatic and highly amorphous. Thanks to its high permeability, PPO is a glassy material suitable for membrane applications.

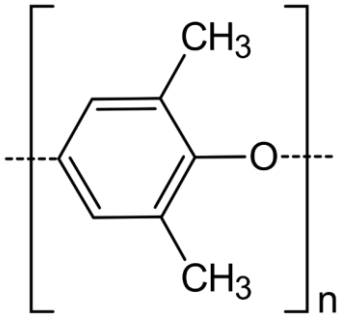

Figure 54, PPO repeating unit. [84]

Solid PPO powder is purchased from Sigma Aldrich, then it is dissolved in high purity chloroform in a solution 5 wt.% by weight of PPO. 10 mL of the prepared solution are poured in a Petri dish and, through solvent casting at 50°C under a fume hood, membranes are obtained. Then, the films are kept in a vacuum oven at 35°C for 1 day in order to promote the elimination of solvent residues.

P84

P84 is a commercial polyimide with higher H_2/CO_2 selectivity than Matrimid.

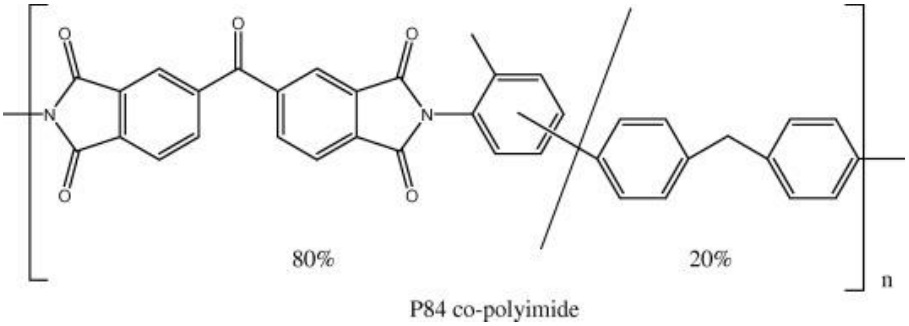

Figure 55, P84 chemical structure [85]

A 4 wt.% solution is prepared by dissolving P84 powder provided by Ensinger in Normal Methyl Pyrrolidone (NMP). The films are then casted on a hot plate with a constant temperature around 50°C.

6.1.3 LbL-Materials

PDDA

Poly(diallyl dimethylammonium chloride) is a polymer that was synthetized for the first time in 1957 by Prof. Butler. It is considered as a strong polyelectrolyte, as it possesses high positive charge density. It can be obtained by a reaction between two equivalents of allyl chloride with dimethylamine. It has been provided by Sigma-Aldrich in a concentrated solution (20 wt.%) and used in order to obtain a polycationic solution with a concentration of 1 wt.% in deionized water.

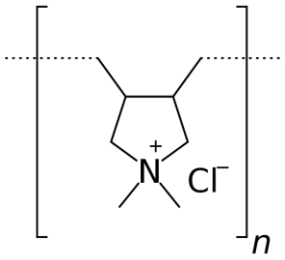

Figure 56, PDDA repeating unit [86]

Graphene

A graphene oxide dispersion, provided by Graphenea, has been used, with a concentration of 0.143 wt.%. The dispersion is sonicated for 4 hours in order to have a homogeneous suspension: a sonication bath is obtained employing an Elmasonic ultrasonic device coupled with a system to maintain the temperature at 35°C. Then, solutions at different concentrations are prepared by diluting the original dispersion: 0.01, 0.004, and 0.007 wt.%.

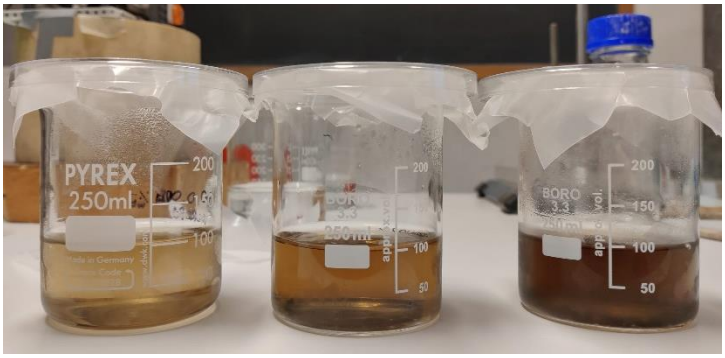

Figure 57, GO solutions at different concentration. From left to right: 0.004, 0.007, and 0.01 wt.%

It is useful to introduce a nomenclature to identify the membranes coming from the different solutions. For instance, the solution with graphene oxide in 0.004 wt.% is named: S4c004, where S4 stands for sonicated 4 hours, c004 gives information about the concentration of GO.

6.2 Methods

6.2.1 LbL Assembly

A multilayer of graphene oxide is deposited onto the polymeric films to obtain nanostructured membranes. Specifically, a layer-by-layer dip coating technique has been used.

Two polyelectrolyte aqueous solutions are prepared: the polycationic solution with a concentration of 1 wt.% of PDDA and the polyanionic solution that is GO at different concentrations by weight as reported in the previous paragraph.

Figure 58, Lego robot used for LbL assembly

The LbL assembly is performed by using a Lego robot to simulate a dip coater and it consists of 4 steps:

1. Immersion in the polycationic solution: the polymeric film is dipped inside the PDDA solution for five minutes
2. Rinsing and immersion in neutralized water (pH=7) for 20 minutes to remove the excess of polyelectrolyte
3. Immersion in the polyanionic solution: the polymeric film is dipped inside the GO solution for five minutes
4. Rinsing and immersion in neutralized water (pH=7) for 20 minutes to remove the excess of polyelectrolyte

Through this technique, a bilayer is deposited on each side of the film: the first one is the polycationic layer (PDDA) and the second is the polyanionic layer (GO).

Once the multilayer has been deposited onto the polymeric film, membranes are left to dry and then they are positioned under an infrared lamp at 60°C for 30 minutes to remove water residues.

6.2.2 Permeation test

Permeation tests are performed by using a manometric apparatus called permeometer, developed according to the ASTM D1434-82 (2015)e1.

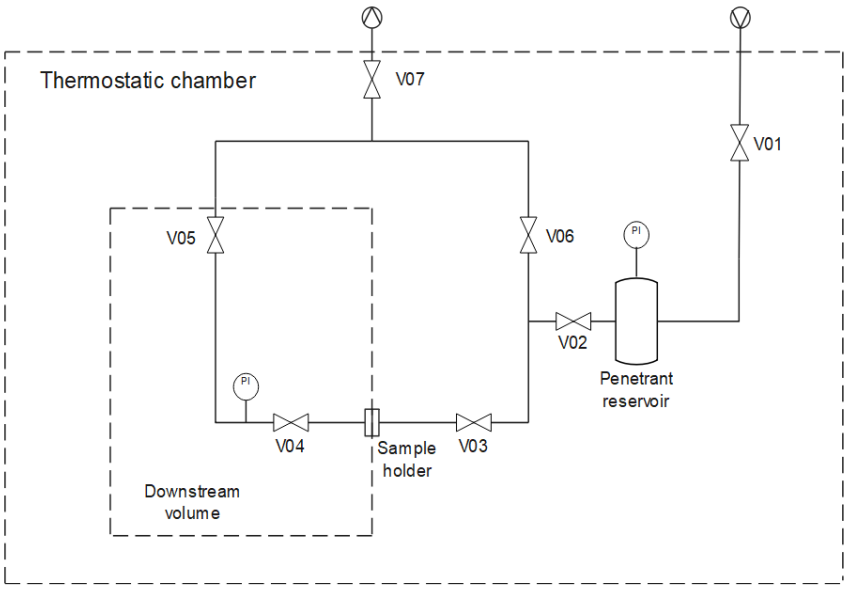

Figure 59, Layout of the permeometer apparatus

The system consists of a thermostatic chamber to set specific temperature conditions and a pressure difference is maintained across the two sides of the sample. The membrane is cut in the shape of a circle with a diameter of 25 mm by means of a die cutter. Afterward it is placed inside a permeation cell that is composed of two chambers separating the upstream and the downstream volume. The presence of an O-ring ensures the sealing of the system, thus preventing any leakage.

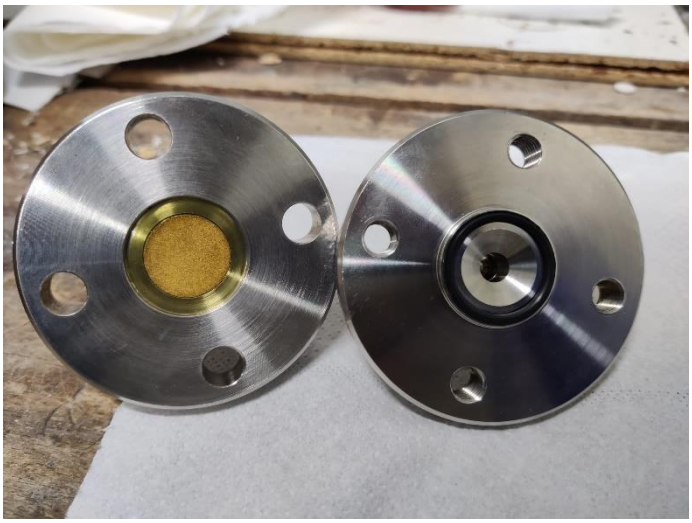

Figure 60, Permeation cell with the membrane

The downstream volume should be as small as possible to have high sensitivity, whilst the upstream volume is a reservoir that can be filled with the penetrant gas and a manometer will measure its pressure. The downstream pressure is then monitored by a high precision manometer over time. Two types of manometers have been used: Baratron MKS and Barocel, both of them working in the range 0-100 mbar and showing a resolution of 10^{-3} mbar.

Before the test, the sample needs to be evacuated in order to allow the desorption of all the chemical species that may be contained in the membrane: to that aim, a vacuum pump is used.

At the beginning of the test, the upstream volume is kept at a constant pressure; whilst the downstream volume is kept at practically 0 pressure, through the use of the vacuum pump. Then, upstream valves are opened and the contact between the gas and the polymeric film starts. From that point onward, it is possible to measure the pressure downstream that is related to the flux of the gas able to cross the membrane.

$$|J|_{SS} = \left(\frac{dp_1}{dt}\right)_{t\to\infty} \cdot \frac{V}{RT} \cdot \frac{1}{A} \qquad (34)$$

Where V is the downstream volume, A the membrane area, and T is the temperature.

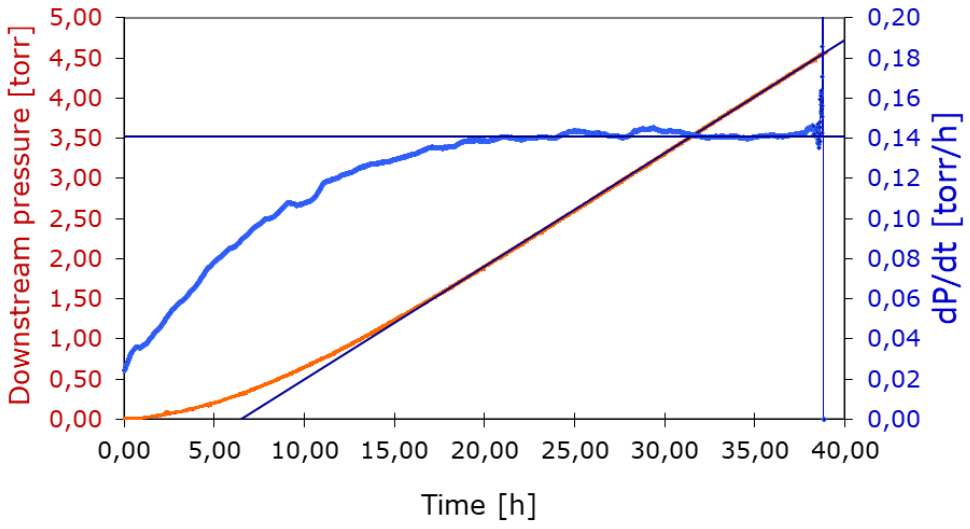

Figure 61, Gas permeation test output

The transfer rate (T.R.) or permeance can be defined as the flux normalized by the driving force, which, in this case, is the pressure difference.

$$T.R. = \frac{|J|_{SS}}{(p_1 - p_2)} = \left(\frac{dp_1}{dt}\right)_{t\to\infty} \cdot \frac{V}{RT} \cdot \frac{1}{A} \cdot \frac{1}{(p_1 - p_2)} \qquad (35)$$

Since the permeance depends on the thickness of the sample (i.e., geometric features of the membrane), it is preferable to use the permeability that has already been defined in Chapter 2 and it can be rewritten as:

$$P = T.R. \cdot l = \left(\frac{dp_1}{dt}\right)_{t\to\infty} \cdot \frac{V}{RT} \cdot \frac{l}{A} \cdot \frac{1}{(p_1 - p_2)} \qquad (36)$$

Permeability is usually expressed in barrers from the name of who started measuring the permeability of membranes:

$$1\ Barrer = 10^{-10}\ \frac{cm^3_{(STP)}}{cm^2\ s} \cdot \frac{cm}{cmHg} = 3.35 \cdot 10^{-16}\ \frac{mol}{m^2 s\ Pa/m} \qquad (37)$$

The transfer rate through a multilayer film can be approached with a series resistance model:

$$\frac{1}{T.R.} = \sum_i \frac{l}{(T.R.)_i} = \sum_i \frac{l_i}{P_i} \qquad (38)$$

Dealing with a dense polymeric film coated with a multilayer, this relationship becomes:

$$\frac{1}{T.R._{\cdot multilayer}} = \frac{1}{T.R._{\cdot substrate}} + 2 \cdot \frac{1}{T.R._{\cdot coating}} \qquad (39)$$

And it is possible to evaluate the intrinsic permeability of the coating:

$$\frac{1}{T.R._{\cdot coating}} = \frac{l_{coating}}{P_{coating}} = \frac{1}{2}\left(\frac{l_{multilayer}}{P_{multilayer}} - \frac{l_{substrate}}{P_{substrate}}\right) \qquad (40)$$

An analogic micrometric thickness gauge with a sensitivity of 0.001 mm is used to estimate the thickness of the polymeric support that generally is about 40-50 μm.

6.2.3 Zeta Potential Test

The zeta potential is a physical property that describes the charge at solid-liquid, liquid-liquid and gas-liquid interface. Zeta potential can be used to characterize colloidal systems and solid surfaces. Dealing with membranes, therefore solid surfaces, zeta potential gives insights of chemistry of the outermost solid surface. Zeta potential tests have been performed by using Anton Paar SurPASS 3 analyzer which exploits the streaming potential technology for macroscopic solids.

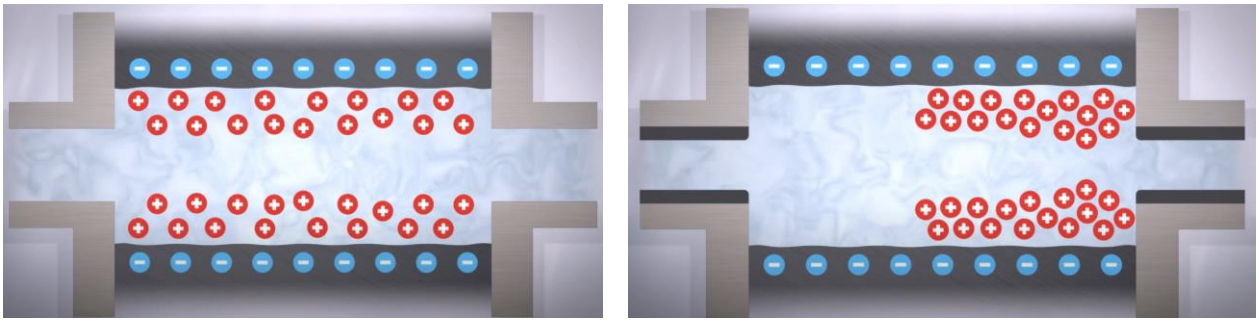

Figure 62, Charge generation and streaming potential in the measuring cell of the zeta-potential analyzer [90]

The membrane is mounted on a suitable measuring cell, a capillary channel is created and the contact between an electrolytic solution (0.001 mol/l aqueous NaCl or KCl solution) and the solid surface starts. In this way, charges are formed due to acid/basic interactions. Then, a pressure gradients is applied to the electrolyte solution and charges move with the liquid flowing, causing

the accumulation of charges on one side of the cell and giving rise to streaming potential. Since there are two electrodes at both ends of the cell, they can measure the streaming potential as a function of the applied pressure.

For planar solids, zeta potential is calculated according to the following equation:

$$\zeta = \frac{dU_{str}}{d\Delta p}\frac{\eta}{\varepsilon \cdot \varepsilon_0}\kappa \qquad (41)$$

Where $\frac{dU_{str}}{d\Delta p}$ is the slope of streaming potential and differential pressure, ε is the dielectric coefficient of the electrolyte, ε_0 is the permittivity, κ is the electrolyte conductivity. [91]

7. Results

The initial tests carried out were permeation tests on the polymeric support, which is Matrimid. These tests were conducted at 35°C for helium, hydrogen, carbon dioxide and argon and the following table reports permeability values expressed in Barrer.

Permeability [Barrer]			
He	**H_2**	**CO_2**	**Ar**
23.9	*24.5*	*6.7*	*0.6*

Table 10, Pure Matrimid permeability at 35°C

The importance of this first slot of tests is related to the need of estimating the properties of pure coating, as reported in equation 40, with the aim of using it on different types of polymeric substrates.

Successive tests, performed with the GO-coated membranes, are instead focused on hydrogen and carbon dioxide, only. Perm-selectivity data of one membrane sample are reported in the table below.

	Matrimid	*Composite system*	*GO coating*	*Membrane Thickness*
H_2 Permeance [GPU]	0.76	0.127	0.30	
CO_2 Permeance [GPU]	0.20	0.003	0.006	32.2 μm
Selectivity H_2/CO_2	3.8	42.3	50	

Table 11, Permeance and selectivity for pure Matrimid, composite membrane and GO coating.

The composite system comprises the Matrimid support and the coating together. Since the aim of the project is to analyze the graphene oxide multilayer performances, coating data acquires relevance.

From XRD tests, the d-spacing, which represents the thickness of a bilayer, can be estimated. In this case, the d-spacing was found to be 1.4 nm and assumed to be constant. This allows for the calculation of the thickness of the coating alone.

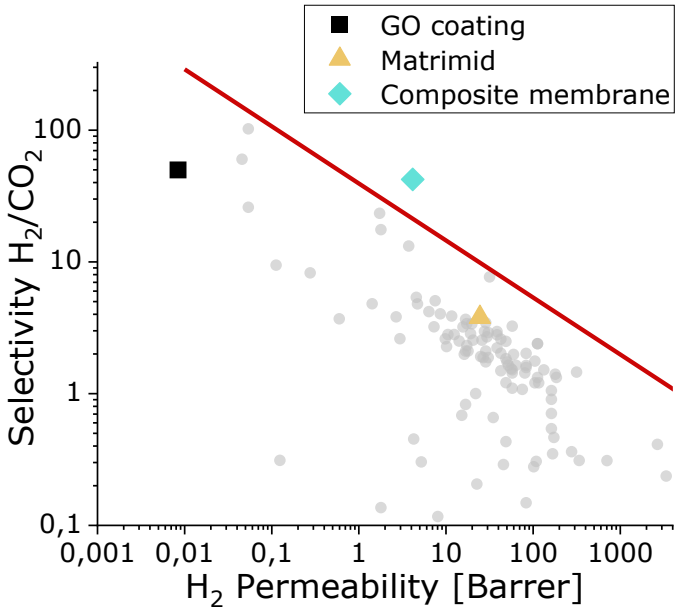

Figure 63, Perm-selectivity of Matrimid, composite membrane and GO coating.

It is clear that the permeability of the coating is a very small value and it is not significant to make a comparison with permeability of other polymeric bulk systems. The proposed multilayered GO coating is much thinner than commercial bulk membranes. Finally, from this point onward, Robeson upper bound plots have been converted in permeance vs selectivity charts, using a reference thickness of 1 μm. This allows for a consistent comparison.

7.1 Effect of concentration

The concentration of the GO solution is a relevant factor in the membrane production process. Decreasing the concentration leads to lower amount of deposited graphene oxide onto the membrane, as could be easily expected. A curious phenomenon is that there is a range of concentrations in which the solution is stable. When GO is dispersed in water, the oxygen-containing functional groups ionize forming negative charges. As a result, GO sheets present high

surface charge density which promotes the attraction between different GO sheets and, also, between GO sheets and water molecules. Increasing the concentration of GO in solution leads to attractive forces that overcome repulsive ones: GO sheets precipitates in a phenomenon called coagulation. When concentration is increased up to 0.01 wt.% the solution is stable; when GO concentration is 0.015 wt.% macroscopically the solution seems to be stable, but the deposition on Matrimid support results not homogeneous even macroscopically (see Figure below).

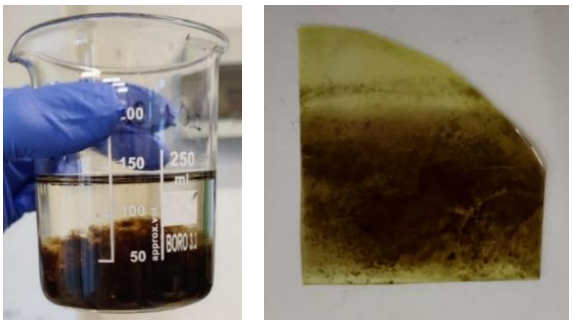

Figure 64, Coagulated GO in solution and non homogeneous deposition on Matrimid film

Similarly, when the concentration of GO is too low, GO precipitates. Also in this case, the explanation could be find in electrostatic forces: at low concentrations repulsive forces between GO sheets are particularly weak and this will cause agglomeration of graphene oxide. Indeed, an attempt to prepare a solution 0.0001 wt.% has been made, but after a while GO coagulated. Overall, the concentration window of membranes produced and tested is 0.004-0.01 wt.%.

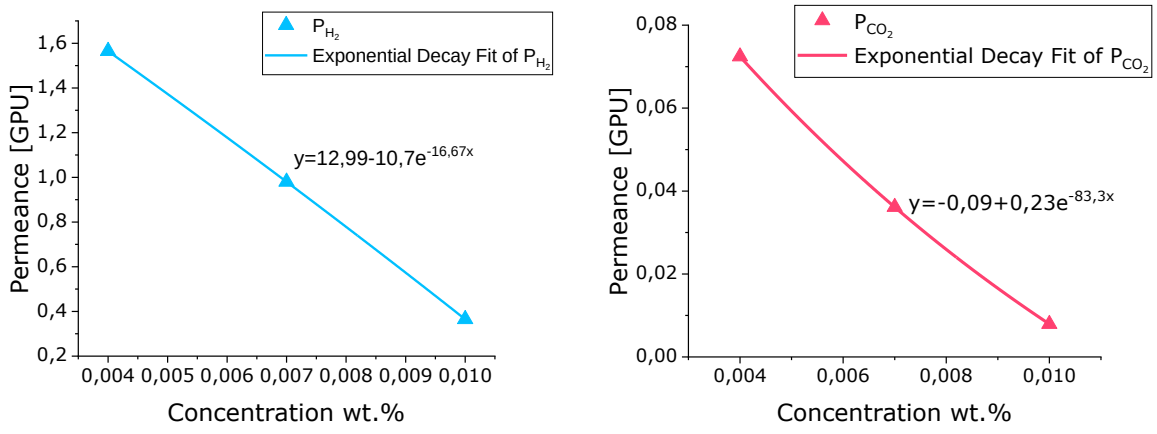

Figure 65, Coating permeance as a function of GO concentration

Lowering GO concentration, permeance increases in a relevant way but, as a drawback also H_2/CO_2 selectivity decreases.

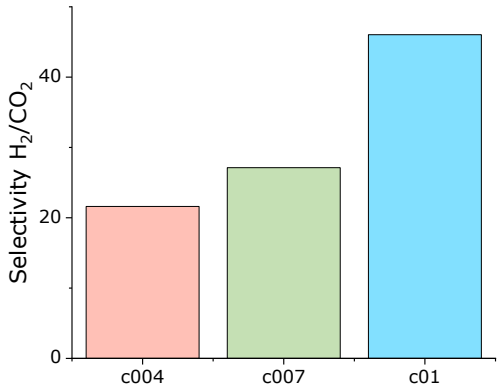

Figure 66, Coating selectivity depending on GO concentration

By comparing the results with the Robeson upper bound, it is noteworthy that by changing the concentration of the GO solution, the performances will follow the same slope as the Robeson limit.

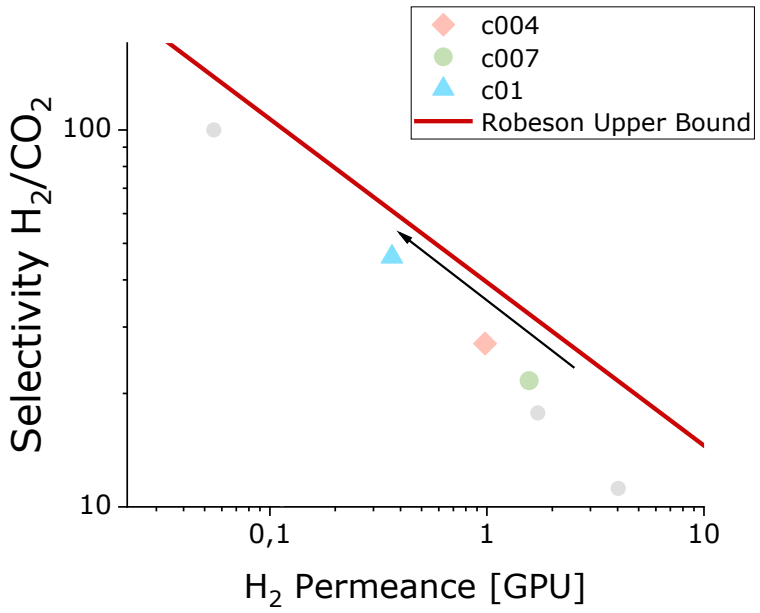

Figure 67, Comparison between membranes obtained at different concentrations and Robeson Upper Bound

7.2 Thermal reduction

From the previous paragraph, the best selectivity is obtained from the membrane c01, but as a drawback it is the system showing the lowest permeability. To overcome such limitation, one sample has been thermally reduced at 150°C. In this way holes are created on the coating: at that temperature, water is released, but also CO and CO_2 are removed from oxygen containing functional groups. These nano-holes allow the formation of extra transport pathways leading to a great improvement on permeability. Hydrogen permeance increases by a factor 4.1 from 0.36 to 1.56 GPU, on the other hand also carbon dioxide permeance increases, but the factor is 1.65: overall a great improvement on selectivity is achieved.

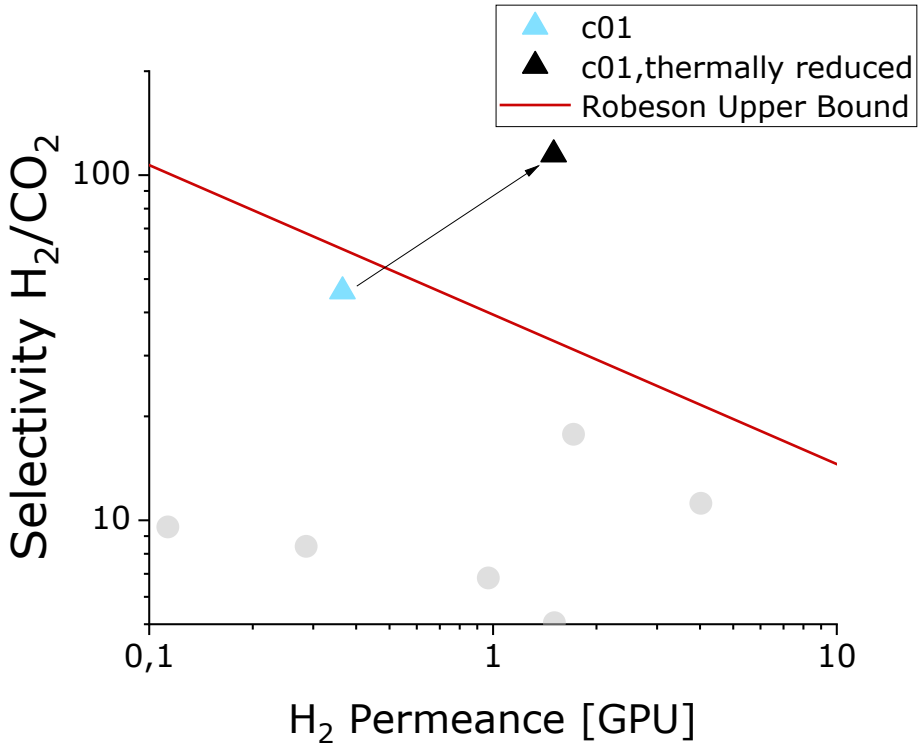

Figure 68, Effect of thermal reduction on membrane performances

7.3 Effect of temperature

As industrial hydrogen purification processes can occur at temperatures different from ambient and typically at higher temperatures, it has been decided to perform permeation tests at different temperatures to analyze the behavior of the produced membranes.

The effect of temperature on Matrimid was analyzed at first for hydrogen to estimate the activation energy of permeability. Results were coherent with data present in literature, so that CO_2 data have been taken from previous tests carried out in the same laboratory following the same procedure. For the sake of completeness and to have a proper comparison, tests have been repeated also for helium and still, results were comparable with previous ones. These data of pure Matrimid will be a key factor to better understand the effect of temperature on perm-selectivity of the coating.

Permeability [Barrer]

He				H_2				CO_2			
Test temperatures				*Test temperatures*				*Test temperatures*			
35°C	45°C	55°C	65°C	35°C	45°C	55°C	65°C	35°C	45°C	55°C	65°C
23.9	27.5	30.5	34.4	24.6	28.1	30.7	35	6.7	7.4	8.1	8.8

Table 12, Matrimid Permeability at different temperatures

Of course, as a second step, the effect of temperature on performances has been analyzed for the GO-coating, at the different concentrations.

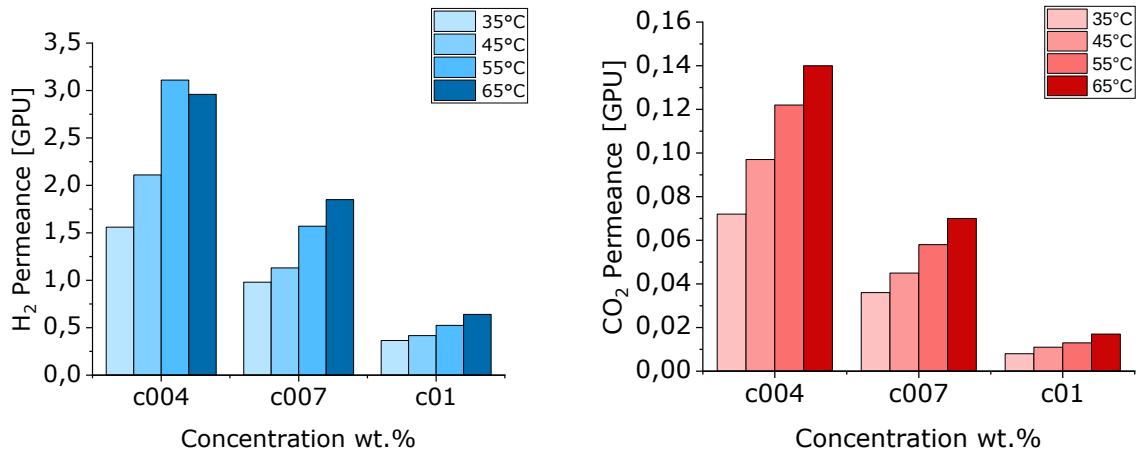

Figure 69, Effect of temperature on H_2 coating permeance (on the left) and CO_2 coating permeance (on the right)

As one can see, the gas transfer rate generally increases with temperature for both hydrogen and carbon dioxide. However, the behavior of the selectivity is more complex. Typically, selectivity increases with temperature in glassy polymers, as demonstrated by Rowe et al. in 2010 (reported in chapter). Specifically, the Robeson upper bound for H_2/CO_2 gaseous mixtures was shifted to higher values of selectivity with increasing temperature. Upon analyzing our results, there is no an apparent relevant trend for selectivity.

Temperature [°C]	*PH_2 [GPU]*	*PCO_2 [GPU]*	*Selectivity*
35	1.56	0.072	21.6
45	2.10	0.097	21.7
55	3.11	0.122	25.5
65	2.96	0.14	21.2

Table 13, Temperature effect on permeance and selectivity of the GO coating

The investigation of the impact of temperature on gas permeability indicates that the resulting values conform to the Arrhenius behavior anticipated in chapter 2. In the following plot it is reported the exponential trend for both H_2 and CO_2 permeance with respect to temperature.

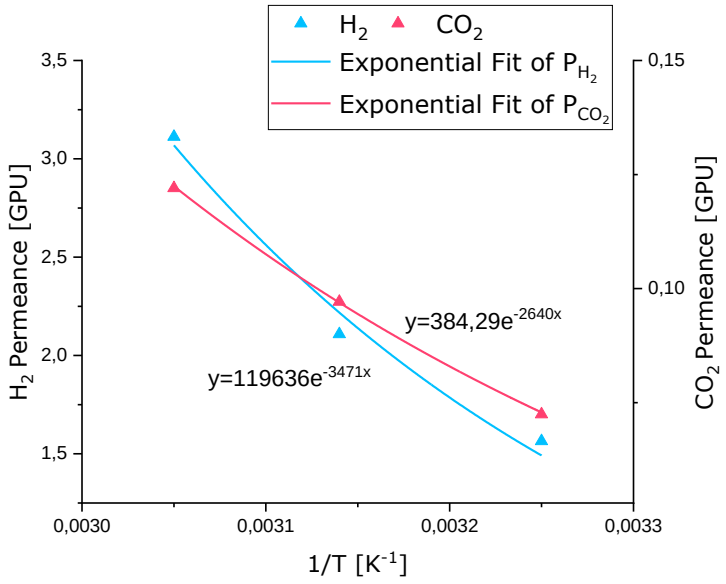

Figure 70, Arrhenius-like exponential fitting of H_2 and CO_2 permeance as a function of temperature

The estimation of the activation energy has been conducted for all the membranes coming from the solutions at different concentrations. Numerical values are reported in the table below.

	H_2		CO_2	
	P_{H2} [GPU]	E_{H2}	P_{CO2} [GPU]	E_{CO2}
Matrimid	0.51	9.93	0.14	8
GOS4c004	1.56	28.9	0.07	19.1
GOS4c007	0.98	19.3	0.04	19.35
GOS4c01	0.36	16.6	0.007	21.4

Table 14, Activation energy and permeance at 35°C

In most cases, the activation energy of hydrogen is higher than the one of CO_2. As temperature increases, the thermal energy of molecules also increases making them more likely to find the transport pathway and cross the membrane. Moreover, this effect should be more pronounced for smaller molecules, such as hydrogen, than for larger ones, like carbon dioxide. On the other hand, the solubility contribution for CO_2 that is a condensable gas, is more relevant.

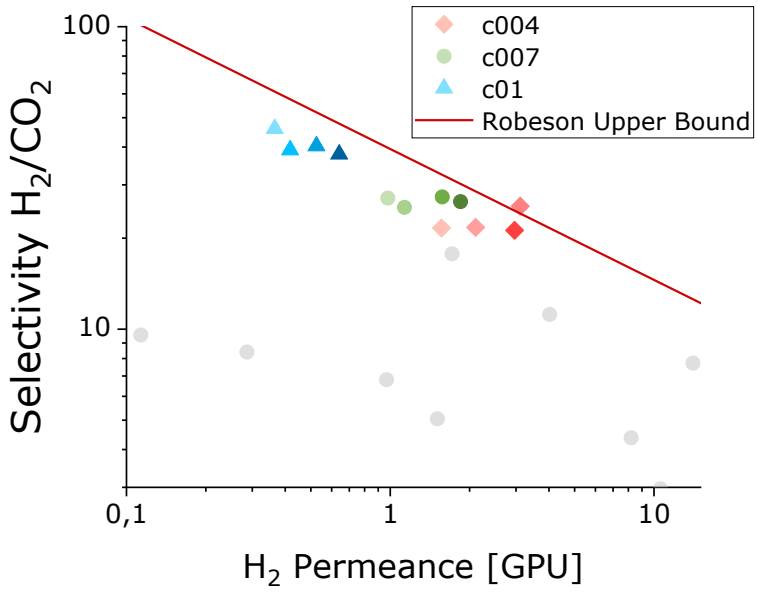

Figure 71, Membranes perm-selectivity depending on temperature and concentration. The darker the color, the higher the temperature: 35°C, 45°C, 55°C, 65°C

From this plot it is possible to see that the selectivity behavior depends on the GO concentration in solutions. Upon examination of low GO concentration case (c004), it is noted that selectivity improves with temperature, which is congruent with the Arrhenius trend and the greater activation energy of hydrogen. However, at 65°C, selectivity diminishes due to a reduction in hydrogen permeance, which could possibly be attributed to compaction of GO multilayer and the potential existence of a non perfectly constant temperature inside the permeometer.

Temperature could also induce permanent modifications on the coating, causing for instance the formation of micropores. For this reason, after the highest temperature (i.e., 65°C), a permeation experiment at 35°C is repeated.

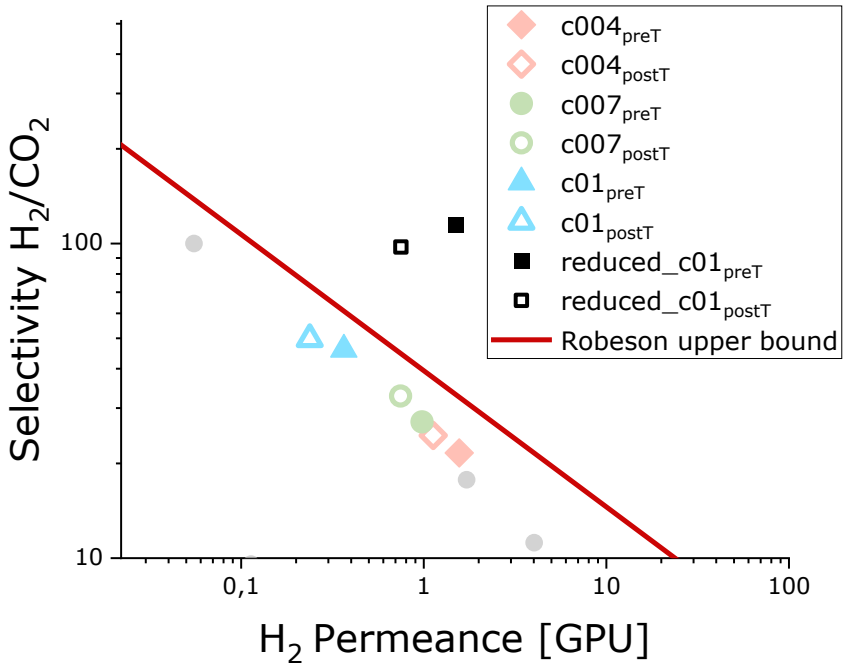

Figure 72, Effect of water loss on perm-selectivity

In this plot there are permeance data at 35°C before and after the membrane has been kept in vacuum at the different temperatures. It is possible to state that the expected permanent modification of the membrane takes place only in part. There is no evidence of thermal reduction that would lead to an increase in the transfer rate. But there is a sort of compaction of the coating related to the elimination of water molecules still present in the graphene oxide multilayer. Indeed,

water is typically absorbed by hydrophilic functional groups of the multilayered structure and it can act as a spacer between the different layers achieving certain permeability. By keeping the membrane in vacuum for long time, water is removed and all the layers become more tightly packed causing, as a result, a slight reduction in permeance.

	PH_2 *[GPU]*	PH_2 *[GPU]*	*Change in permeance*
Testing conditions	35°C pre temperature cycle	35°C post temperature cycle	
S4c004	1.56	1.13	28%
S4c007	1.03	0.78	24%
S4c01	0.37	0.24	35%

Table 15, Change in permeability due to water removal.

The highest change in permeance is obtained by the membrane with the highest concentration of GO: this may be somehow related to the amount of graphene oxide that is deposited onto the membrane. The more relevant the amount of GO in the solution, the higher the density of hydrophilic functional groups, therefore the amount of water that is absorbable.

The compaction of GO coating should be considered as an antagonist to the temperature effect: from one side the temperature enhances the gas permeation, from the other side the reduction of interlayer height causes a decrease in permeability. Indeed, after changing the temperature of the permeometer, a night is waited in order not to have temperature gradients: this means that when membranes are tested at 65°C, they have been under vacuum for at least 5 days.

Such effect of losing water is present also in the case of the thermally reduced membrane. It is unlikely that a thermally reduced GO membrane would contain water because the thermal reduction process involves heating the membrane to a high temperature. However, since the affinity of graphene oxide and water is very high thanks to the presence of oxygen containing functional

groups, once the membrane is taken out from the oven, it can easily reabsorb water coming from humidity of the environment.

7.4 Hydrolyzation

In paragraph 6.2, it is reported that hydrolyzation was needed to allow proper deposition of the coating onto the Matrimid polymeric support. Such a need derives form the hydrophobic nature of pure Matrimid that can cause problems in the deposition of a multilayer starting from aqueous solutions.

Actually, by performing measurements of the zeta potential it can be seen that there is no particular difference between the case of hydrolyzed membranes and non-hydrolyzed ones. Zeta potential is the electrical potential at the interface between the surface of a solid material and the mobile fluid medium. It can be used to determine the surface charge of solid materials. In the specific case of GO-coated membranes, having an indication of the zeta potential of the different layers may be an estimation of the correct deposition of the coating. Indeed, one should expect that integer bilayers numbers are characterized by the zeta potential of pure GO, instead, in case of even bilayers the zeta potential should coincide with that of PDDA. Tests have been performed for 9.5 and 10 BLs to spot differences not only regarding the GO layer, but also the PDDA layer.

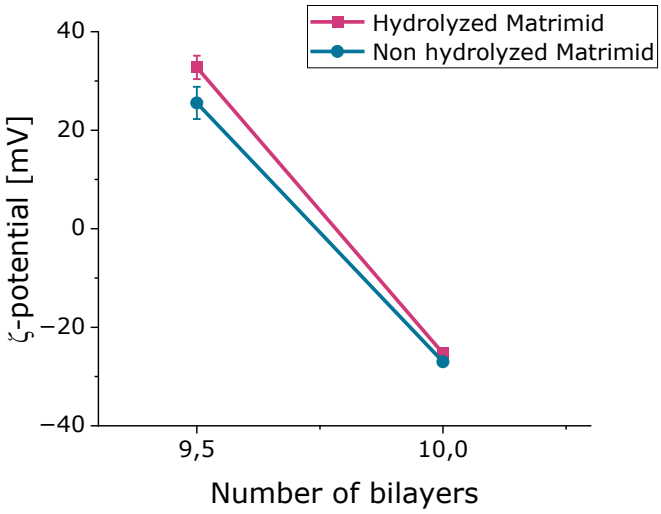

Figure 73, Zeta-potential of GO coated membranes starting from hydrolyzed and non hydrolyzed Matrimid

In both cases zeta-potential values of PDDA are in agreement to the ones reported in literature, for instance Zhu et al. talk about 34.7 mV [81] . Graphene oxide values are also coherent with literature data that are between -25 and -40 mV. [82] In general the relevant aspect is that there is alternating positive and negative values for polycationic and polyanionic layers respectively, and, these values are always about the same.

Furthermore, also by carrying out the permeation tests, there was no difference on hydrogen transfer rate of the two different systems and the transport mechanism still exploits its sieving capacity.

	H_2 Permeance [GPU]
S4c004 with hydrolyzed Matrimid	0.320
S4c004 with non-hydrolyzed Matrimid	0.318

Table 16, Permeance values for membranes starting from hydrolyzed and non hydrolyzed Matrimid

From these results comes that multilayer assembly is applicable with and without hydrolysis, and the resulting membranes will exhibit similar structure and separation performance.

7.5 Effect of coating on one side only

Another parameter that needs to be optimized is the velocity of tests. To that aim, the coating has been deposited just on one side of the membrane. In particular, since graphene oxide can be easily peeled away from solid surfaces, after the coating deposition on both sides of the polymeric support it is peeled away by using adhesive tape. Coating permeability results to be consistent with the values obtained for both-side coated membranes and tests are much more rapid. The transport properties of the coating were not affected by this variation; on the contrary, the permeability of the entire system was. This is due to the fact that there is one less resistance to mass transport across the membrane.

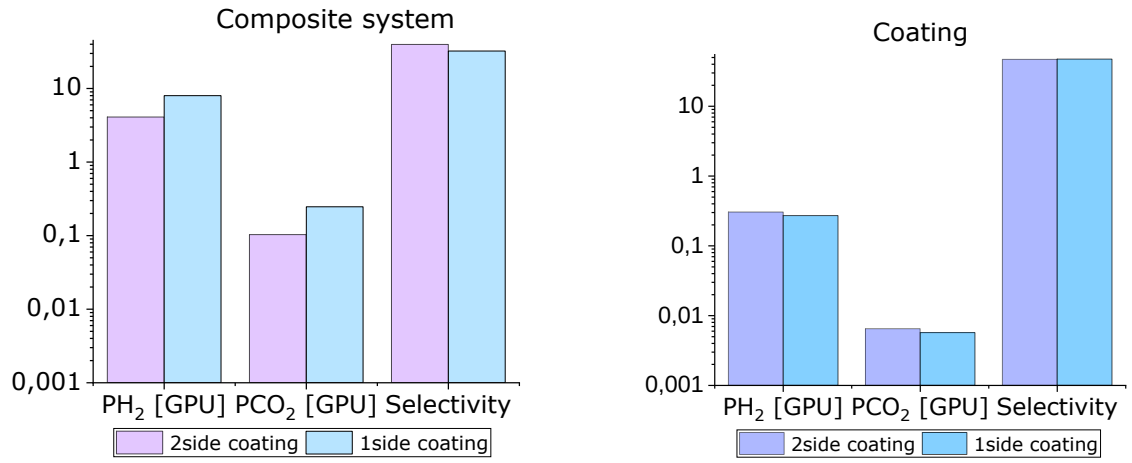

Figure 74, Comparison of permeance and selectivity among 2 side coated membranes and 1 side coated membranes: on the left the overall system (Matrimid + GO multilayer); on the right only the coating

7.6 Effect of the number of Bilayers

The performance of membranes is also affected by the number of bilayers present in the coating. A bilayer is composed of the polycationic layer represented by PDDA and the polyanionic one, that is GO. To investigate this effect, four samples were prepared: 10, 8, 5 and 3 bilayers (BLs).

The following bar plot shows the permeance values of the coating for these samples.

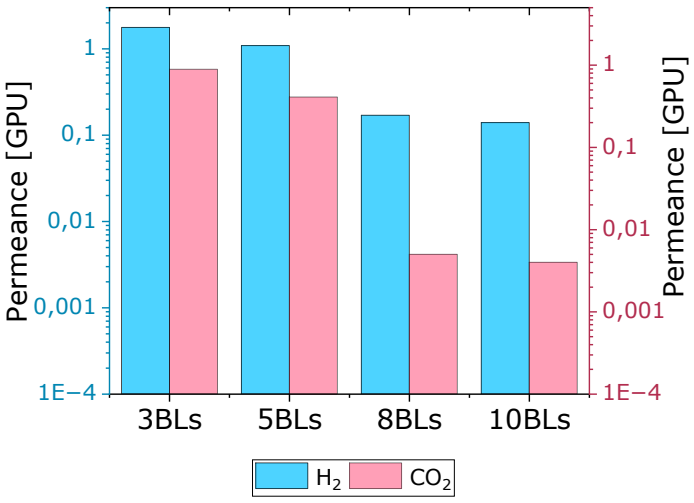

Figure 75, Permeance as a function of the number of bilayers

If the coating assembly has reached nanometric effectiveness, the coating permeability should be consistent, regardless of the specific number of bilayers. As a result, the permeability of different tested membranes can be calculated, considering the d-spacing measurement of 1.4 nm.

	H_2 Permeability [Barrer]	*CO_2 Permeability [Barrer]*	*H_2/CO_2 Selectivity*
c004_3BLs	7.43E-03	3.74E-03	1.99
c004_5BLs	7.63E-03	2.87E-03	2.66
c004_8BLs	1.96E-03	5.6E-05	33.3
c004_10BLs	1.96E-03	5.6E-05	33.9

Figure 76, Coating permeability as a function of the number of bilayers

As one can see, in the case of 10 and 8 Bilayers, permeability of the coating is the same. Instead, in the case of 3 and 5 this is not true, probably because this number of layers is not enough to guarantee the needed ordered structure of the multilayer. Then the deposition of further layers improves the uniformity of the coating. By analyzing the selectivity of these two systems, it is much lower than the others not giving an improvement to the pure Matrimid.

In general, reducing the number of bilayers in a membrane can be done without any negative impact on its performance, up to a certain point. This critical point lies between 5 and 8 BLs and, below it the assembly becomes not accurate. 8 BLs sample serves as evidence that optimizing the membrane by reducing the number of BLs is possible. Doing so would not only decrease the amount of GO used, but also accelerate the assembly process.

7.7 Standardization

The next step in this experimental study has been the standardization of all procedures. Standardization is important for several reasons, including:

- Consistency: to have membranes that show reproducibility and reliability in order to extend the use of this coating to industrial products
- Performance of the membranes: by standardizing the procedure, one may manage to control all the different factors affecting performances

- Scalability

The first aspect that needs to be considered is the mode in which the membrane is dipped inside the GO solutions. In this step, it is crucial that the membrane do not touch the bottom of the beaker. If this happens, the coating deposition is altered by the contact of the polymer and the beaker itself. Indeed, in the first experiments two membranes were produced from the same Matrimid film. But after the coating deposition, depending on the point from where the sample was taken, different perm-selectivity was obtained. Such a phenomenon can be explained by considering that the coating becomes stable and fixed on the membrane only after drying; otherwise, it can be easily altered and removed. To overcome this problem, smaller Matrimid pieces are used and membranes are produced one at a time.

By repeating the membrane production and permeation tests after 3 months from the first membranes, it has been noted that properties changed in a relevant way. When approaching a LbL procedure, one of the large advantages is that the technique is highly tunable. As a drawback, there is a remarkably high number of parameters that can affect the final properties of membranes. Environmental conditions need to be kept as similar as possible. Specifically, the factor that changed the most in these three months is temperature due to the shift from a hot autumn to winter.

These considerations have led to move the Lego under a thermostatic chamber where temperature can be kept reasonably constant: temperature is set at 22°C, with fluctuations within ±2°C.

Then, the attention was focused on the sonication time because, there was still a sensitive change in properties for membranes produced starting from the same batch of solution. During sonication, high frequency waves are used to create cavitation bubbles of water and break the GO flakes to generate a homogeneous dispersion. The longer the sonication time, the more stable the solution up to a certain critical sonication time, above which degradation of graphene oxide flakes occurs.

When membranes are prepared, evaporation occurs causing a concentration of the solution which may lead to precipitation or agglomeration of GO flakes: a sort of GO aging takes place. Macroscopically this can be seen only in extreme cases, but in the nanometric structure, things change fast.

	PH_2 [GPU]	*PCO_2 [GPU]*	*Selectivity*	*Notes*
M1	0.27	0.006	47.9	Day 0 New GO solution
M2	0.22	0.01	22.1	1-day old GO, sonicated 4h
M3	0.19	0.03	6.63	2-days old GO, non sonicated
M4	0.11	0.006	20.73	3-days old GO, re-diluted and sonicated 4 h

Table 17, GO aging effect on membrane performances.

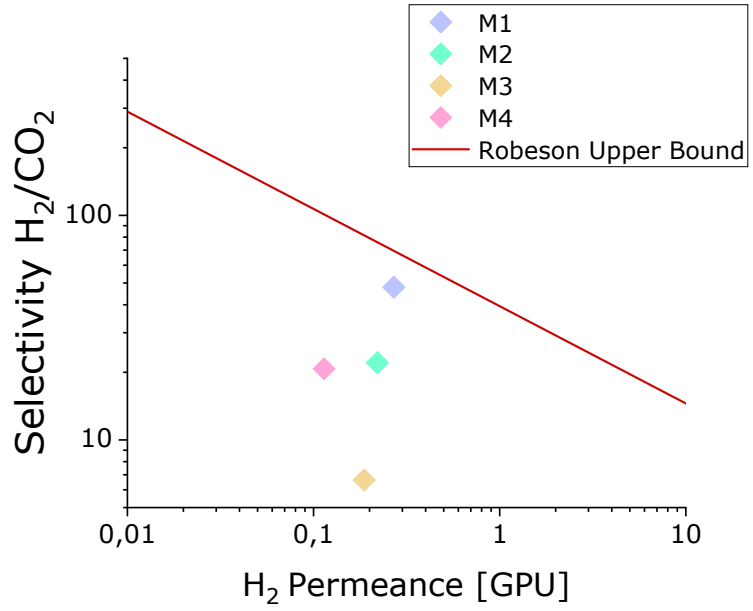

Figure 77, Performances variability due to GO aging.

As one can see from these values, permeance decreases, and also selectivity. It is likely that GO flakes agglomerate, causing the formation of bigger GO sheets deposited onto the membrane and the partial occlusion of transport pathways. Moreover, having these agglomerates also leads to a more disordered multilayer so that selectivity does not remain the same. When the solution is re-diluted and sonicated again, it seems to increase its selectivity.

More precisely, day 0 is when the solution is produced and sonicated 4 hours. A membrane is produced overnight, and the same solution is used the following day, after another 4 hours of sonication. Then, since evaporation has caused a strong decrease in the volume of the solution, it has been re-diluted and sonicated again. These results suggest that once aging started, 4 hours of

sonication are not sufficient anymore. The idea is to sonicate for 8 hours in order to avoid this aging effect and, indeed, it seems that after 8 hours of sonication, perm-selectivity improves.

	PH_2 [GPU]	*PCO_2 [GPU]*	*Selectivity*	*Notes*
M5	0.12	0.005	24.21	New GO solution
M6	0.14	0.004	33.98	2 days old GO solution, sonicated 8 h

Table 18, Effect of higher sonication time

7.8 Results analysis

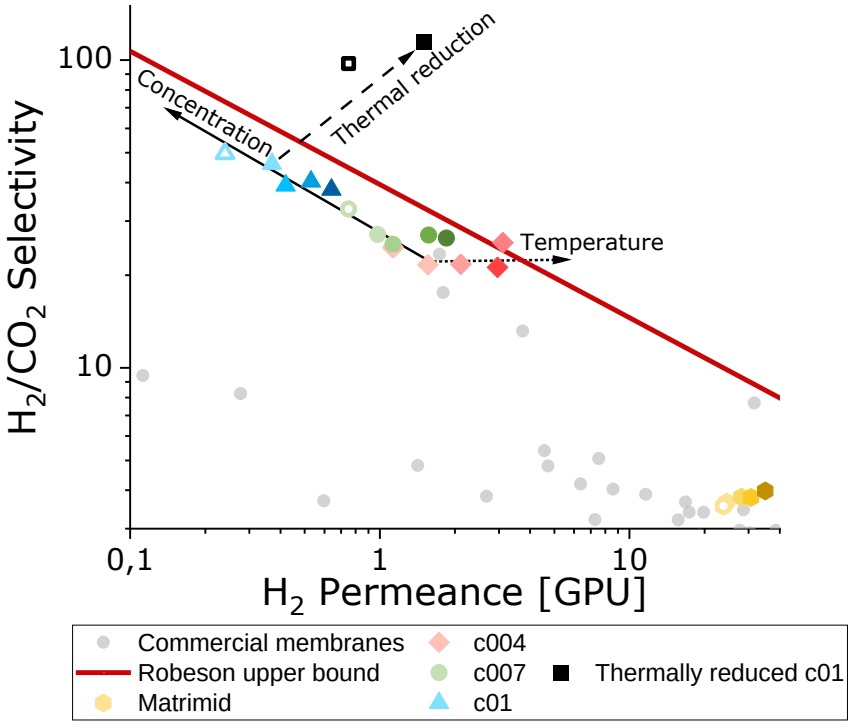

Figure 78, Summary of temperature, concentration and thermal reduction effects on coating performances

The first aspect to note is that the addition of GO multilayered coating onto a Matrimid support leads to a significant improvement in perm-selectivity across all cases. Moreover, coating consistently performs very close to, and even surpasses, the Robeson upper bound in some cases.

Several factors affecting membrane performance have been analyzed. From the plot, it is possible to observe three primary directions of movement with respect to the Robeson upper bound.

Temperature is indicated by the increase in color intensity, and it is apparent that increasing the temperature results in higher permeability. Selectivity behavior with temperature is concentration dependent. With low amounts of GO, selectivity increases with temperature, except for the last point of c004 that is not consistent with the Arrhenius-like behavior. On the other hand, as the concentration of GO rises, selectivity remains the same or may slightly decrease.

When focusing on concentration, it follows the same slope of the upper bound. Permeability and selectivity can be adjusted independently, but it is not possible to improve both aspects of gas separation simultaneously. This is not necessarily a negative effect because even the lowest concentration considered, the system still exhibits good selectivity in the range 21-25.

The best treatment is thermal reduction, which strongly overcomes the limitations of polymeric membranes in the case of the lowest permeability. This is achieved by combining a dense polymeric material with a nanoporous multilayered coating that benefits from the high selectivity of the multilayer and the increased permeability of a nanoporous thin system. Additionally, the hollow points on the plot represent the different membranes after being in vacuum for at least 5 days in the presence of increasing temperatures. In all cases, there is a decrease in permeability due to the compaction of the coating, but this effect is not so relevant and it does not significantly modify the analyzed systems.

The structure of the coating results to be well assembled. Tests with the coating on only one side of the polymeric support showed that the performance of the coating remained the same. Furthermore, reducing the number of bilayers provided interesting insights. The deposition of the first layers was not effective: tests on 3 and 5 bilayers showed that the coating is not selective. However, there is no difference in perm-selectivity between 8 and 10 bilayers. This paves the way for an optimization process that allows for faster testing and production of membranes while maintaining accuracy and reproducibility and, on the other hand, for the use of a smaller amount of graphene oxide onto the polymeric films.

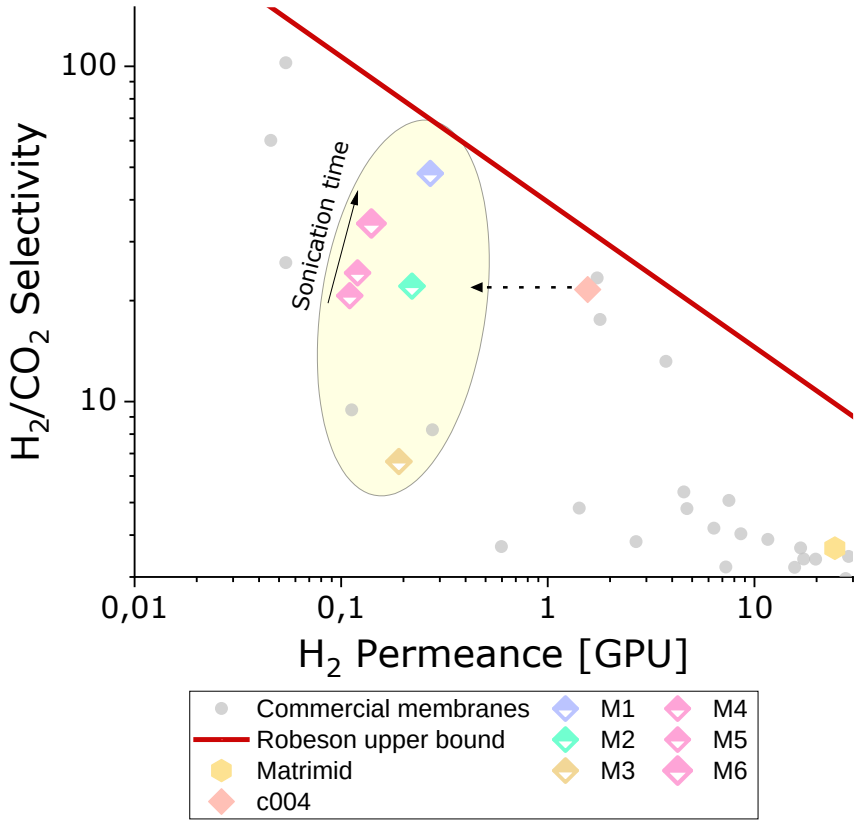

Figure 79, Summary standardization procedure effect on coating performance

In this plot, membranes starting from the same concentration of GO solutions are reported. After some months from the first tests, all coatings shifted towards lower values of permeability. This is due to the aging of GO that tends to agglomerate as a result of electrostatic interactions causing a loss in reproducibility. At this regard the points representing the coatings are spread out over a large area on the plot. However, this issue can be addressed by standardizing the procedure to eliminate any uncertainties and by increasing the sonication time that exfoliates more GO agglomerates. The results labeled M4, M5 and M6 were obtained by performing the LbL assembly at controlled temperature, and M6 was sonicated for 8 hours rather than 4 because the solution was 1-day old.

8. Conclusions

Hydrogen market is experiencing exponential growth due to its great potentiality for decarbonizing hard-to-abate systems. As a result, pure hydrogen production has become increasingly important in recent years.

Graphene-based materials are considered as rising stars among low dimensional materials thanks to their extraordinary properties. In gas separation systems, they can be used to produce nanoporous single layer membranes or multilayered membranes, which have shown excellent performance results. The multilayered structure can be obtained using several different deposition techniques, among which Layer By Layer has emerged as a versatile technology that allows for nanometric tunability of the multilayer. However, understanding all the possible effects of the different parameters that influence the preparation of these membranes is challenging.

This experimental study focuses on GO multilayered membranes that were prepared using LbL assembly techniques for H_2/CO_2 separation. Matrimid was used as the main polymeric support, and various effects were investigated, such as GO concentration, thermal reduction and testing temperature. In all cases, there was a significant change in the resulting coating perm-selectivity.

GO concentration is a key parameter, as increasing amount of graphene oxide dispersed in solutions leads to a higher amount of GO deposited on the membrane. There is a strong correlation between the GO concentration and separation performance of the membranes. A high density of GO sheets on the polymeric substrate leads to a more tortuous path, allowing only the passage of smaller molecules, such as hydrogen, resulting in higher selectivity. However, as a drawback, permeability decreases and this is something that should be avoided not to have a loss in the productivity of the system. This problem can be overcome by performing a thermal reduction on GO membranes, which forms nano holes in the multilayered coating, resulting in higher permeability and selectivity.

Testing temperature also has a significant effect on the permeability of the membranes. There is an Arrhenius-like behavior of permeability that comes from the combination of diffusivity and solubility that depend both on temperature. In general, permeability increases with temperature, but there is no evidence of a peculiar trend for selectivity.

The presence of water inside the membranes also affects permeability, as keeping the membrane in vacuum for an extended period removes water and compacts the multilayer, resulting in decreased permeability and slightly increased selectivity.

Reduction of the number of bilayers is an interesting aspect. In the first 5 layers, the coating deposition is not uniform causing a decrease in perm-selectivity. However, once the ordered structure has been formed, coating performances remain constant.

Several factors exhibit their effects simultaneously, making it challenging to standardize the procedure and achieve reproducibility. The assembly temperature and GO solution aging are two examples of indeterminations that hindered reproducibility, leading to the need to standardize the procedure as much as possible. The final part of this experimental work is focused on standardization and optimization of the assembly.

Attempts were made to use different polymeric substrates , but several problems arose. Matrimid thin film onto a porous support were produced, but their thickness was not uniform, making it impossible to obtain accurate results. PPO and P84 films were also produced, but both the polymers caused GO coagulation, which is likely due to the presence of solvent residues that contaminated GO solutions.

To conclude, GO coated membranes show good separation performance, with results very close to the Robeson upper bound that limits permeability and selectivity of polymeric membranes, and in some cases, even higher. LbL assembly is confirmed to have high potentiality which can be fully exploited by continuing to understand all the variable parameters. GO coating can also be easily deposited onto other substrates to extend the achieved separation performances at the industrial scale.

References

1. Ritchie, H. (2020, May 11). *Emissions by sector*. Our World in Data. https://ourworldindata.org/emissions-by-sector
2. Stolten, D., & Emonts, B. (2016b). *Hydrogen Science and Engineering: Materials, Processes, Systems and Technology*.
3. Ag, E. (n.d.). *The colors of hydrogen: an overview*. EWE AG. https://www.ewe.com/en/shaping-the-future/hydrogen/the-colours-of-hydrogen
4. *Hydrogen Production: Natural Gas Reforming*. (n.d.). Energy.gov. https://www.energy.gov/eere/fuelcells/hydroge-n-production-natural-gas-reforming
5. T. (n.d.). *Blue, green, gray: the colors of hydrogen*. http://www.chem4us.be/blue-green-gray-the-colors-of-hydrogen/
6. Scipioni, A., Manzardo, A., & Ren, J. (2017). *Hydrogen Economy: Supply Chain, Life Cycle Analysis and Energy Transition for Sustainability*. Academic Press.
7. Liu, K., Song, C., & Subramani, V. (2010). *Hydrogen and Syngas Production and Purification Technologies*. John Wiley & Sons.
8. Naimi, Y., & Antar, A. (2018). Hydrogen Generation by Water Electrolysis. *InTech EBooks*. https://doi.org/10.5772/intechopen.76814
9. Zoulias, E. & Varkaraki, Elli & Lymberopoulos, N. & Christodoulou, Chris & Karagiorgis, George. (2004). A Review on Water Electrolysis. TCJST. 4. 41-71.
10. Ursúa, A., Abad, A., & Sanchis, P. (2012). Hydrogen Production From Water Electrolysis: Current Status and Future Trends. *Proceedings of the IEEE*, *100*(2), 410–426. https://doi.org/10.1109/jproc.2011.2156750
11. *Global Hydrogen Review 2022 – Analysis - IEA*. (n.d.). IEA. https://www.iea.org/reports/global-hydrogen-review-2022
12. *Carbon Capture, Utilisation and Storage – Analysis - IEA*. (n.d.). IEA. https://www.iea.org/reports/carbon-capture-utilisation-and-storage-2
13. *Carbon capture, storage and utilisation*. (n.d.). Energy. https://energy.ec.europa.eu/topics/oil-gas-and-coal/carbon-capture-storage-and-utilisation_en

14. I., Change, I. P. O. C., & Group, I. P. O. C. C. W., III. (2005a). *Carbon Dioxide Capture and Storage: Special Report of the Intergovernmental Panel on Climate Change*. Cambridge University Press.
15. *Fig. 1 -Block diagrams illustrating post-combustion, pre-combustion,*ResearchGate. https://www.researchgate.net/figure/Block-diagrams-illustrating-post-combustion-pre-combustion-and-oxy-combustion-systems_fig1_222431915
16. Voldsund, M., Jordal, K., & Anantharaman, R. (2016). Hydrogen production with CO2 capture. *International Journal of Hydrogen Energy*, *41*(9), 4969–4992. https://doi.org/10.1016/j.ijhydene.2016.01.009
17. Du, Z., Liu, C., Zhai, J., Guo, X., Xiong, Y., Su, W., & He, G. (2021). A Review of Hydrogen Purification Technologies for Fuel Cell Vehicles. *Catalysts*, *11*(3), 393. https://doi.org/10.3390/catal11030393
18. Sharma, S. (2009). FUELS – HYDROGEN PRODUCTION | Gas Cleaning: Pressure Swing Adsorption. *Elsevier EBooks*, 335–349. https://doi.org/10.1016/b978-044452745-5.00307-5
19. *Dynamic Sorption - Gas Separation, Gas Purification*. (n.d.). https://www.dynamicsorption.com/applications/gas-separation/
20. *Zeochem*. (n.d.). Zeochem. https://www.zeochem.com/news/psa-vs-tsa-whats-the-difference
21. Mason, J. A.; Sumida, K.; Herm, Z. R.; Krishna, R.; Long, J. R. Evaluating metal-organic frameworks for post-combustion carbon dioxide capture *via* temperature swing adsorption. *Energy Environ. Sci.*, 2011, 4, 3030–3040
22. Hinchliffe, A. B., & Porter, K. (2000). A Comparison of Membrane Separation and Distillation. *Chemical Engineering Research & Design*, *78*(2), 255–268. https://doi.org/10.1205/026387600527121
23. Today, C. (n.d.). *Adsorption, Absorption and Desorption - What's the Difference?* Chromatography Today. https://www.chromatographytoday.com/news/hplc-uhplc/31/breaking-news/adsorption-absorption-and-desorption-whats-the-difference/31397#:~:text=Physical%20absorption%20%E2%80%94%20A%20non%2Dreactive,atoms%20or%20molecules%20are%20absorbed

24. Rackley, S. A. (2010). Absorption Capture Systems. *Elsevier EBooks*, 103–131. https://doi.org/10.1016/b978-1-85617-636-1.00006-7
25. Pakzad, P., Mofarahi, M., Ansarpour, M., Afkhamipour, M., & Lee, C. H. (2020). CO2 absorption by common solvents. Elsevier EBooks, 51–87. https://doi.org/10.1016/b978-0-12-819657-1.00003-7
26. Rackley, S. A. (2010b). Absorption Capture Systems. *Elsevier EBooks*, 103–131. https://doi.org/10.1016/b978-1-85617-636-1.00006-7
27. Mulder, J. (1996). *Basic Principles of Membrane Technology*. Springer.
28. Ismail, A. F., Khulbe, K., & Matsuura, T. (2015). *Gas Separation Membranes: Polymeric and Inorganic*. Springer.
29. Baker, R., & Baker, R. W. (2004). *Membrane Technology and Applications*. John Wiley & Sons.
30. Ho, W., & Sirkar, K. (2012). *Membrane Handbook*. Springer Science & Business Media.
31. Pierleoni, D. (2018). *Novel experimental methods and modeling of solvent induced glass transition and structural relaxation in polymers* [PhD Dissertation]. University of Bologna.
32. Hollaway, L. (2011). Key issues in the use of fibre reinforced polymer (FRP) composites in the rehabilitation and retrofitting of concrete structures. *Elsevier EBooks*, 3–74. https://doi.org/10.1533/9780857090928.1.3
33. Ansaloni, L. (2014). *POLYMERIC MEMBRANES FOR CO2 SEPARATION: EFFECT OF AGING, HUMIDITY AND FACILITATED TRANSPORT* [PhD Disseration]. UniBO.
34. Li, N. N., Fane, A. G., Ho, W. S. W., & Matsuura, T. (2011). *Advanced Membrane Technology and Applications*. John Wiley & Sons.
35. Shao, L., Low, B. Y., Chung, T., & Greenberg, A. E. (2009). Polymeric membranes for the hydrogen economy: Contemporary approaches and prospects for the future. *Journal of Membrane Science*, *327*(1–2), 18–31. https://doi.org/10.1016/j.memsci.2008.11.019
36. Farnam, M., Mukhtar, H., & Shariff, A. M. (2021). A Review on Glassy and Rubbery Polymeric Membranes for Natural Gas Purification. *ChemBioEng Reviews*, *8*(2), 90–109. https://doi.org/10.1002/cben.202100002
37. Ockwig, N. W., & Chapman, K. W. (2007). Membranes for Hydrogen Separation. *Chemical Reviews*, *107*(10), 4078–4110. https://doi.org/10.1021/cr0501792

38. Robeson, L. M. (2008). The upper bound revisited. *Journal of Membrane Science*, *320*(1–2), 390–400. https://doi.org/10.1016/j.memsci.2008.04.030
39. Rowe, B. W., Robeson, L. M., Freeman, B. D., & Paul, D. R. (2010). Influence of temperature on the upper bound: Theoretical considerations and comparison with experimental results. *Journal of Membrane Science*, *360*(1–2), 58–69. https://doi.org/10.1016/j.memsci.2010.04.047
40. Robeson, L. (1999). Polymer membranes for gas separation. *Current Opinion in Solid State & Materials Science*, *4*(6), 549–552. https://doi.org/10.1016/s1359-0286(00)00014-0
41. Han, Y., & Ho, W. S. W. (2021). Polymeric membranes for CO2 separation and capture. *Journal of Membrane Science*, *628*, 119244. https://doi.org/10.1016/j.memsci.2021.119244
42. Al-Rowaili, F. N., Khaled, M., Jamal, A., & Zahid, U. (2023). Mixed matrix membranes for H2/CO2 gas separation- a critical review. *Fuel*, *333*, 126285. https://doi.org/10.1016/j.fuel.2022.126285
43. Dong, G., Li, H., & Chen, V. (2013). Challenges and opportunities for mixed-matrix membranes for gas separation. *Journal of Materials Chemistry. A, Materials for Energy and Sustainability*, *1*(15), 4610. https://doi.org/10.1039/c3ta00927k
44. Goh, P. S., & Ismail, A. F. (2020). Structure and gas transport of nanocomposite membranes. -. https://doi.org/10.1016/b978-0-12-819406-5.00003-4
45. Armano, A., & Agnello, S. (2019). Two-Dimensional Carbon: A Review of Synthesis Methods, and Electronic, Optical, and Vibrational Properties of Single-Layer Graphene. *C*, *5*(4), 67. https://doi.org/10.3390/c5040067
46. Lowe, D. B. (2016). *The Chemistry Book: From Gunpowder to Graphene, 250 Milestones in the History of Chemistry*. Sterling.
47. Singh, R., Kumar, R., & Singh, D. (2016). Graphene oxide: strategies for synthesis, reduction and frontier applications. *RSC Advances*, *6*(69), 64993–65011. https://doi.org/10.1039/c6ra07626b
48. Dreyer, D. R., Park, S., Bielawski, C. W., & Ruoff, R. S. (2010). The chemistry of graphene oxide. *Chemical Society Reviews*, *39*(1), 228–240. https://doi.org/10.1039/b917103g

49. Jiříčková, A., Jankovský, O., Sofer, Z., & Sedmidubský, D. (2022). Synthesis and Applications of Graphene Oxide. *Materials*, *15*(3), 920. https://doi.org/10.3390/ma15030920
50. Luo, L., Peng, T., Yuan, M., Sun, H., Dai, S., & Wang, L. (2018). Preparation of Graphite Oxide Containing Different Oxygen-Containing Functional Groups and the Study of Ammonia Gas Sensitivity. *Sensors*, *18*(11), 3745. https://doi.org/10.3390/s18113745
51. Krishnamoorthy, K., Veerapandian, M., Yun, K., & Kim, S. H. (2013). The chemical and structural analysis of graphene oxide with different degrees of oxidation. *Carbon*, *53*, 38–49. https://doi.org/10.1016/j.carbon.2012.10.013
52. ASTM, Zeta potential of colloids in water and wastewater. ASTM Standard D 4187–82. American Society for Testing and Materials; 1985
53. Chen, D., Feng, H., & Li, J. (2012). Graphene Oxide: Preparation, Functionalization, and Electrochemical Applications. *Chemical Reviews*, *112*(11), 6027–6053. https://doi.org/10.1021/cr300115g
54. Eigler, S. (2016). Graphene. An Introduction to the Fundamentals and Industrial Applications Edited by Madhuri Sharon and Maheshwar Sharon. In *Angewandte Chemie* (Vol. 55, Issue 17, p. 5122). Wiley. https://doi.org/10.1002/anie.201602067
55. Yoo, B. M., Shin, J. E., Lee, H. D., & Park, H. B. (2017). Graphene and graphene oxide membranes for gas separation applications. Current Opinion in Chemical Engineering, 16, 39–47. https://doi.org/10.1016/j.coche.2017.04.004
56. Yuan, W., Chen, J., & Shi, G. (2014). Nanoporous graphene materials. *Materials Today*, *17*(2), 77–85. https://doi.org/10.1016/j.mattod.2014.01.021
57. Zhou, F., Fathizadeh, M., & Yu, M. (2018). Single- to Few-Layered, Graphene- Based Separation Membranes. Annual Review of Chemical and Biomolecular Engineering, 9(1), 17–39. https://doi.org/10.1146/annurev-chembioeng-060817-084046
58. Guirguis, A., Maina, J., Kong, L., Henderson, L. C., Rana, A., Li, L., Majumder, M., & Dumée, L. F. (2019). Perforation routes towards practical nano-porous graphene and analogous materials engineering. *Carbon*, *155*, 660–673. https://doi.org/10.1016/j.carbon.2019.09.028

59. Liu, G., Jin, W., & Xu, N. (2015). Graphene-based membranes. *Chemical Society Reviews*, *44*(15), 5016–5030. https://doi.org/10.1039/c4cs00423j
60. Tsou, C., An, Q., Lo, S., De Guzman, M. R., Hung, W., Hu, C., Lee, K., & Lai, J. (2015). Effect of microstructure of graphene oxide fabricated through different self-assembly techniques on 1-butanol dehydration. *Journal of Membrane Science*, *477*, 93–100. https://doi.org/10.1016/j.memsci.2014.12.039
61. Chen, J. C., Guo, Y., Huang, L., Xue, Y., Geng, D., Liu, H., Wu, B., Yu, G., Hu, W., Liu, Y., & Zhu, D. (2014). Controllable fabrication of ultrathin free-standing graphene films. *Philosophical Transactions of the Royal Society A*, *372*(2013), 20130017. https://doi.org/10.1098/rsta.2013.0017
62. Branco, C. M., Sharma, S., De Camargo Forte, M. M., & Steinberger-Wilckens, R. (2016). New approaches towards novel composite and multilayer membranes for intermediate temperature-polymer electrolyte fuel cells and direct methanol fuel cells. *Journal of Power Sources*, *316*, 139–159. https://doi.org/10.1016/j.jpowsour.2016.03.052
63. Rha, S., Yoon, H. M., Yoon, S., Yoo, B. S., Ahn, B. T., Cho, Y. M., Shin, H. W., Yang, H., Paik, U., Kwon, S., Choi, J., & Park, H. S. (2013). Selective Gas Transport Through Few-Layered Graphene and Graphene Oxide Membranes. *Science*, *342*(6154), 91–95. https://doi.org/10.1126/science.1236098
64. *File:Spincoating.svg - Wikimedia Commons*. (2015, February 26). https://commons.wikimedia.org/wiki/File:Spincoating.svg
65. Nie, L., Chuah, C. Y., Bae, T., & Lee, J. (2021). Graphene-Based Advanced Membrane Applications in Organic Solvent Nanofiltration. *Advanced Functional Materials*, *31*(6), 2006949. https://doi.org/10.1002/adfm.202006949
66. Zhao, G., Han, W., Dong, L., Fan, H., Qu, Z., Gu, J., & Meng, H. (2022). Sprayed separation membranes: A systematic review and prospective opportunities. *Green Energy & Environment*, *7*(6), 1143–1160. https://doi.org/10.1016/j.gee.2022.04.001
67. Ahmad, Z., Khan, A. U., Farooq, R., Saif, T., & Mastoi, N. (2016). Mechanism of Corrosion and Erosion Resistance of Plasma- Sprayed Nanostructured Coatings. *InTech EBooks*. https://doi.org/10.5772/64316

68. Dai, Z., Ansaloni, L., & Knuutila, H. K. (2016). Recent advances in multi-layer composite polymeric membranes for CO2 separation: A review. *Green Energy & Environment*, *1*(2), 102–128. https://doi.org/10.1016/j.gee.2016.08.001
69. Ji, G., & Zhao, M. (2017). Membrane Separation Technology in Carbon Capture. *InTech EBooks*. https://doi.org/10.5772/65723
70. Decher, G. (1997). Fuzzy Nanoassemblies: Toward Layered Polymeric Multicomposites. *Science*, *277*(5330), 1232–1237. https://doi.org/10.1126/science.277.5330.1232
71. Richardson, J. J., Cui, J., Björnmalm, M., Braunger, J. A., Ejima, H., & Caruso, F. (2016). Innovation in Layer-by-Layer Assembly. *Chemical Reviews*, *116*(23), 14828–14867. https://doi.org/10.1021/acs.chemrev.6b00627
72. Lee, T., Min, H. K., Gu, M., Jung, Y. K., Lee, W., Lee, J. U., Seong, D. G., & Kim, B. C. (2015). Layer-by-Layer Assembly for Graphene-Based Multilayer Nanocomposites: Synthesis and Applications. *Chemistry of Materials*, *27*(11), 3785–3796. https://doi.org/10.1021/acs.chemmater.5b00491
73. Kruk, T., & Warszyński, P. (2021). Conductive Nanofilms with Oppositely Charged Reduced Graphene Oxides as a Base for Electroactive Coatings and Sensors. *Colloids and Interfaces*, *5*(2), 20. https://doi.org/10.3390/colloids5020020
74. Park HB, Suh IY, Lee YM: Novel pyrolytic carbon membranes containing silica: preparation and characterization. Chem. Mater. 2002, 14:3034-3046.
75. Suda H, Haraya K: Gas permeation through micropores of carbon molecular sieve membranes derived from Kapton polyimide. J. Phys. Chem. B 1997, 101:3988-3994.
76. Pierleoni, D., Minelli, M., Ligi, S., Christian, M., Funke, S., Reineking, N., Morandi, V., Doghieri, F., & Palermo, V. (2018). Selective Gas Permeation in Graphene Oxide–Polymer Self-Assembled Multilayers. *ACS Applied Materials & Interfaces*, *10*(13), 11242–11250. https://doi.org/10.1021/acsami.8b01103
77. Liu, H., Bandyopadhyay, P., Kshetri, T., Kim, N., Ku, B., Moon, B., & Lee, J. H. (2017). Layer-by-layer assembled polyelectrolyte-decorated graphene multilayer film for hydrogen gas barrier application. *Composites Part B-Engineering*, *114*, 339–347. https://doi.org/10.1016/j.compositesb.2017.02.007

78. Zeynali, R., Ghasemzadeh, K., Sarand, A. B., Kheiri, F., & Basile, A. (2018). Performance evaluation of graphene oxide (GO) nanocomposite membrane for hydrogen separation: Effect of dip coating sol concentration. *Separation and Purification Technology*, *200*, 169–176. https://doi.org/10.1016/j.seppur.2018.02.032
79. Lyn, F. H., Tan, C. P., Zawawi, R. M., & Hanani, Z. N. (2021). Effect of sonication time and heat treatment on the structural and physical properties of chitosan/graphene oxide nanocomposite films. *Food Packaging and Shelf Life*, *28*, 100663. https://doi.org/10.1016/j.fpsl.2021.100663
80. Roh, J. S., Choi, T. H., Lee, T. H., Yoon, H. M., Kim, J., Rha, S., & Park, H. S. (2019). Understanding Gas Transport Behavior through Few-Layer Graphene Oxide Membranes Controlled by Tortuosity and Interlayer Spacing. *Journal of Physical Chemistry Letters*, *10*(24), 7725–7731. https://doi.org/10.1021/acs.jpclett.9b03082
81. Manning, G. S. (2006). The Persistence Length of DNA Is Reached from the Persistence Length of Its Null Isomer through an Internal Electrostatic Stretching Force. *Biophysical Journal*, *91*(10), 3607–3616. https://doi.org/10.1529/biophysj.106.089029 https://www.ncbi.nlm.nih.gov/pmc/articles/PMC1630458/
82. Guiver, M. D., Robertson, G. P., Dai, Y., Bilodeau, F., Kang, Y. S., Lee, K. L., Jho, J. Y., & Won, J. (2002). Structural characterization and gas-transport properties of brominated matrimid polyimide. *Journal of Polymer Science Part A*, *40*(23), 4193–4204. https://doi.org/10.1002/pola.10516
83. Castro-Muñoz, Roberto & Fila, Vlastimil. (2018). Progress on Incorporating Zeolites in Matrimid®5218 Mixed Matrix Membranes towards Gas Separation. Membranes. 8. 30. 10.3390/membranes8020030.
84. Wikipedia contributors. (2023, February 8). *Poly(p-phenylene oxide)*. Wikipedia. https://en.wikipedia.org/wiki/Poly%28p-phenylene_oxide%29#/media/File:Polyphenylenether.svg
85. Li, X., & Chung, T. (2014). Thin-film composite P84 co-polyimide hollow fiber membranes for osmotic power generation. *Applied Energy*, *114*, 600–610. https://doi.org/10.1016/j.apenergy.2013.10.037

86. Wikipedia contributors. (2021, December 12). *PolyDADMAC*. Wikipedia. https://en.wikipedia.org/wiki/PolyDADMAC#/media/File:Polyquaternium-6.svg
87. Schöttler, M. (2021, October 5). *Water electrolysis explained – the basis for most Power-to-X processes*. PtX Hub. https://ptx-hub.org/water-electrolysis-
88. Borhani, T. N., Azarpour, A., Akbari, V., Alwi, S. R. W., & Manan, Z. A. (2015). CO2 capture with potassium carbonate solutions: A state-of-the-art review. *International Journal of Greenhouse Gas Control*, *41*, 142–162. https://doi.org/10.1016/j.ijggc.2015.06.026
89. Wikipedia contributors. (2023a, January 29). *Ethanolamine*. Wikipedia. https://en.wikipedia.org/wiki/Ethanolamine#/media/File:Ethanolamine-2D-skeletal-A.png
90. Anton Paar GmbH. (2022, June 22). *SurPASS 3: Solid surface charge analysis made easy*. YouTube
91. Anton Paar GmbH. (2019, July 31). *Characterizing the Zeta Potential of Materials from the Nano to the Macro Scale* [Video]